MAGNETIC EXTRACTION OF THE PROTON BEAM FROM THE MCGILL SYNCHROCYCLOTRON

by

Robert B. Moore

A thesis submitted to the Faculty of Graduate Studies and Research of McGill University, in partial fulfilment of the requirements for the degree of Doctor of Philosophy

Radiation Laboratory
McGill University
April, 1962

TABLE OF CONTENTS

ACKNOWLEDGEMENT

Professor J. S. Foster, the founder and previous director of this laboratory suggested in 1959 that some improvement of the McGill synchrocyclotron should be considered. When Professor R. E. Bell became director of the laboratory in June 1960, he pointed out that an improved external beam system would be a great advantage and suggested that an improvement of the extraction system should be undertaken. It was decided that a non-linear regenerative type of extraction system should be installed. In September 1960, Dr. W. Frisken from the University of Birmingham joined the laboratory and assumed directorship of the extraction project. In September 1961, Dr. W. Link from Brookhaven National Laboratories, joined this laboratory and helped in the focusing and transport of the extracted proton beam. The author gratefully acknowledges the guidance, the encouragement and the help of these men in the work described in this thesis.

In the actual construction of the extraction system, the ingenuity and the industry of Mr. S. Doig and Mr. G. Belley were invaluable.

The author gratefully acknowledges National Research Council of Canada scolarships held throughout the course of this work.

ABSTRACT

This thesis describes the successful extraction of the full energy proton beam from the McGill synchrocyclotron. Extraction was achieved by increasing the radial separation for the last few orbits by the process of non-linear regenerative magnetic deflection, and then leading the last orbit into a magnetic channel.

Design and installation of the magnetic regenerator and the magnetic channel are described in the main body of this thesis, and theoretical development of the design criteria is given in the appendix.

The extracted beam has been focused to a spot 1.3 x 4.8 mm with a divergence of 1° at a position 15 feet from the channel exit. It has a pulsed time structure consisting of 15×10^{-6} sec. bursts repeated 400 times per second, and an average intensity of 4×10^{-9} amperes.

LIST OF FIGURES

LIST OF PLATES

CHAPTER 1

INTRODUCTION

Introduction

This section of the thesis describes the design and installation of a magnetic extraction system for the McGill 82 inch synchrocyclotron. This machine, which accelerates protons to a little less than 100 Mev, was primarily intended for the production of neutron deficient radioactive nuclei. These can be produced by (p,xn) reactions in targets placed inside the machine to intercept the internal beam. The reasons for installing the extraction system, and the reasons for deciding on the type chosen, are outlined in this introduction.

When the McGill synchrocyclotron was first put into operation (about 1950) there was little information on radioactive nuclei. With the proton energy available in the machine, (p,xn) reactions on stable nuclei could be used to produce many radioactive nuclei for the first time. Although synchrocyclotrons have a much lower beam intensity than fixed frequency cyclotrons, they have other advantages. Their higher energy protons can produce radioactive nuclei that the fixed frequency cyclotrons cannot. Furthermore, the single dee system permits target bombardment at almost any radius inside the machine and so the energy of the reaction protons may be very easily selected. The McGill machine was therefore very useful in obtaining nuclear data which helped in the building up of systematics of the nuclei. About 40 new isotopes were produced in the machine and many isomeric states were also discovered. Decay schemes have been proposed for most of these and for a great many others.

However, for the higher energy synchrocyclotrons put into operation at the same time, the most exciting work was in the fields of nucleon-nucleon scattering, nucleon-nucleus scattering and the production of pions. (For a discussion of the relative merits of cyclotrons and synchrocyclotrons at this time, see Livingston (1952)). The difficulties of doing such work in the internal beam of a synchrocyclotron were overwhelming and so there was a great demand for external beams from these machines. In fact the development of magnetic extraction systems centered around these larger machines. With the external beams of these larger machines and, later, with the even higher energy external beams of the proton synchrotrons, nucleon-nucleon scattering experiments have been carried out over a wide range of energies. Along with high energy electron scattering experiments on nucleons and with systematics of nuclei, these experiments have led to a fairly good phenomenological picture of some aspects of the nuclear force. For example, by assuming velocity independent nuclear forces, a potential function may be devised to fit the scattering data fairly well. At the same time theories of nuclear forces are making progress in high energy particle physics. For a good review of most of the present knowledge of the two nucleon interaction see Phillips (1959).

With the development of nuclear physics along these two fronts in the past 12 years, an external beam from a smaller machine has become much more desirable. By now, many body calculations are being performed using the phenomenological two-nucleon potentials. (For an introduction to the methods employed see Eden (1959)). However, so far, these calculations have not given the correct values for even the systematics of nuclear density and binding energy (Brueckner 1961). It is a distinct possibility that the assumption of velocity independence of nuclear forces is incorrect. If this is the case, then there is an infinity of velocity dependent potential functions which will fit the two-nucleon scattering data. In principle, this indeterminacy can be reduced by requiring that the velocity dependent potential functions also explain the systematics of nuclei when applied to the many body problem. The systematics of nuclei and the details of nuclear structure, combined with the two nucleon scattering results, are therefore a much more stringent test of theories of nuclear forces than are the two nucleon scattering results alone.

It is therefore of prime interest to obtain such information about nuclei as can be used directly to help formulate and to test many body calculations of nuclear structure. At the moment this type of information appears to be that concerning the nuclear density distribution, nuclear binding energies, momentum distribution of the nucleons (particularly in the nuclear surface), the surface properties of nuclei and the collective motions of the nucleons (Peierls 1960). Much of this information may still be obtained from accurate analyses of decay schemes of radioactive nuclei, but a great deal could also come from investigation of nucleon-nucleus reactions in the medium energy range.

Use of the internal beam of a synchrocyclotron is limited to the production of radioactivities of which the half-life is long enough to permit extraction of the target. This is because the setting up of experimental apparatus around a target inside the machine is inhibited by the high magnetic field, the necessity of preserving the high vacuum, the proximity of the pole tips of the cyclotron, and the proximity of the circulating beam which has not reached the target.

On the other hand, beam extraction from cyclic machines is generally a difficult problem. It was not until 1955 that the first successful magnetic extraction system was obtained for a synchrocyclotron (Crewe and Gregory (1955) at the University of Liverpool). The difficulty arises simply from the radial stability of the particle motion. The stable motion of the particle is a circle and particles only slightly deflected from this circle will curl back into the machine. For a particle to spiral out of the machine its motion has to become radially unstable.

This condition is met if a slight deflection outward from its equilibrium orbit brings the proton into a region where Br is less than the magnetic rigidity of the particle, i.e. where its radius of curvature is greater than its distance from the center of the machine. This implies that $d(Br)/dr$ is negative for r equal to or greater than r_0 the radius of the equilibrium orbit. (Br is the value of the magnetic field of the machine multiplied by the distance of the particles from the center of the machine).

The variation of Br with r in the McGill synchrocyclotron is shown in Figure 9, Chapter 3. If the particles in a cyclotron could be accelerated to a radius where the value of Br is a maximum, them radial instability would naturally occur and the particles would spiral out of the machine. At this radius $d(Br)/dr \simeq 0$ or $n \simeq -(r/B)dB/dr \simeq 1$ and the beam extraction based on this principle is called "beam extraction at $n \simeq 1$". However, in the interior of synchrocyclotrons the value of n is about 0.05 and, unfortunately, as n increases several severe resonances between radial and vertical oscillations occur. To prevent the energy of the radial oscillations from "exploding" the beam vertically, the energy of the radial oscillations must be minimized. This may be accomplished only by extreme azimuthal uniformity of the magnetic field. However, with sufficient care, it is possible to accelerate most of the particles to the radius at which $n \simeq 1$. A very good extraction system based on this principle is used in the 160 cm fixed-frequency cyclotron-synchrocyclotron at the Institute for Nuclear Research at Tokyo (Suwa et. al. 1959).

However with most synchrocyclotrons the protons cannot be accelerated through the resonance which occurs at $n = 0.2$. In the McGill machine it is seen from Figure 9 that the value of n breaks sharply upward from 0.05 at a radius of about 36 inches. It would therefore seem that to obtain maximum extracted proton energy without danger of losing beam at the $n = 0.2$ resonance, the beam should be extracted from this radius. However, protons orbiting at this radius have a magnetic rigidity which is less than Br for any outward deflection less than about 3 inches (See Figure 9). For deflections exceeding 3 inches the protons will spiral naturally out of the machine.

This magnitude of deflection is impractical but if a region of sufficiently reduced magnetic field can be set up in the machine, then the particles need only be deflected into this region for them to spiral out. Such a region will exist inside a magnetic channel with sufficiently thick vertical iron walls. The proton deflection system then need only deflect the protons into this channel.

At first electrostatic deflectors were tried for synchrocyclotrons. Electrostatic deflection is relatively easy for fixed-frequency cyclotrons but for synchrocyclotrons is much more difficult because of the higher particle momentum and the much smaller radial separation between orbits. To achieve electric field deflection in the Berkeley 184 inch synchrocyclotron, a pulsed deflector had to be used (Fremlin and Gooden 1950). For an investigation of an electrostatic deflector for the McGill cyclotron see Hone (1951).

Coulomb scattering by a heavy nucleus such as uranium is a much simpler means of deflecting protons in a synchrocyclotron into a magnetic channel. However, the yield of protons in a reasonable solid angle for a magnetic channel is very low (about 1 part in 10^4 of the internal beam at best). The fact that such systems were considered worthwhile underscores the desirability of an external beam. (For a description of the scattering extraction system of the McGill cyclotron see Kirkaldy (1953)).

The early demand for good external proton beams from the high energy synchrocyclotrons led to the development of a magnetic extraction system that did not require extreme azimuthal uniformity of magnetic field, that did not require the complex circuitry of the pulsed electrostatic deflector, and that was capable of producing a much more intense external beam than the scattering system. This system is based on a deflection of the internal beam by a coherent regenerative build up of the radial oscillations.

The principle of regenerative deflection was first suggested by Tuck and Teng (1950) at the University of Chicago but the development work was carried out by Le Couteur and his co-workers at the University of Liverpool (Le Couteur (1951, 1953,1955), Le Couteur and Lipton (1955) and Crewe and Gregory (1955)). Regenerative extraction systems have been installed in synchrocyclotrons at the University of Liverpool (Crewe and Gregory (1955)), the University of Chicago (Crewe and Kruse (1956)), Harvard University (Calame et. al. (1957)), at Beunos Aires (Mayo et. al. (1958)) and at Orsay (Verster (1959)).

In 1960 it was decided that a magnetic extraction system of the non-linear regenerative type should be installed in the McGill synchrocyclotron. From the performance of systems already in existence, it was felt that about 1% of the internal beam current, or an average beam current of about 10^{-8} ampere, with an energy of a little less than 100 Mev, could be obtained. This beam would be made up of bursts of about 1.5×10^{8} protons in about 20×10^{-6} seconds, with a repetition rate of 400 per second.

CHAPTER 2

THE REGENERATIVE DEFLECTION SYSTEM

The Regenerative Deflection System

A sustained beam of particles in a cyclotron must have orbital stability in both radial and vertical directions. The equilibrium orbits of particles in a cyclotron which has symmetry about the median plane of its pole gap and azimuthal uniformity of magnetic field, are circles in the median plane, concentric with the axis of the machine. The radius r_o of these circles is determined by the momentum of the particles. For stability, particles whose orbits deviate slightly from these circles must undergo oscillations in the vertical direction about the median plane, and in the radial direction about r_o. For circular machines it is customary to express the frequency of these oscillations as a multiple of the orbital frequency of the equilibrium orbit. The frequencies then become dimensionless and particle velocities may be expressed as derivatives with respect to azimuthal angle rather than time.

Reasonably constrained particle motion requires that there be no oscillatory forces on the particle which are sympathetic to the radial or vertical oscillations. These oscillatory forces may be considered to be external (electrical forces from the dee system with a frequency 1), or internal such as resulting from a magnetic coupling of the modes of oscillation. In the case of internal coupling, the radial oscillation generally contains about 50 times as much energy as the vertical oscillation and so if the two become sympathetic (frequencies become related by some small integer), then the energy transferred from the radial motion to the vertical motion will cause the beam to explode vertically.

The condition for radial stability ($n \ll 1$) has already been discussed in the Introduction. For vertical stability n must have a value greater than zero. The existence of a negative field gradient means that the field lines will be curved as shown in the sketch below.

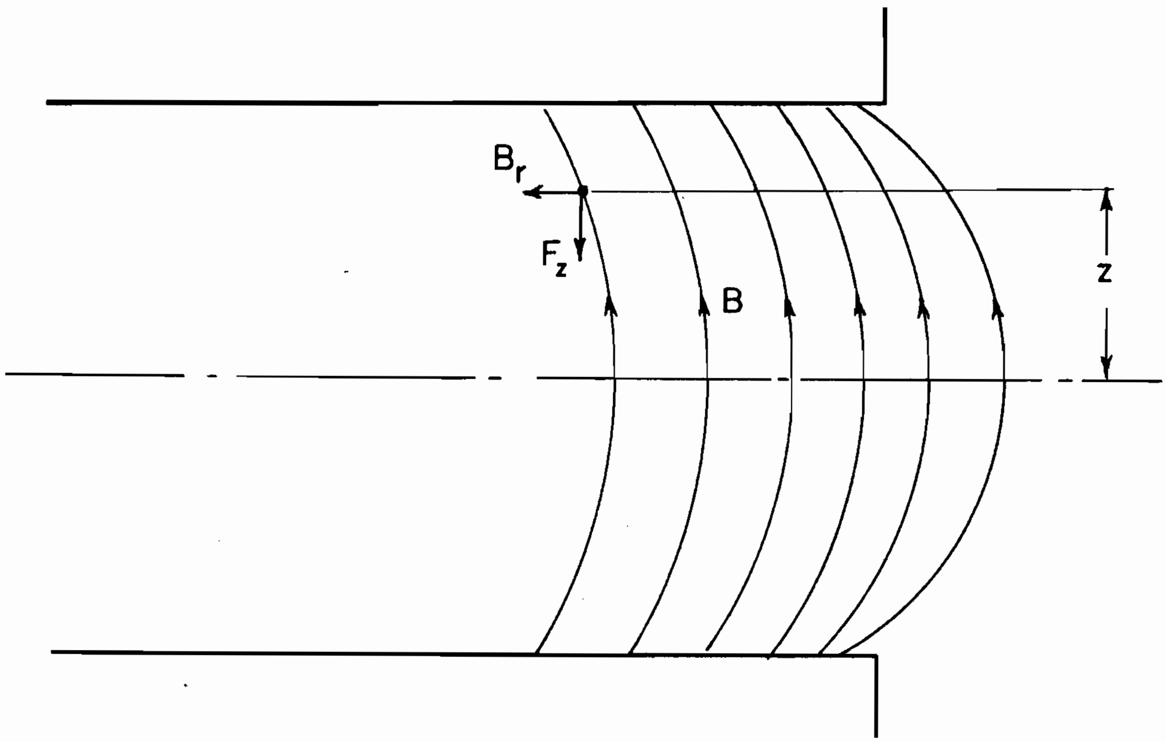

A positively charged particle with displacement z fro the median plane and velocity $r\dot{\theta}$ perpendicular to the plane of the sketch and towards reader will experience a restoring force toward the median plane equal to

$$F_z = er\dot{\theta}B_r \quad .$$

(B_r is negative for positive z and positive for negative z).

To first order, the radial component of magnetic field is given by

$$B_r = \left(\frac{\partial B_r}{\partial z}\right)_o z$$

which, since $\nabla \times B = 0$ becomes

$$B_r = \left(\frac{\partial B_z}{\partial r}\right)_o z$$

where $\left(\frac{\partial B_z}{\partial r}\right)_o$ is the field gradient in the median plane.

The vertical motion of the particle is then described by

$$\frac{d^2z}{dt^2} = \frac{e}{m} r\dot{\theta}\left(\frac{\partial B_z}{\partial r}\right)_o z$$

$$= \dot{\theta}^2 \left(\frac{r}{B}\frac{\partial B}{\partial r}\right)_o z$$

which leads to

$$\frac{d^2z}{d\theta^2} = \left(\frac{r}{B}\frac{\partial B}{\partial r}\right)_o z \equiv -nz$$

The vertical oscillation frequency in units of orbital frequency is then $n^{\frac{1}{2}}$. The more thorough analysis given in Appendix A shows that the radial oscillation frequency is $(1-n)^{\frac{1}{2}}$. A practical value of n is about 0.05. This value should be maintained as evenly as possible out to the fringing field region of the cyclotron, where n increases since the field drops off much more rapidly. As n increases, the first serious resonance between radial and vertical oscillations occurs when the radial frequency is exactly twice the vertical frequency. This is the well known n = 0.2 point where, unless the radial oscillations are very small, the magnetic coupling of the radial oscillations to the vertical oscillations will cause the beam to blow up vertically. The two modes of oscillation are coupled through higher radial derivatives of the magnetic field (see Appendix A).

To understand how a proton may be extracted from a synchrocyclotron before its orbit reaches the n = 0.2 radius it is not necessary to investigate how it got there. Therefore the principle of phase stability and how the proton gets its energy from the dee system will not be discussed here. It is sufficient to realize that the energy of the proton increases with time so that its orbital frequency matches that of the alternating voltage on the dees. The rate of change of the dee frequency of the McGill machine is such that at the maximum radius, the energy gain per orbit is about 7 Kev. Averaged over radial oscillations, the radial increase per orbit is then about 0.0015 inches. This increase is indicated by the dotted line in the sketch below.

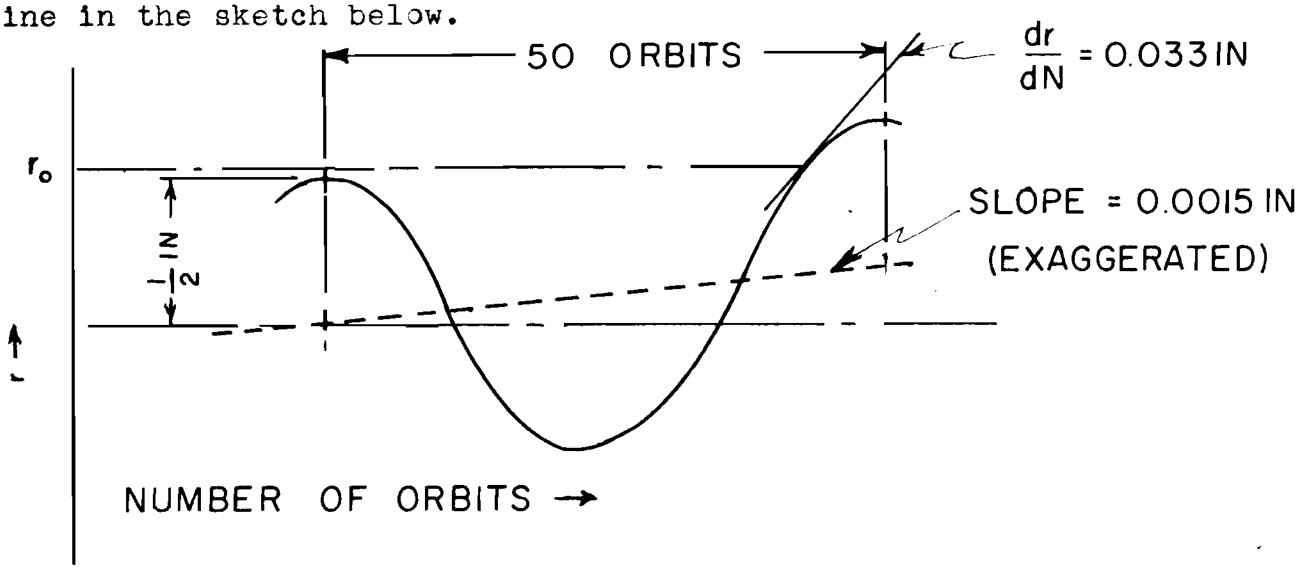

However because of radial oscillations, the radial position of a particle at a given azimuth may change much more than this in one orbit. Consider a particle which has a radial oscillation frequency Ω of 0.98 and amplitude of radial oscillation of 0.5 inch. The precession frequency of its orbit center is $1 - \Omega = 0.02$. Its radial position at a given azimuth, as a function of orbit number is shown in the sketch.

This particular particle will have its maximum possible radial gain per orbit at r_o if it just fell short of r_o on its previous maximum precessional swing. As indicated in the sketch, this radial gain will be approximately 0.033 inches per orbit or about 20 times the radial gain due to the expansion of the orbit from the energy gain.

Even this however is much too small to permit beam extraction by capturing between successive orbits and, of course, particles with radial oscillations of amplitude less than 0.5 inches and different phase of precession will have even smaller radial gain per orbit at r_o. The average gain per orbit for particles reaching r_o for the first time will be of the order of 0.01 inches.

The regenerative deflection of a proton beam is based on a regenerative expansion of the separation between successive orbits. (By regenerative it is meant that the rate of growth of the separation depends on the separation). This is accomplished by introducing segments of field gradient in regions of the machine in such a way as to hold the radial frequency at the orbital frequency. The precessional frequency of the orbit center is now zero and increasing the amplitude of the radial oscillation moves the center of the particle orbit radially outward from the center of the machine.

Energy from the orbital motion can now be transferred sympathetically to the radial motion. This energy increases the amplitude of the radial oscillation. A simple means of acheiving this energy transfer is shown in the sketch below.

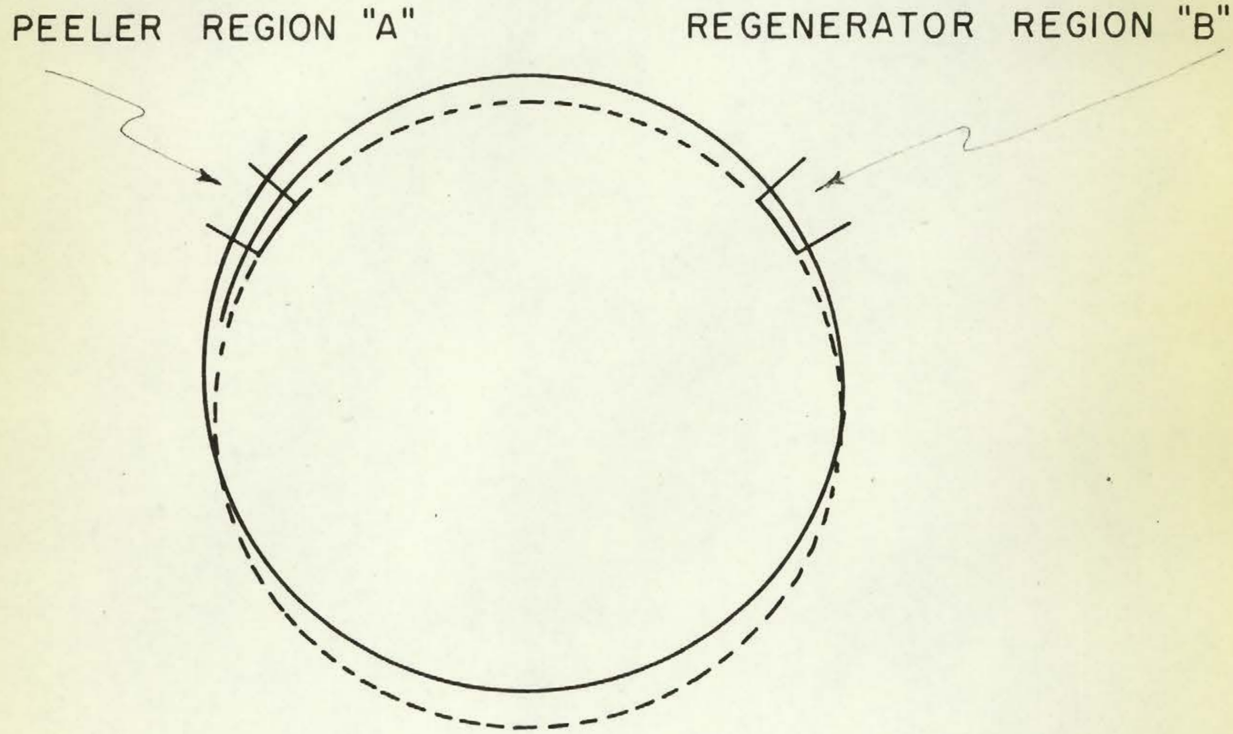

In region A the field is decreasing linearly with radius and in region B it is increasing linearly with radius. When the protons enter the peeler region A for the first time, their paths are straightened slightly so they enter the regenerator region B at some larger radius. The higher field in this region curls them back into the machine but they enter A for the second time with some net radial gain. The field gradients in A and B may be adjusted to satisfy the two conditions of proper phase in the radial motion and necessary radial gain. Careful design can achieve reasonable values of radial gain per orbit while still maintaining vertical stability. This system is called a peeler-regenerator or a linear regenerative deflection system (Le Couteur 1951) and is the type that was installed in the Liverpool 156 inch synchrocyclotron (Crewe and Gregory 1955).

In this linear regenerative system the radial oscillation amplitude increases exponentially. If this increase is continued, the radial separation between orbits becomes sufficient for the particles to enter a magnetic channel. Considering the radius at which the particle first enters the deflection system as r_o, and expressing the radial displacement as $\rho = r - r_o$, the exponential increase in the radial oscillation amplitude may be written as an exponential increase in the maximum value of ρ for the orbits;

$$(\rho_{max})_N = (\rho_{max})_O e^{\lambda N}$$

where $(\rho_{max})_O$ is the value of ρ_{max} for the particle on first entering the system.

The separation between orbits is

$$\Delta \rho_{max} = \lambda (\rho_{max})_O e^{\lambda N}$$

A practical value of e^{λ}, the radial gain factor, is about 1.4. With an initial displacement of the order of 0.01

inches, it would take about 15 orbits to achieve a practical separation of 0.5 inches between orbits.

Constant field gradients in A and B are adequate if the general field gradient of the machine is constant. However the magnetic field in the region n = 0.2 is strongly non-linear. The linear deflection system is thus limited to inner radii where the protons have not reached the full energy that the synchrocyclotron is capable of giving them. However Le Couteur (1955) showed that a practical non-linear system was possible. In fact he showed that, by making effective use of the field gradients in the fringing region of the cyclotron, no peeler would be necessary.

Without the peeler to help in the initial displacement of the beam in the first few orbits in the deflector, the initial gain factor is small (about 1.05). The number of orbits required for sufficient displacement for extraction is then about 50, of which about 30 occur in the first 0.1 inches of displacement.

Either regenerative deflection system has the advantage of good energy selection. Particles of lower energy which reach the deflection system early because of large radial oscillations have too low a magnetic rigidity to be deflected and will be left to orbit until they reach the required momentum. Consequently, the energy and the time distribution of the deflected particles is much sharper than the energy and time distribution of the particles which are intercepted by a target inside the the machine. This effect was easily seen experimentally as is described in Chapter 5.

An extraction system based on non-linear regenerative deflection has been installed in the McGill synchrocyclotron. The design requirements for the deflection system are calculated in Appendix A. Since the field decrease in the fringing region of the McGill machine is slightly different from what appears to be the pattern for most other synchrocyclotrons, the original development of Le Couteur had to be reworked to obtain a suitable regenerator design. For this purpose an accurate map of the magnetic field of the cyclotron for radii greater than the radius for $n = 0.2$, was required.

CHAPTER 3

PRELIMINARY FIELD MAP

Preliminary Field Map

To calculate the design requirements for the magnetic field of the regenerator of the extraction system, it is necessary to have an accurate map of the cyclotron magnetic field at the outer radii of the machine. Therefore the initial part of the extraction project involved the setting up and calibration of accurate magnetic measuring gear.

The magnetic field sensing element was a Hall Generator FC34 manufactured by Siemens. This element is InSb encased in ceramic and having overall dimensions 22mm x 12mm x 1.5mm. The control current perpendicular to the magnetic field was set at 200ma regulated to better than 0.1%. The Hall voltage, which appears across the element perpendicular to the field and to the control current direction, can be measured with a potentiometer to give a measuring sensitivity of about 30×10^{-6} volt/gauss. A thermistor controlled heater was used to hold temperature variations to $\pm$ 0.1^{o} centigrade corresponding to a Hall voltage variation of about $\pm$ 0.02%.

The circuit diagram for the magnetic field probe and control circuits is shown in Figure 2. The parts enclosed by the dotted lines are encased in aluminum with outside dimensions of 35mm x 20mm x 8mm. About 12 feet of instrument leads connect the probe to a terminal board on which are mounted the shunting resistors. The Hall current shunting resistors are used so that the Hall voltage is a more linear function of magnetic field. Any length of 8 conductor cable may be used between the terminal board and the potentiometer and recording instruments.

The probe was calibrated by nuclear magnetic resonance in hydrogen. The highly uniform magnetic field necessary for nuclear magnetic resonance was generated by a 4 inch electro-magnet. The field gradients were measured directly by swinging a small coil through the pole gap on a rotating arm. The signals from this coil were detected through mercury contacts to the rotating arm and displayed on an oscilloscope. In this way non-uniformities in the magnetic field could be easily detected and corrected. Typical oscilloscope traces are shown in Figure 1. The highest uniform field obtained in the magnet was 15,000 gauss.

To detect the resonance, the marginal oscillator of Cowen and Tantilla (1958) was used with a 0.5 cm^3 sample of H_2O doped with Manganese Sulfate. The frequency at which nuclear magnetic resonance occured was set up on a General Radio Standard Frequency Generator by beating with the marginal oscillator on an oscilloscope display. Simultaneously, the frequency of the generator was measured by a quartz crystal controlled electronic counter (Hewlett Packard Model No. 524B). The resulting calibration curve of the Hall probe is shown in Figure 3. This curve is the result of a mean square deviation "Forsythe" fitting of a third order polynomial to the calibration points.

Plate 1 and Plate 2 show the layout of the calibration gear (excluding the electronic counter) and the Hall probe control and measuring circuitry. Plate 3 shows the mount which was employed for the nuclear magnetic resonance probe and the Hall probe so that the position of the two could be easily interchanged.

PLATE 1

4 INCH ELECTROMAGNET AND NUCLEAR MAGNETIC RESONANCE PROBE

Photograph shows 4 inch electromagnet, nuclear magnetic resonance detector and mechanism for detecting field gradients in the electromagnet. The control panel in the lower center of the photograph is for a set of current shims to correct for field gradients.

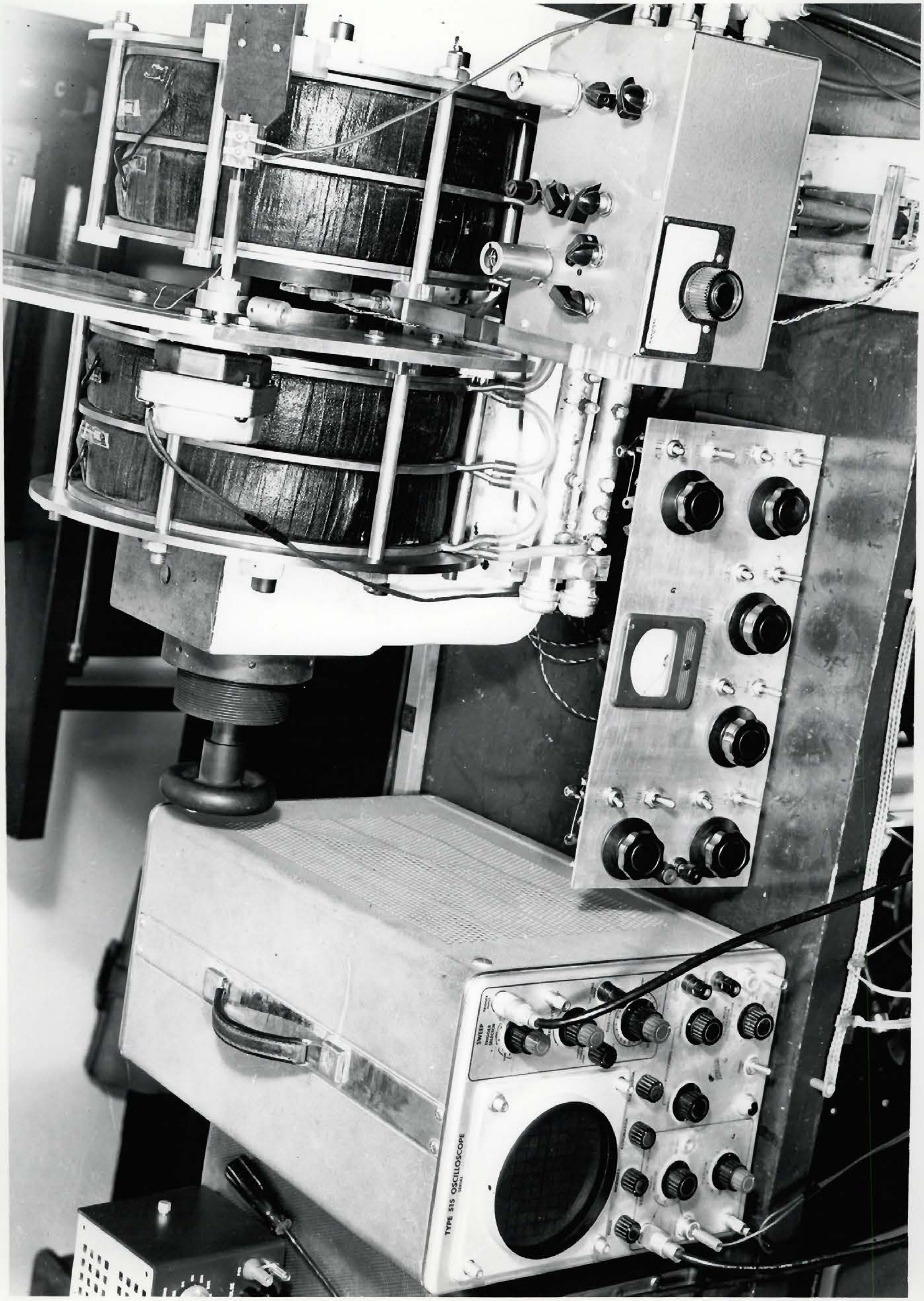
SWEEP
TYPE 515 OSCILLOSCOPE

PLATE 2

HALL PROBE MEASURING CIRCUIT

Photograph includes (left to right) temperature recorder-regulator, current supply, audio generator of nuclear magnetic resonance detector, current regulator for 4 inch electromagnet, Hall control current recorder, potentiometer and Hall voltage recorder.

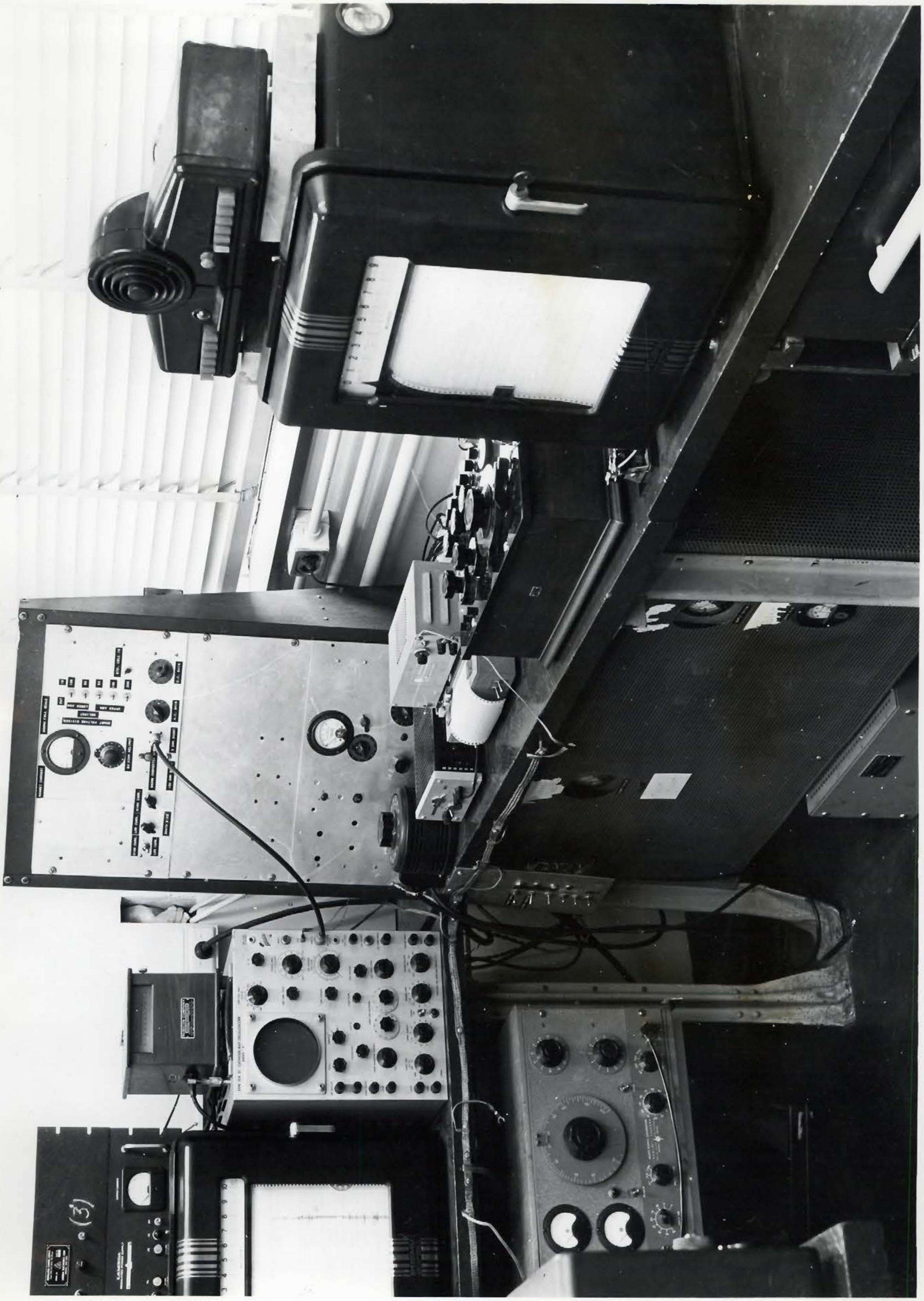

PLATE 3

MOUNT FOR HALL PROBE AND NUCLEAR MAGNETIC RESONANCE PROBE

Photograph shows the probes ready to be inserted into the $\frac{1}{2}$ inch gap of the 4 inch electromagnet.

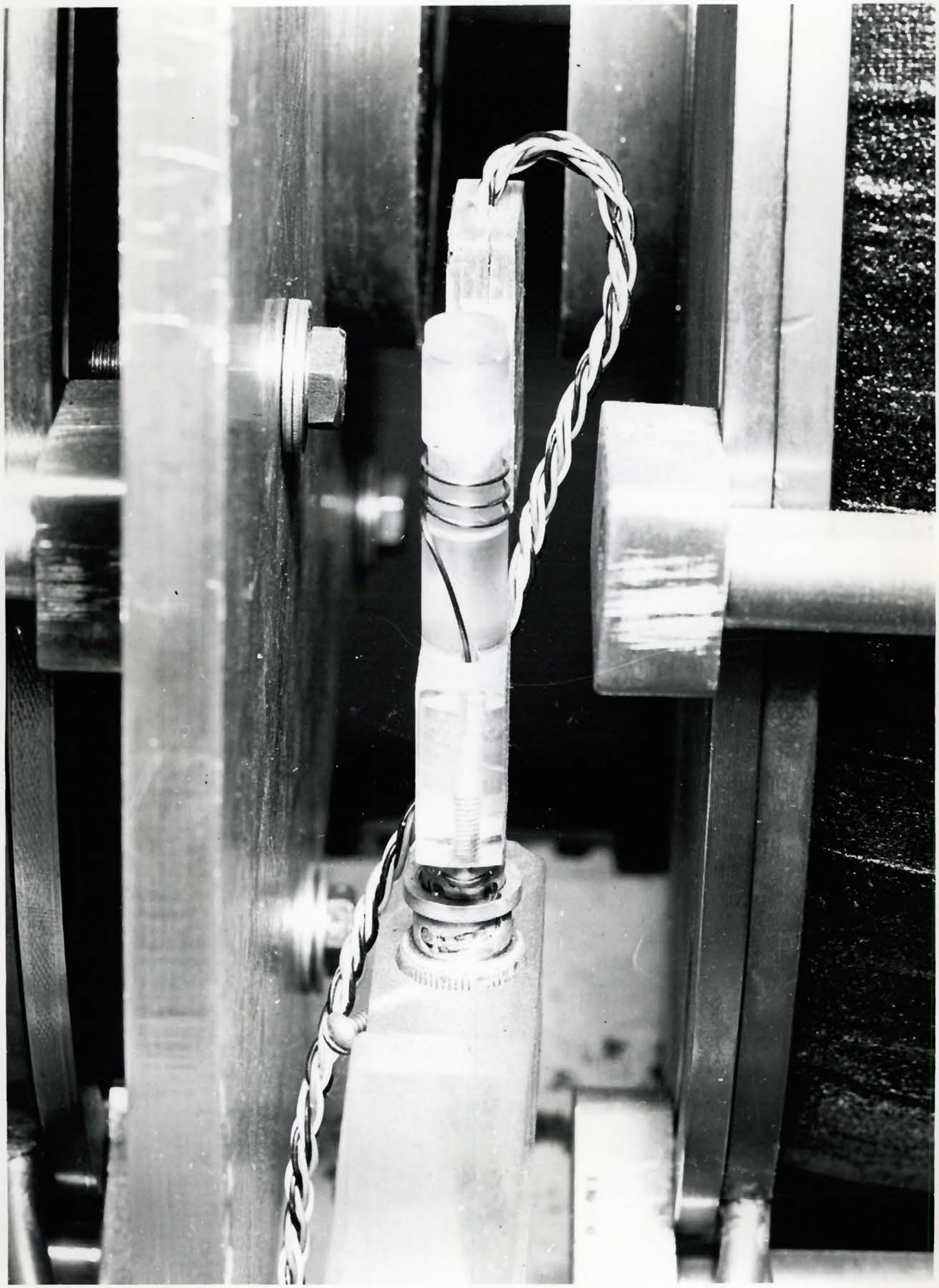

FIGURE 1

FIELD DERIVATIVES IN TEST MAGNET

These oscilloscope traces were obtained from a coil sweeping through the field region on an arm 10 inches long. The complete pulse shape is of the form shown in the picture on the left. Sweeps through the 4 inch magnet are shown in the other two pictures. The effect of pole tip saturation at high fields is clearly shown in the middle picture where the gradients are considerably greater than in the picture on the right. 15,000 gauss was the highest field at which nuclear magnetic resonance could be obtained.

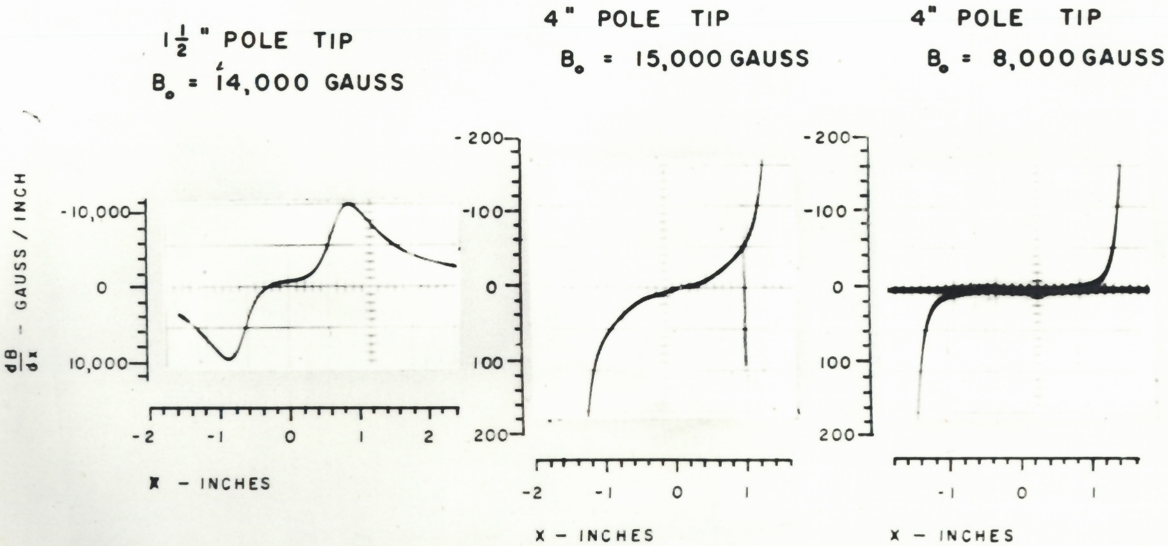

FIG. 1 - FIELD DERIVATIVES IN TEST MAGNET

FIGURE 2

MAGNETIC FIELD PROBE CIRCUIT

The circuit elements within the dotted lines are encased in an aluminum capsule 35mm x 20mm x 8mm. The exterior shunting resistors are mounted on the terminal board which is separated from the field probe by 12 feet of instrument lead wire. Any length of cable may be used to connect this terminal board to the measuring and control apparatus. Only eight conductors of the indicated nine conductor cable are used.

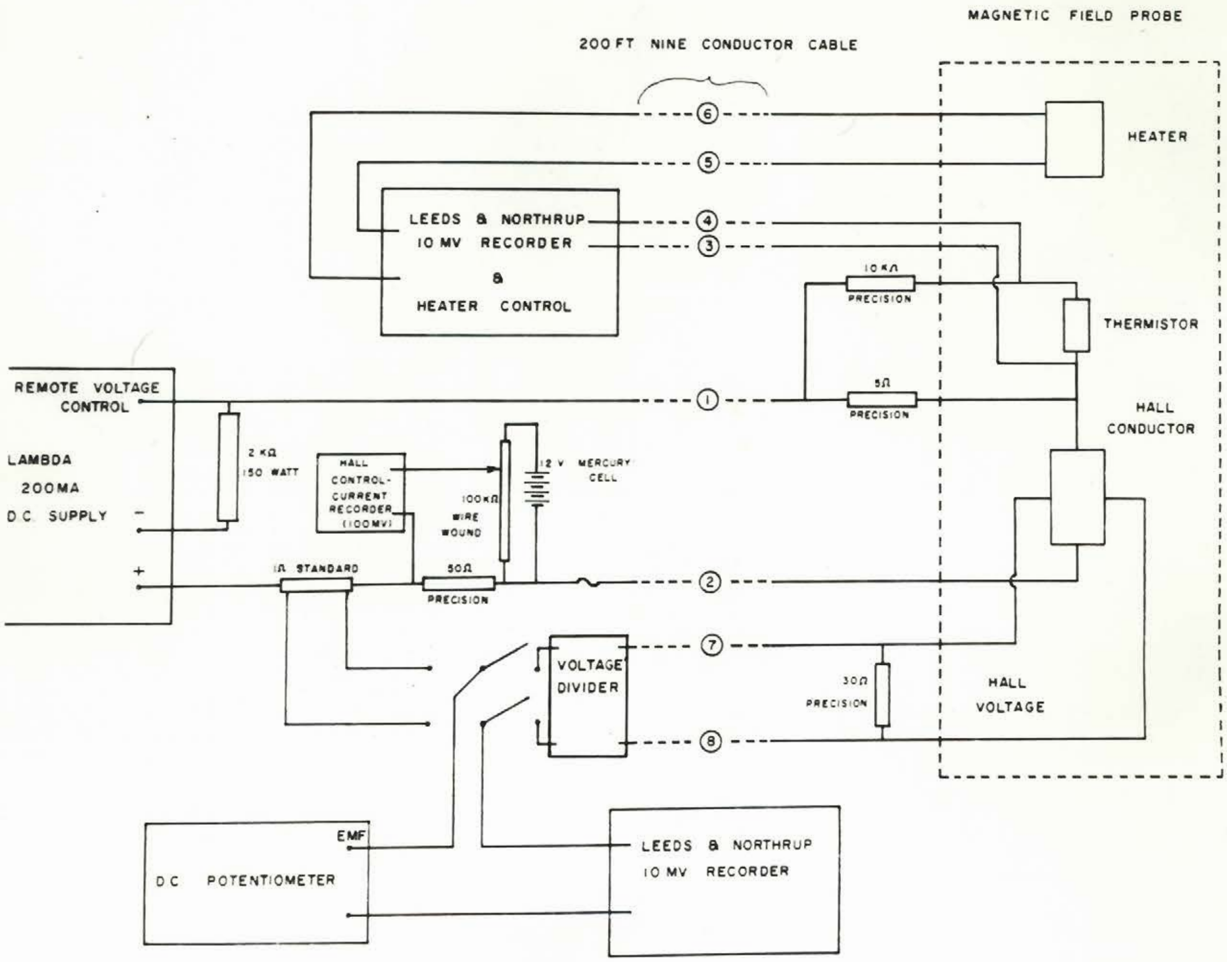

FIG. 2 - MAGNETIC FIELD PROBE CIRCUIT

FIGURE 3

MAGNETIC FIELD PROBE CALIBRATION CURVE

This calibration curve was obtained by nuclear magnetic resonance (see text). Frequencies of the nuclear magnetic resonance were measured with a Hewlett Packard Electronic Counter model 524B (a frequency counter based on a quartz oscillator). The curve is a Forsythe fitting of a third order polynomial to the calibration points and the dotted region is an extrapolation beyond the range of measurement.

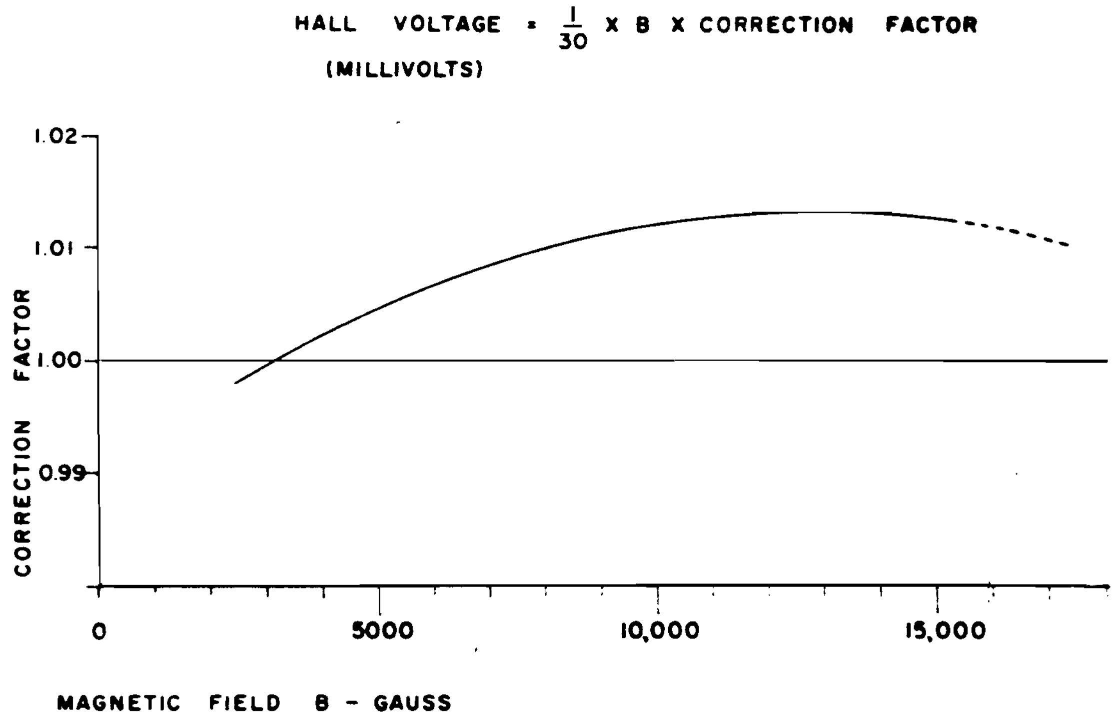

FIG. 3 - MAGNETIC FIELD PROBE CALIBRATION CURVE

For the field map of the cyclotron, the Hall probe was mounted on a rotating arm which was driven by a synchronous motor through a gear chain. The mechanism was designed to operate in the cyclotron pole gap without requiring the removal of the live dee. It was necessary to remove the dummy dee but this was a comparatively simple matter.

Balancing most of the probe output with a potentiometer and feeding the difference into a 10 mv chart recorder gave a continuous map of field versus azimuthal angle at a fixed radius. Degree marker pulses produced through contacts on the drive mechanism of the rotating arm could be fed into the recorder as well. This safe-guarded against slippage but proved to be unnecessary. A typical field map (with marker pulses at 0° and 180°) is shown in Figure 4. The small variations of about 0.1 mv which are apparent in the flat region at 180° show the effect of heating cycles in the temperature control.

Although for the extraction problem it was only necessary to have a field map at outer radii, a more or less complete field map was carried out. It was hoped that such a map might show some reason for the known loss of internal beam current at various radii. Indeed some correlations were found. For example it was found that fractions of the internal beam were lost in regions where the average value of the negative field gradient was diminished. Also it was found that at reduced cyclotron magnet currents the protons did not reach the orbit radius at which $n = 0.2$ (about $36\frac{1}{2}$ inches) because of a positive field gradient at 35 inches. This positive gradient exists

FIGURE 4

TYPICAL FIELD MAP

This map was taken with a cyclotron magnet current of 620 amperes (control console meter). The sweep time was 4 minutes per revolution and the sweep started at about - 20°. The heating cycles have a period of about one minute and cause an error amplitude at peak temperature deviation of about 3 gauss. The reason for the magnetic field anomaly of about 100 gauss at 0° is not clear.

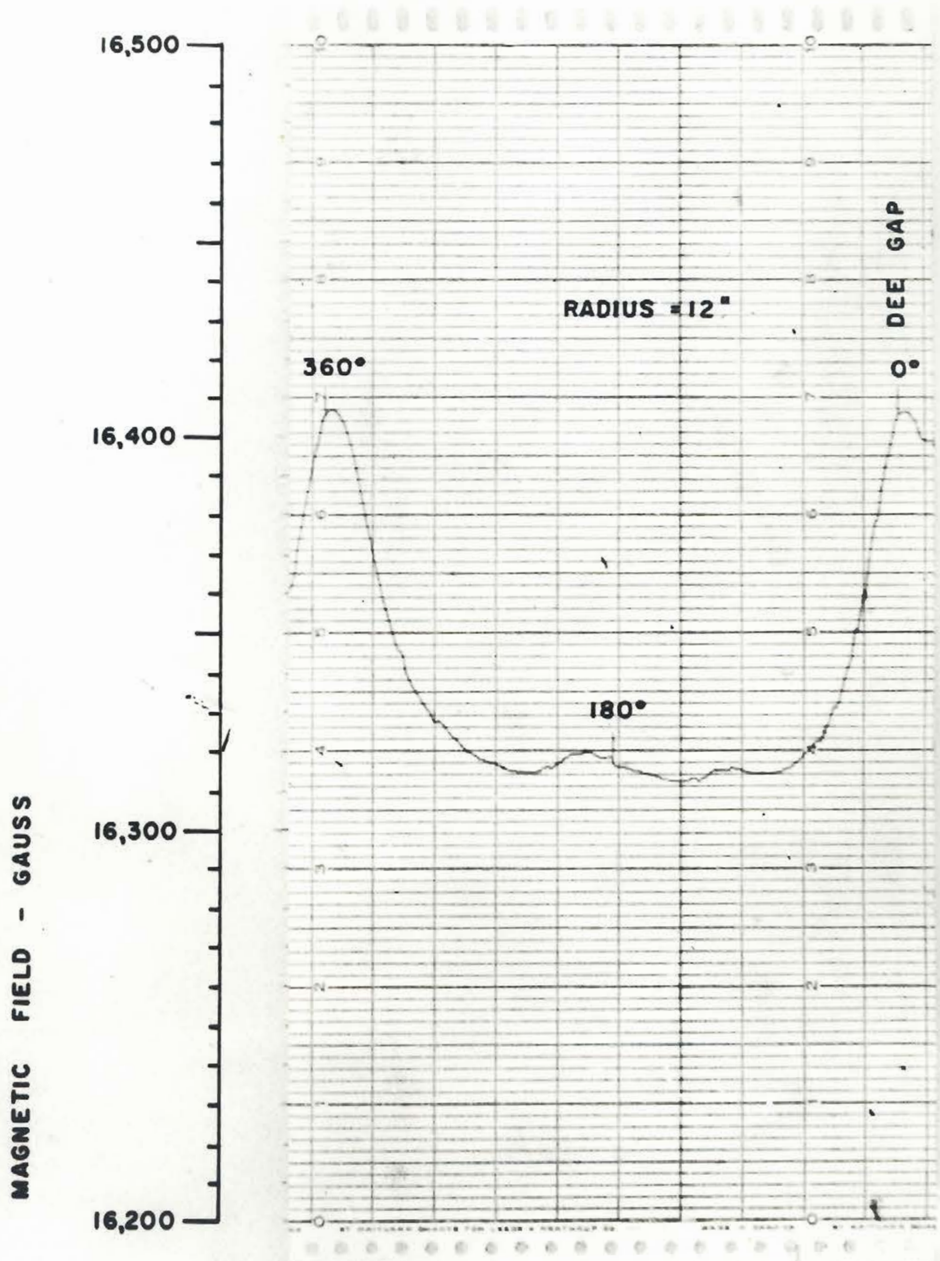

3. — TYPICAL FIELD MAP

at reduced magnet currents because the ring shim (shown in Figure 5) could only be designed for one particular field value due to its saturated condition. For the production of an external beam the magnet current was set at 675 amperes (control console meter) as this gave what appeared to be the best field gradient out to a radius of $36\frac{1}{2}$ inches.

The output Hall voltage was read from the chart record and processed in the IBM 650 computer at McGill to give the corresponding magnetic fields. This involved applying the calibration curve with necessary temperature corrections and taking into account any deviation in control current from 200 ma. The magnetic field values obtained were plotted on the contour map shown in Figure 6 and were used to calculate the field azimuthal average plotted in Figure 7 and the asymmetries plotted in Figure 8. (A complete circular map beyond 38 inches was impossible because of the live dee and the then existing magnetic channel for the scattering extraction system and so the "azimuthal average" for radii beyond 37 inches was obtained by a sample of 4 azimuths in the open side of the cyclotron). Various parameters depending on the average magnetic field are shown as a function of radius in Figure 9.

It is seen from Figure 9 that n is fairly constant up to r = 36 inches but increases rapidly with further increase in radius. It was considered then, that r = 36 inches would be a good radius from which to attempt the extraction. In regenerator design calculations then, r = 36 inches was considered to be r_o, the radius of the last stable orbit before extraction. In these calculations it is necessary to know the effective values of dB/dr, d^2B/dr^2, and higher

FIGURE 5

GEOMETRY OF EDGE OF POLE TIP

Shown is a vertical section through the outer region of the cyclotron pole gap. No attempt is made to show the circular geometry. The ring shim of outer radius $38\frac{1}{2}$ inches is designed so that the useful region of the machine is extended out to about 36 inches for the maximum design field of the cyclotron.

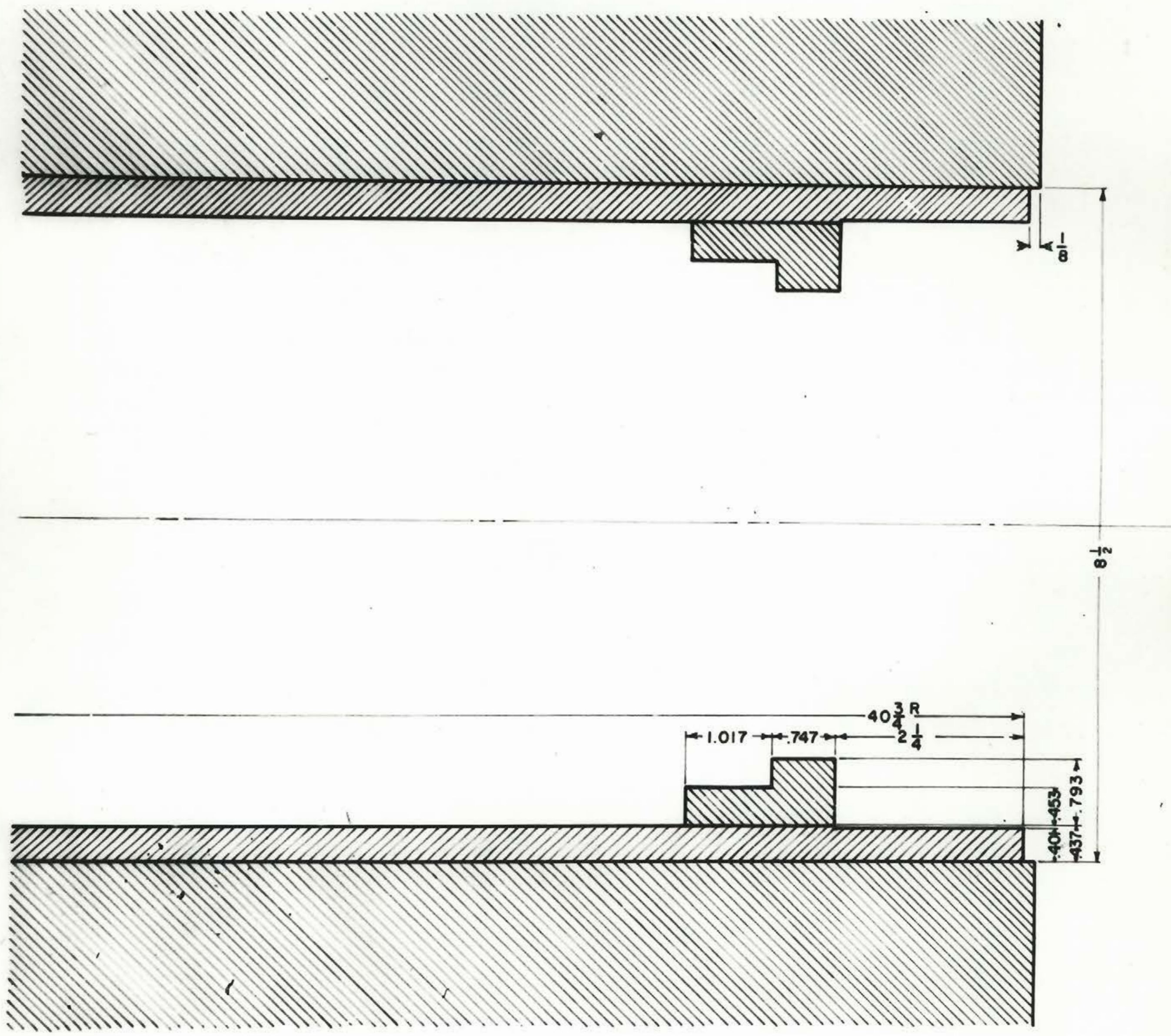

- GEOMETRY OF EDGE OF POLE TIP

FIGURE 6

CONTOUR MAP OF CYCLOTRON MAGNETIC FIELD

This map was obtained with a cyclotron magnet current of 670 amperes (control console meter). The anomaly at 0^{o}, at a radius from about 5 inches to about 20 inches, still exists at this magnet current but is not as pronounced as for a current of 620 amperes. The anomalies at the outer radii at about 60^{o} to the dee gap are due to the magnetic channel of the uranium scatterer extraction system which was not removed for this mapping.

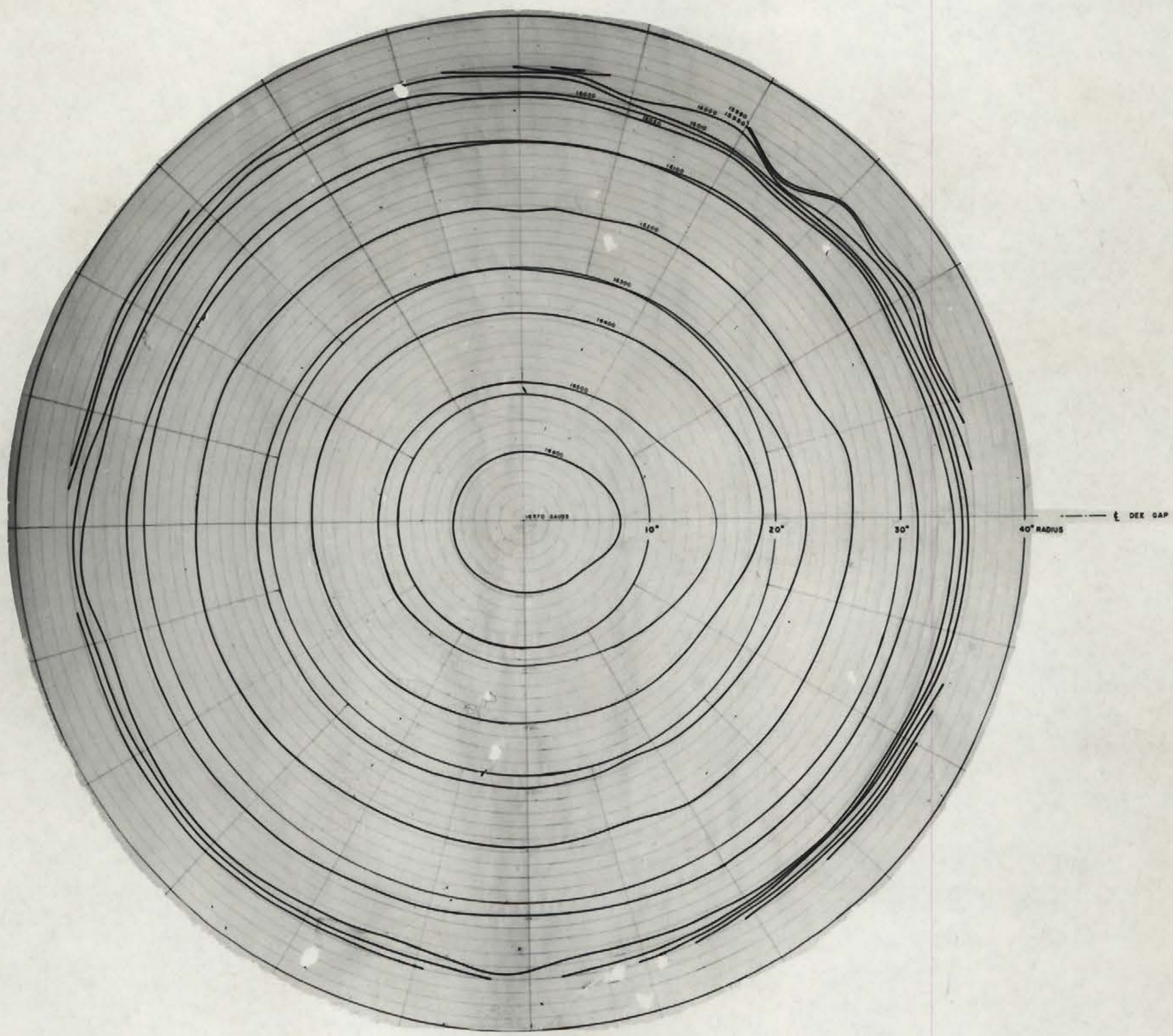

FIG. 6 - CONTOUR MAP OF CYCLOTRON MAGNETIC FIELD

FIGURE 7

CYCLOTRON MAGNETIC FIELD (AZIMUTHAL AVERAGE)

This field average was obtained with a cyclotron magnet current of 670 amperes (control console meter).

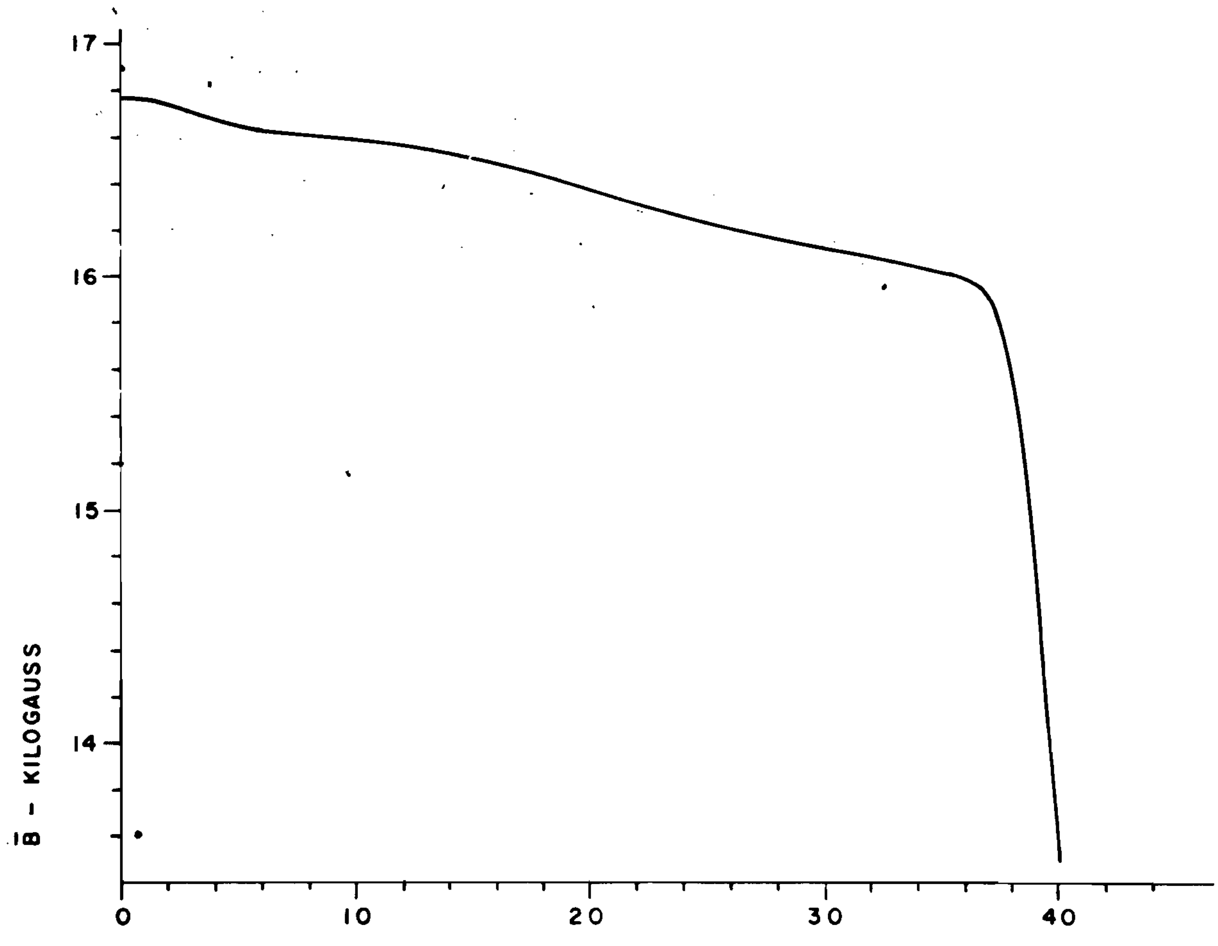

FIG 7 - CYCLOTRON MAGNETIC FIELD (AZIMUTHAL AVERAGE)

FIGURE 8

PLOT OF CYCLOTRON MAGNETIC FIELD ASYMMETRIES

These plots indicate the extent to which the cyclotron field is not azimuthally uniform when the magnet current is 670 amperes (control console meter). The large values of A_1 and A_2 in the region r $\simeq$ 5 inches to 20 inches, are due to the anomaly in the magnetic field south of the center of the machine along the dee gap (0°). Small values of A_1 and A_2 are necessary if the radial oscillations are to be kept small, but the radial gradient of the average field is much more important with regard to beam losses in the synchrocyclotron.

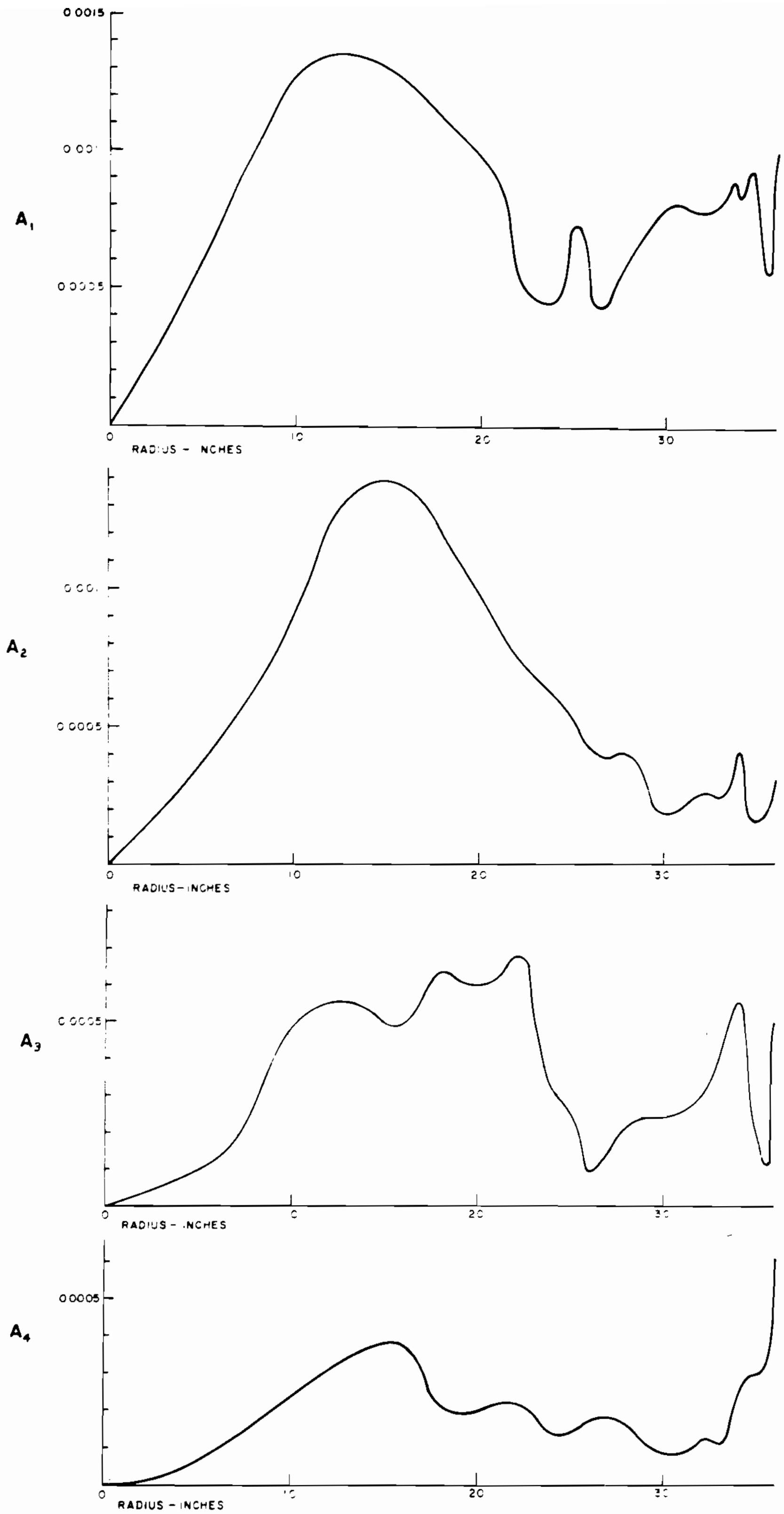

FIG 8 - PLOT OF CYCLOTRON MAGNETIC FIELD ASYMMETRIES

$$\left(B(\theta) = \bar{B}(1 + A_1 \sin(\theta + \phi_1) + A_2 \sin(2\theta + \phi_2) + \dots)\right)$$

FIGURE 9

CYCLOTRON FIELD PARAMETERS

The parameters shown here are derived from the curve of the azimuthal average of the cyclotron magnetic field.

In synchrocyclotrons, acceleration of protons is difficult beyond $n = 0.2$ where n is defined as $-(r/B)dB/dr$ (see text). The protons are therefore extracted from the region where n begins to increase ($r = 36$ inches). At this radius the protons have $Br = 575$ kilogauss-inches and energy 97 Mev. It may be noted that the magnetic field has the value $Br = 575$ kilogauss-inches at $r = 39$ inches also. Without a magnetic channel, protons would therefore have to be deflected beyond this radius to spiral out of the machine.

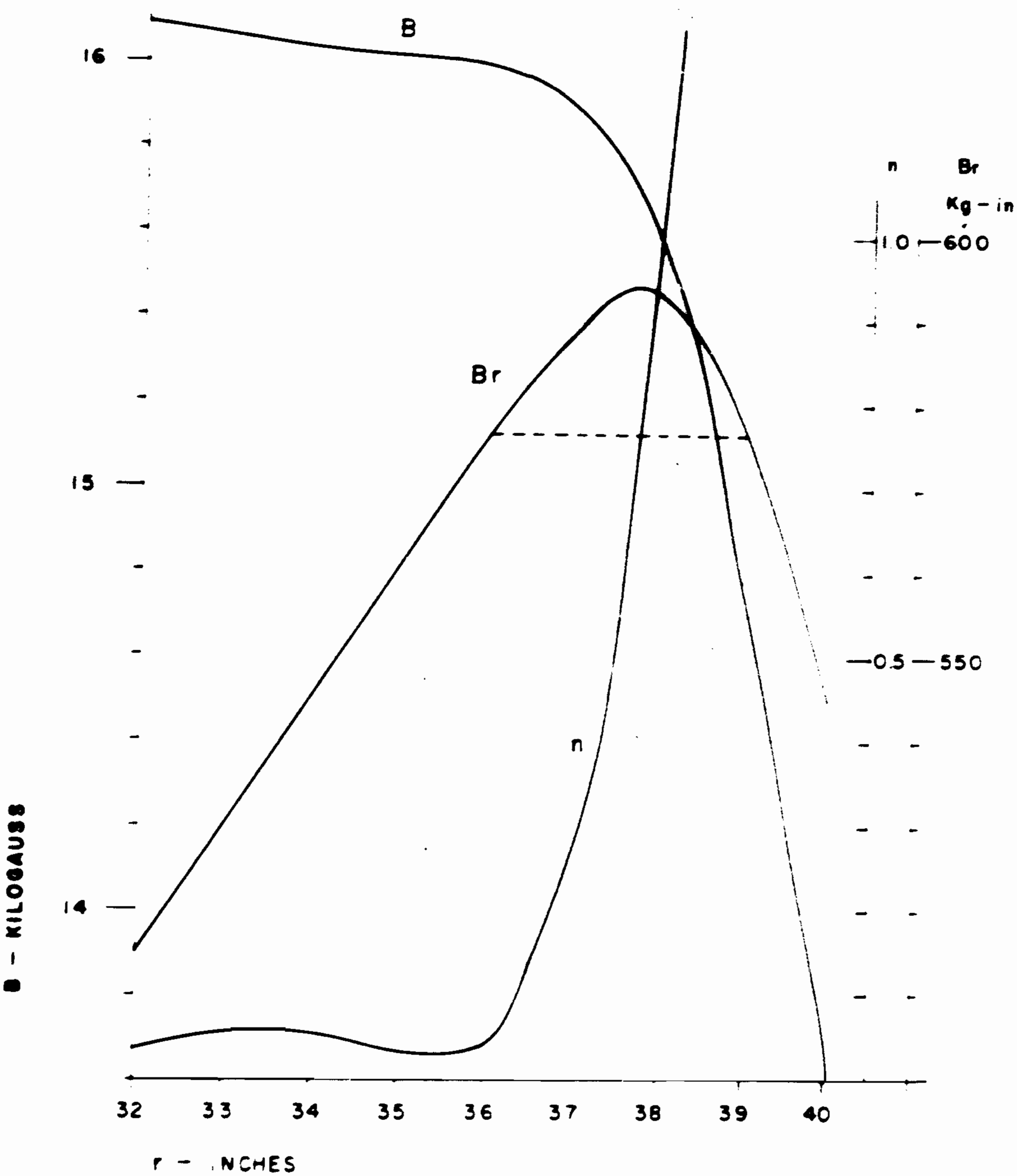

FIG 9 - CYCLOTRON FIELD PARAMETERS

derivatives at r_o. In the approximation of the calculation of Appendix A, dB/dr is considered to take a sharp break at $r = r_o$. The second derivative d^2B/dr^2 and higher derivatives are therefore double valued at $r = r_o$; zero when r_o is approached from smaller radii but non-zero when r_o is approached from larger radii. What are required here are the values when r_o is approached from larger radii.

The values of these derivatives are obtained by a mean square deviation fit of a polynomial in $\rho = r-r_o$ to the measured values of average field in the region $0 \leq \rho \leq 2$ inches. Writing

$$B = B_o + a\rho + b\rho^2 + c\rho^3 + - - - \quad ,$$

it was found that an adequate numerical fit was obtained by including terms only up to third order. The resulting coefficients were; a = -0.024 Kilogauss/inch, b = -0.054 Kilogauss/inch^2, and c = -0.016 Kilogauss/inch^3. The values of the necessary derivatives may be obtained by considering the polynomial as a Taylor's expansion of B about $r = r_o$. Then $a = dB/dr$, $b = 1/2\ d^2B/dr^2$, and $c = 1/6\ d^3B/dr^3$. The resulting values of the derivatives are used in Appendix A to calculate the design reguirements of the regenerative deflector.

The reasons for the strange system of units (Kilogauss-inch) are historical. The diameter of the machine has always been expressed in inches and the magnetic field in kilogauss. The author apologizes for not having the courage to introduce a more logical system.

CHAPTER 4

REGENERATOR DESIGN AND INSTALLATION

Regenerator Design and Installation

The regenerator strength at a radius r in the machine is defined in Appendix A as

$$S_r \equiv \frac{r_o}{B_o} \int_{regen} \Delta B(r,\theta)\, d\theta$$

The field increment $\Delta B(r,\theta)$ is integrated over the whole azimuthal region whose field intensity is affected by the presence of the regenerator. As indicated in Chapter 2, the problem in designing a regenerative deflection system is to obtain a regenerator strength that will increase the radial oscillation and at the same time preserve the proper phase of the radial oscillation to keep the motion of the orbit center outwards toward the extraction channel.

Since the orbiting protons are to be undisturbed by the regenerative deflector until they reach r_o, the regenerator strength at $r = r_o$ must be zero. The regenerator strength as a function of r may then be written as a polynomial in ρ ;

$$S_r = A\rho + B\rho^2 + C\rho^3 + - - -$$

For facility in design, the regenerator strength is assumed to have at most a quadratic dependence. The parameters A and B are then adjusted until the proper regenerative deflection can be obtained. Optimum values of A and B were calculated from Appendix A to be about A = 0.2 and B = 0.4 (for r and ρ measured in inches, θ in radians).

The method used to calculate the field intensity in the vicinity of iron blocks placed in the cyclotron pole gap is described in Appendix B. Calculations indicated that two blocks $1\frac{1}{2}$ inches x $1\frac{1}{2}$ inches x 8 inches placed symmetrically above and below the median plane of the cyclotron and separated by $2\frac{1}{4}$ inches, should give a regenerator strength characterized by the above values of A and B and negligible values for the coefficients of higher order terms.

A non-magnetic stainless steel open jaw frame holding soft iron blocks of this geometry was designed, built and installed in the cyclotron gap. For convenience in any adjustment of the regenerator strength that might prove necessary, the blocks were made up of 1/8 inch plates.

To check the calculated regenerator strength, the magnetic field in the regenerator was measured with the measuring gear described in Chapter 3. A typical scan of the region in the regenerator is shown in Figure 10. The integrated field defect $\int \Delta B d\theta$ is shown as a function of r in Figure 11. A second order polynomial adequate to describe the curve of measured integrated field defect has values of A = 0.2 and B = 0.43. These compared well with the design values of A = 0.2 and B = 0.4 but in any case they were tested for proper regenerative effect by the calculations of Appendix A. The results indicated that the vertical expansion of the beam should not become critical until ρ = 2 inches and that the radial separation between orbits would be adequate for entrance into a magnetic channel before this deflection was reached.

The field reduction in the area adjacent to the regenerator is partly due to the geometry of the iron blocks but mostly to the saturation of the cyclotron pole tips in their vicinity. To restore the average field at inner radii

FIGURE 10

TYPICAL REGENERATOR FIELD MAP

This map was carried out with a sweep time of 16 minutes per revolution or 2 2/3 seconds per degree .

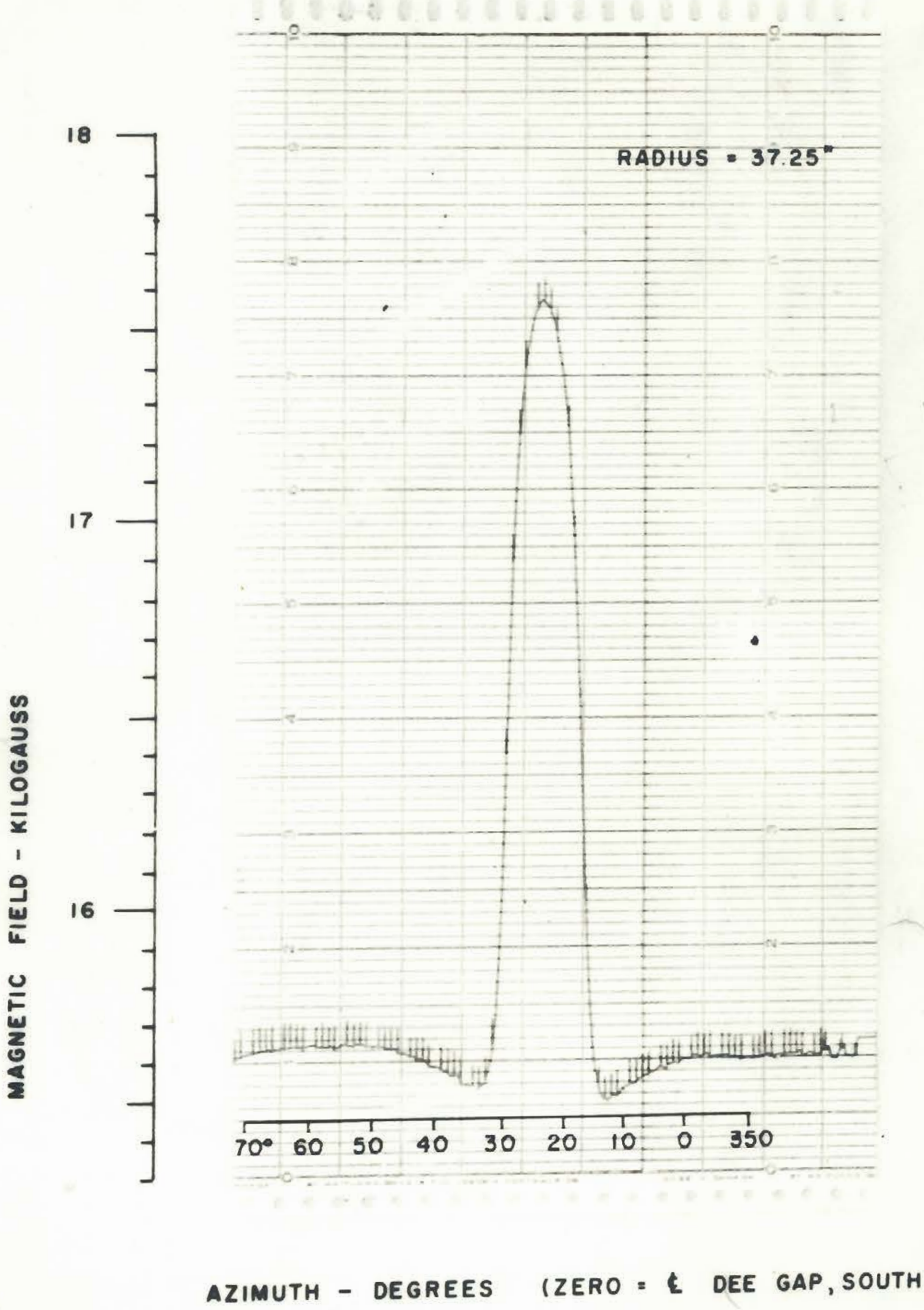

FIG. 10- TYPICAL REGENERATOR FIELD MAP

FIGURE 11

REGENERATOR FIELD DEFECT

The field defect is defined as $\int \Delta B d\theta$ where $\Delta B = \Delta B(r,\theta)$ is the field change introduced by the regenerator and the integration at r is carried out over the region in θ where ΔB is considered significant.

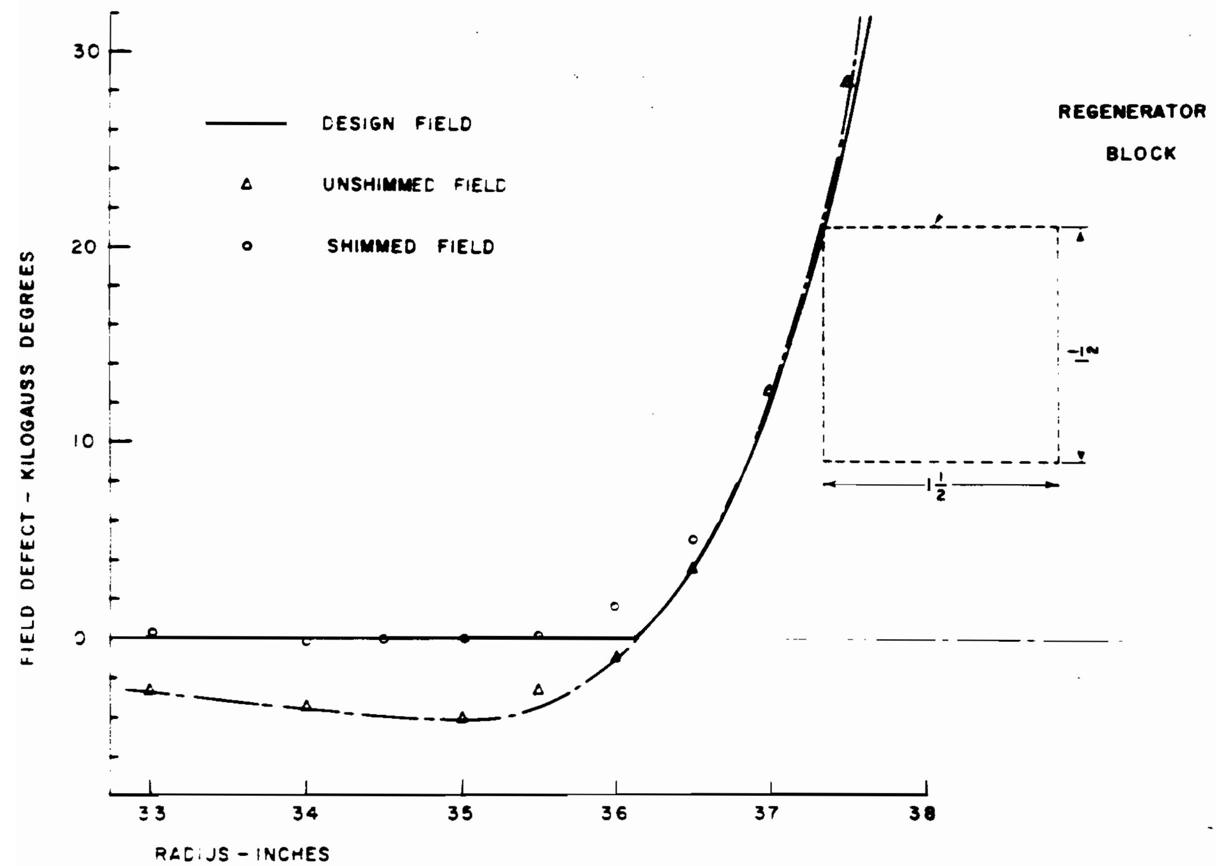

FIG II - REGENERATOR FIELD DEFECT

to its original value, thin vertical shims tangential to the orbits were placed above and below the median plane at various radii. Typically these shims were about 1/32 to 1/64 inch thick and the vertical gap between matching sets of shims was about $2\frac{1}{2}$ inches. The magnetic iron used throughout was Armco Magnetic Ingot Iron.

The vertical shims were mounted on racks attached to the regenerator frame. Details of the regenerator frame and shim mount are given in Figure 12 and a photograph of the regenerator ready for installation is shown in Plate 4. The regenerator installation is shown in Plate 5. It may be seen that the radial position of the whole array of regenerator blocks and vertical shims can be adjusted from outside the cyclotron vacuum tank. The motion is accomplished by a micrometer screw connected to the stainless steel regenerator frame. One complete revolution of the graduated barrel gives a radial motion of 0.1 inch. The regenerator frame is spaced away from the pole tips of the cyclotron by aluminum plates held against the pole tips by jacks. The radial motion of the frame is guided by a groove in the bottom of the frame which rides over a cylinder attached to the bottom aluminum plate. The groove is visible in the photographs.

When the field defect in the interior of the machine was sufficiently corrected by shimming, the system was tested for regenerative deflection of the cyclotron beam. The variation of beam intensity with radius at the best position of the regenerator is shown in Figure 13. The intensity was

FIGURE 12

DETAIL OF REGENERATOR

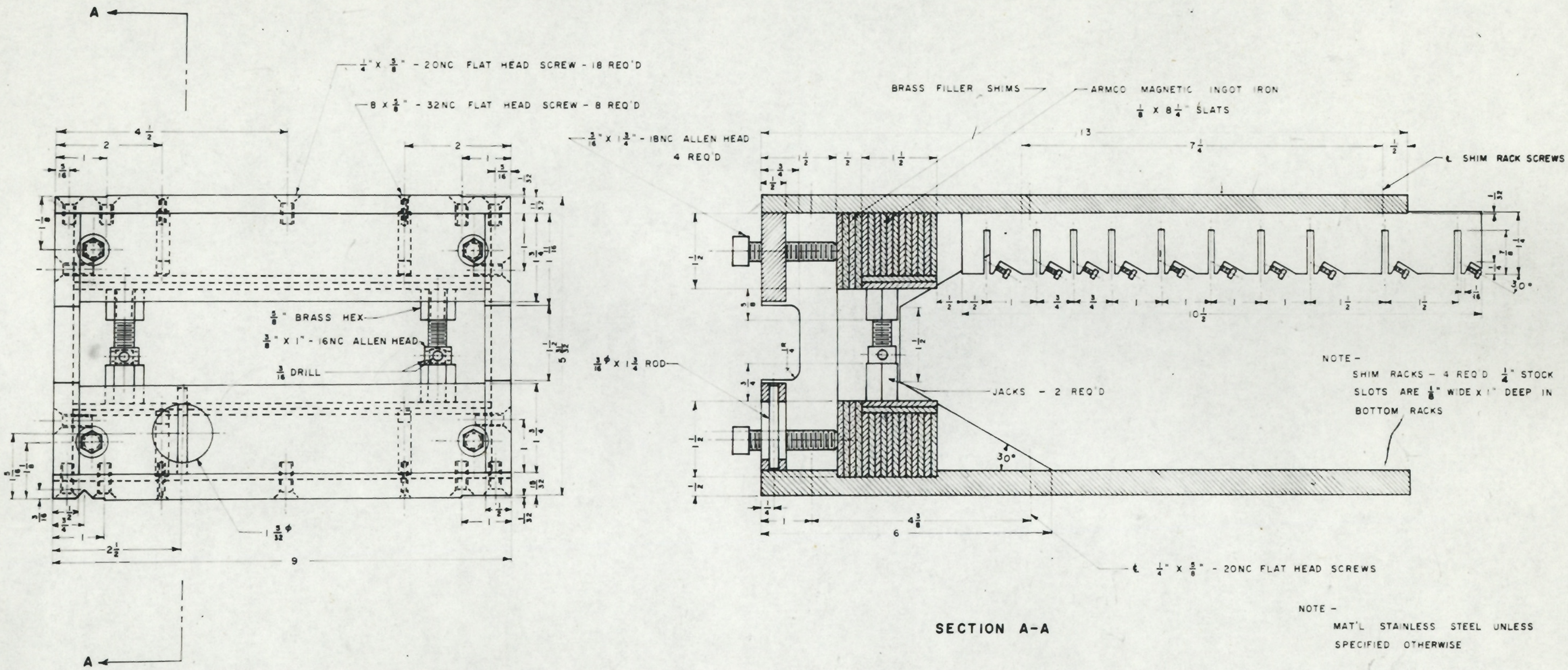

SECTION A-A

MCGILL UNIVERSITY **RADIATION LABORATORY**	
DETAIL OF REGENERATOR	
SCALE - FULL SIZE	DATE - AUG. 15, 1961 DR'WN BY -

PLATE 4

REGENERATOR FRAME WITH BLOCKS & SHIMS IN POSITION

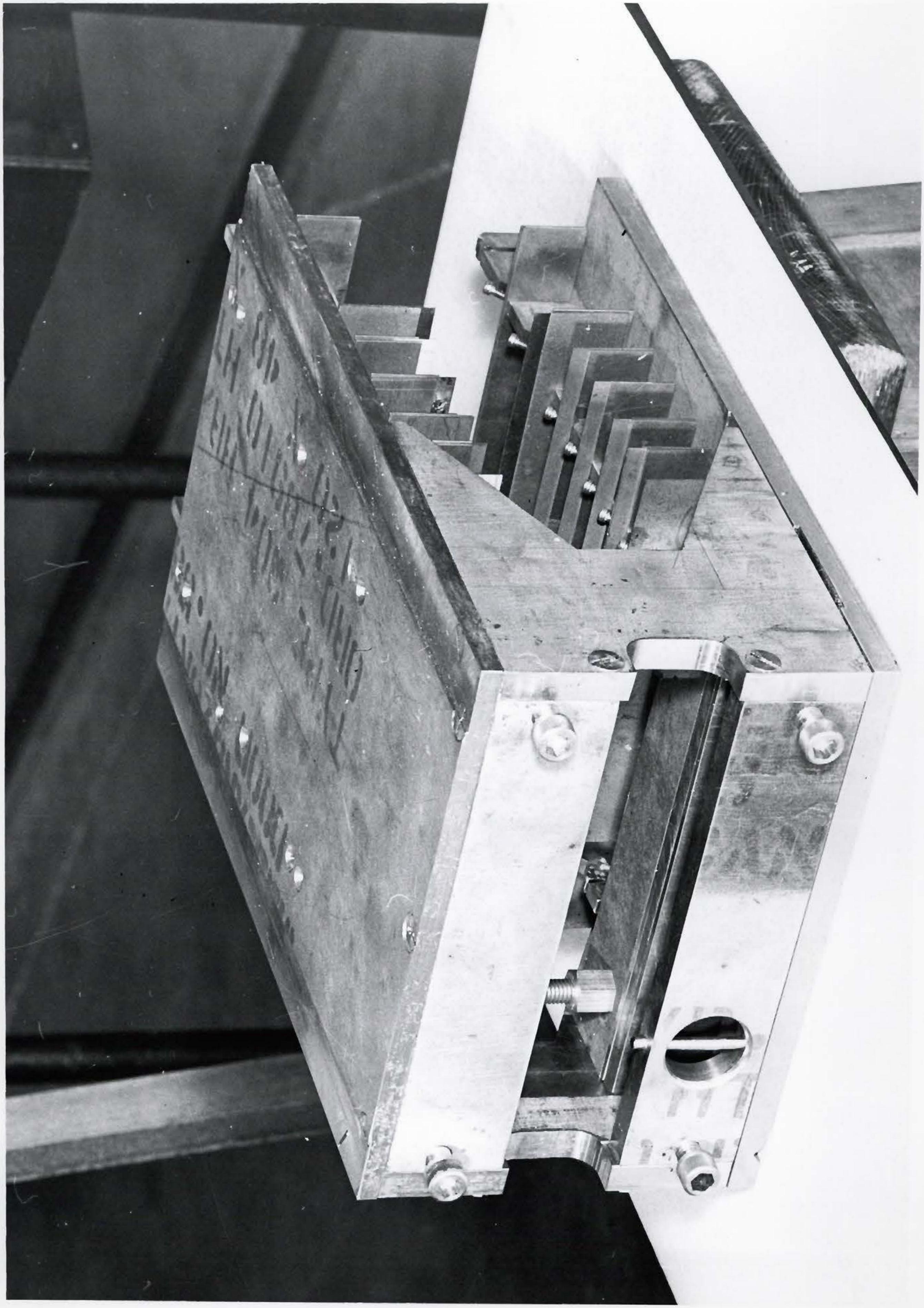

PLATE 5

EXTRACTION SYSTEM INSTALLED FOR MAGNETIC FIELD MEASUREMENTS

This photograph is intended to show principally the regenerator installation. The drive mechanism for the position adjustment of the regenerator is bolted to a short dummy section of vacuum tank wall. The drive mechanism for the Hall probe is seen in the foreground. The exit of the magnetic channel may be seen in the background.

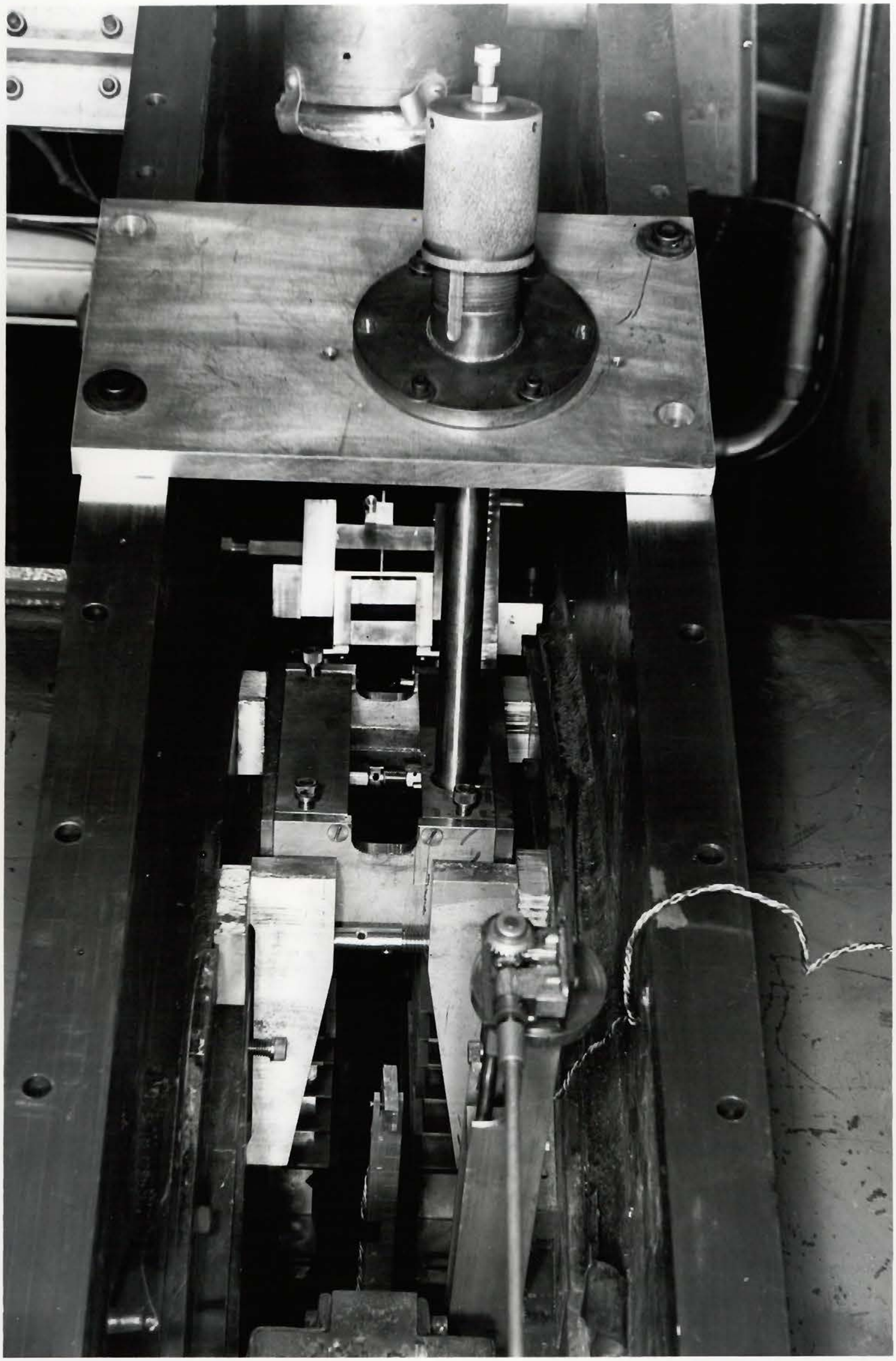

FIGURE 13

VARIATION OF MAXIMUM BEAM CURRENT WITH RADIUS

These measurements were obtained from the height of the beam pulse as viewed on an oscilloscope. When the measurements for the curve were taken, the average beam current at $r = 20$ inches was about 0.5×10^{-6} ampere. Measurements were taken with the regenerator at the best position for the regenerative deflection of the beam.

The reason for the minimum at $r = 37$ inches is a sharp change in beam pulse shape. The beam pulse at 38 inches appeared to have only about half the time spread of the beam pulse at 36 inches (about 30×10^{-6} second).

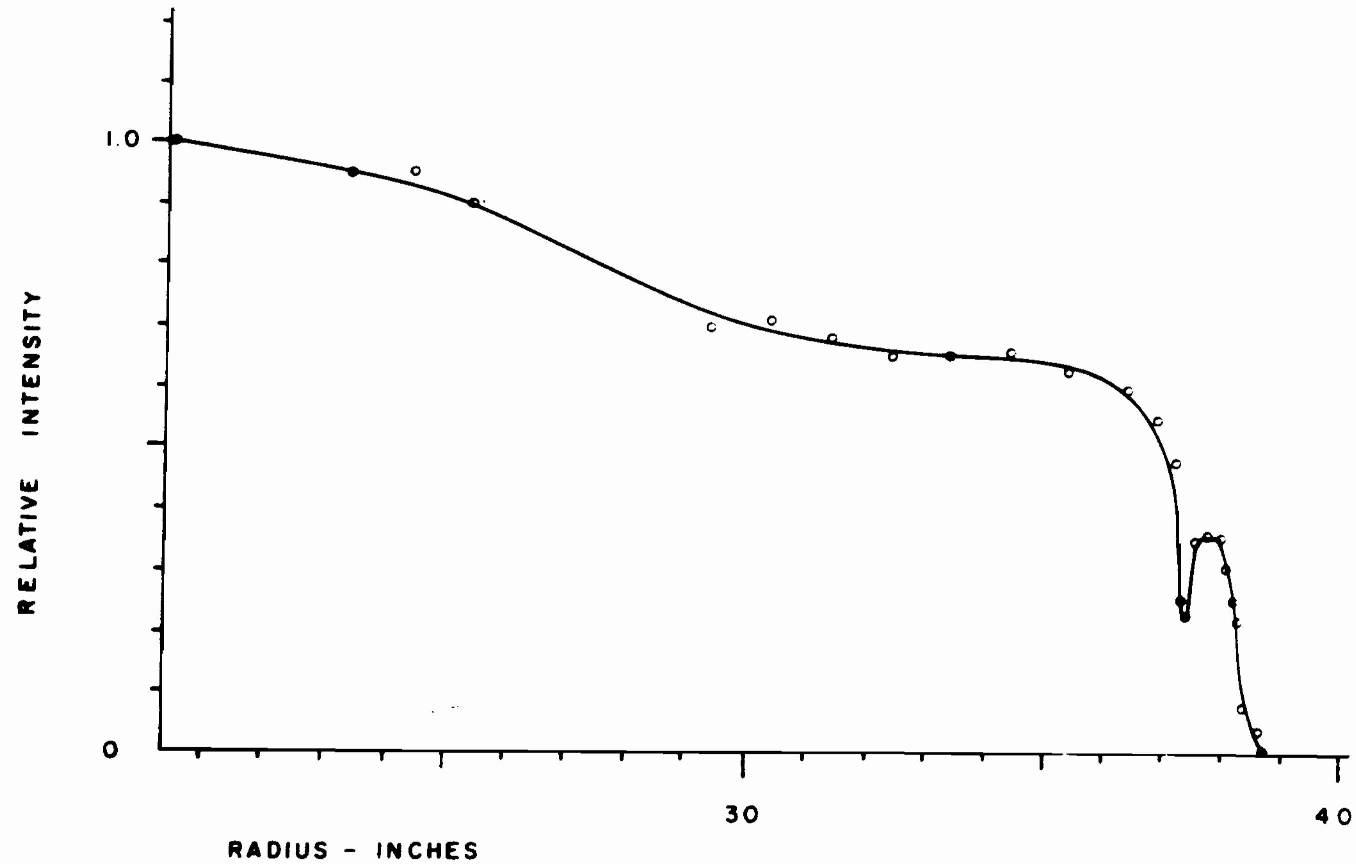
1.0
0
RELATIVE INTENSITY
30
40
RADIUS - INCHES

obtained by measuring the current pulse of protons collected on a copper block placed in the beam. It is seen in Figure 13 that part of the circulating beam is maintained out to 38 inches.

To test for sufficient separation between orbits, a grounded copper block 3/8 inch thick was placed radially inward from the copper block which measured the beam pulse. Both blocks moved together as a unit. The deflected beam intensity is shown in Figure 14. About 25% of the beam circulating at 36 inches was sufficiently deflected to clear the grounded copper block. The variation of this deflected beam intensity with regenerator position (Figure 15) was rather sharp, indicating that the geometry of the regenerator was rather critical.

It appeared that the system was indeed energy selective in deflecting the cyclotron beam (see Chapter 2). An oscilloscope trace of the beam pulse was much sharper in time than the oscilloscope trace of the internal beam pulse. This selection in time suggests a selection in energy. The reduction in time spread viewed on the oscilloscope was a factor of 2 or 3.

FIGURE 14

DEFLECTED BEAM CURRENT

The measurements for this curve were obtained under the same conditions as those for Figure 13 except that a 3/8 inch thick grounded copper block was placed immediately inward of the current measuring block.

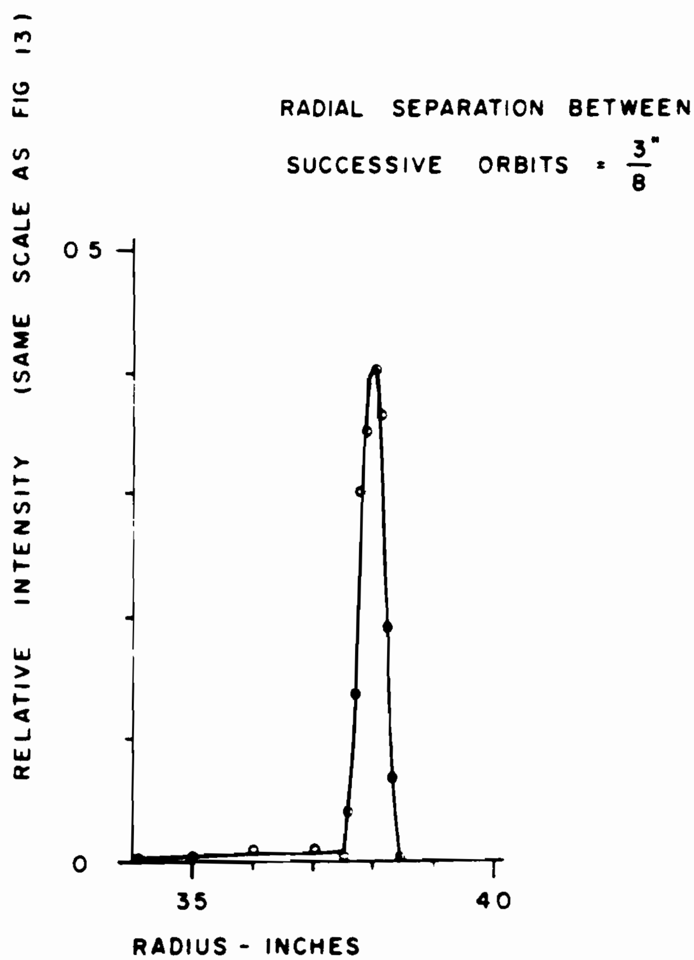
RADIAL SEPARATION BETWEEN
SUCCESSIVE ORBITS = 3"/8
RELATIVE INTENSITY (SAME SCALE AS FIG 13)
0 5
0
35
40
RADIUS - INCHES

FIGURE 15

DEFLECTED BEAM CURRENT VS REGENERATOR POSITION

The reading on the micrometer barrel increases for radial motion into the machine. Each point on the curve is the peak from curves such as Figure 14.

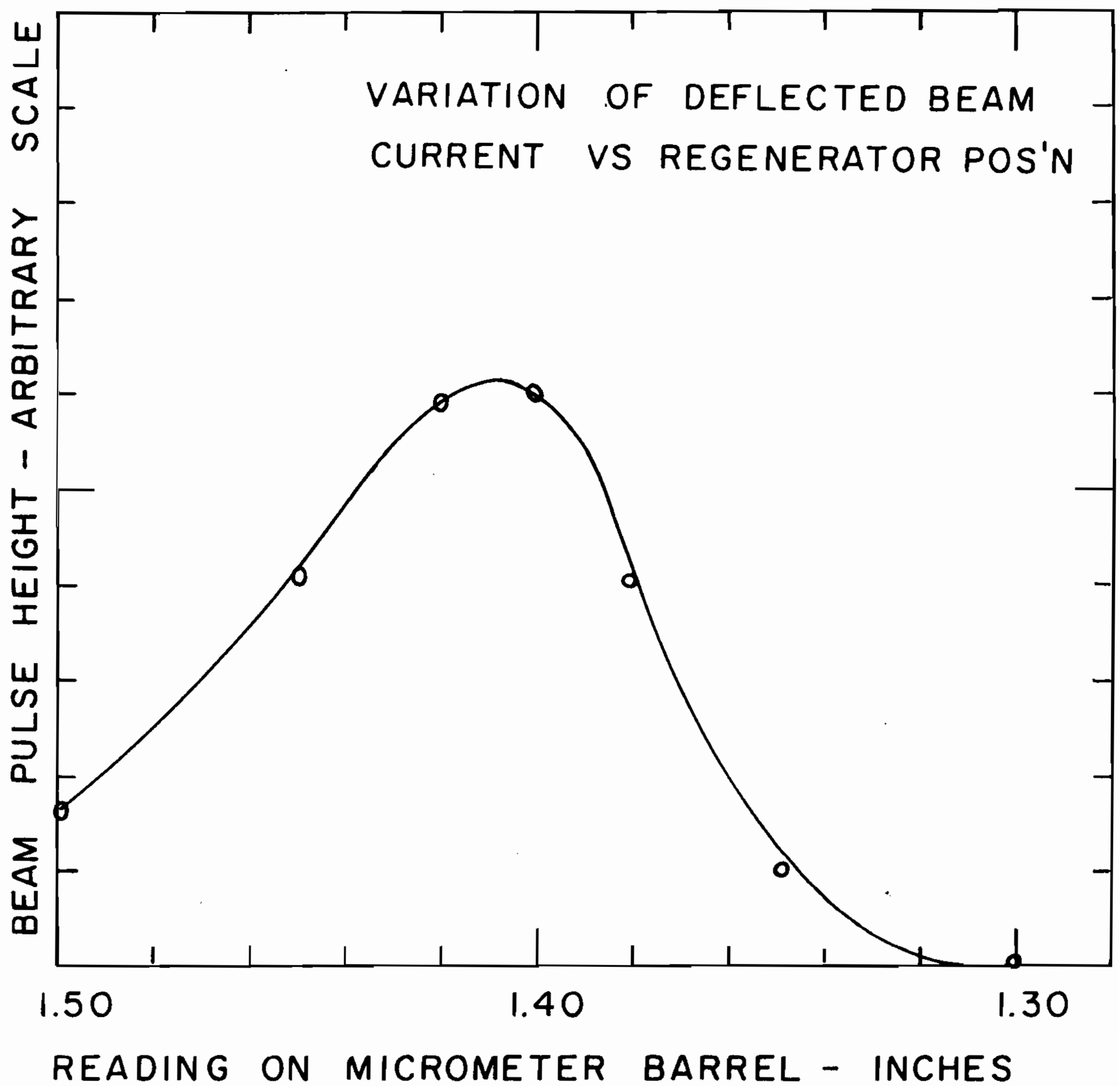
VARIATION OF DEFLECTED BEAM
CURRENT VS REGENERATOR POS'N
BEAM PULSE HEIGHT - ARBITRARY SCALE
1.50
1.40
1.30
READING ON MICROMETER BARREL - INCHES

CHAPTER 5

DESIGN AND INSTALLATION OF THE MAGNETIC CHANNEL

The Design and Installation of the Magnetic Channel

In principle, a regenerative deflection system could deflect the proton beam of a cyclotron out to a radius of the machine for which the magnetic field is sufficiently reduced for Br to be less than the magnetic rigidity of the protons. The protons would then spiral out of the machine.

However the regenerator strength for such a deflection is not practically attainable. Therefore a localized region of reduced magnetic field must be set up inside the cyclotron and the protons extracted by deflecting them into this region (Chapter 1). The channel between two vertical slabs of magnetic iron is such a region. The deflection system must then give sufficient separation between orbits so that the protons clear the inner face of the inner slab on one orbit and enter the channel on the next.

It is important that the channel walls be as thick as the deflection system will allow in order to gain as much field reduction in the channel as possible. This is because protons spiraling out through the fringing area of the cyclotron field, encounter severe negative radial field gradients even inside the magnetic channel, and these tend to diverge the proton beam horizontally. To minimize this horizontal divergence of the beam, the protons must be made to spiral rapidly through the fringing region by reducing their curvature as quickly as possible.

The thickness of the inner wall at the channel entrance is limited by the radial separation between successive orbits that is practical with the regenerative deflector. In the McGill machine this separation appears to be about 3/8 inch. As the protons travel along the channel they move away from the last orbit before extraction and the wall thickness may be increased.

It is inadvisable to further reduce the field by making the outer wall thicker than the inner wall. This would make more severe the negative field gradient which is already troublesome.

Where the negative field gradient is most severe it is possible to reduce it by reducing the thickness of the outer wall of the channel. However the field reduction in the channel is then not as great, and furthermore, the gradient is not constant across the width of the channel. This non-uniform field gradient can cause distortions in the proton beam optics which are difficult to correct later along the flight path. It was felt therefore that the channel should have inner and outer walls of equal thickness and that strongly positive field gradients should be introduced over a short length of flight path when horizontal refocusing was necessary. Sufficiently strong positive gradients of reasonable uniformity can be achieved by the self excited quadrupoles described later in this chapter.

The height of the channel wall and the channel width were decided on the basis of uniformity of field in the region of the channel occupied by the proton beam. Again, non-uniformity of field can cause troublesome distortions in the proton beam optics. The vertical focusing of the cyclotron field gradient keeps the vertical extent of the beam to about $\frac{3}{4}$ inch overall. It was felt that 2 inches of channel height would give adequate uniformity in this region. While a somewhat greater field reduction may be obtained by reducing the channel height for the same wall thickness, the greater beam distortions that such a channel might introduce could offset the advantage of the greater field reduction. To further minimize non-uniformity the channel width was made as small as possible, and $\frac{1}{2}$ inch was felt to be adequate to clear the proton beam.

The channel was made up of sections each 4 inches long. The design of the wall thickness of each section was carried out as follows.

For various azimuthal positions the radial separation between successive orbits was calculated from Appendix A. The wall thickness for a channel entrance placed at this azimuth was then taken as slightly less than this separation. The magnetic field in an entrance channel section with this wall thickness was then calculated from the methods of Appendix B. From the known motion of the protons entering the channel, it was then possible to calculate the increase in separation between the proton beam in the channel and the last orbit before entering the channel, at the end of the first 4 inch section. The permissible increase in wall thickness for the second section was thus determined. The actual increase was made a little less than this permissible limit to reduce the distortion in the magnetic field traversed by the protons on their last orbit before entering the channel.

In this way the trajectory of the beam as it was led out of the machine for various azimuthal positions of the channel entrance was computed for what appeared to be the best channel geometry. From these computations and from practical consideration involving the space available in the machine, the channel layout shown in Figure 16 was chosen.

Of course no amount of computation can give the exact coordinates of the beam at any point and so each channel section was made adjustable in the horizontal position of both ends. The adjusting mechanisms were designed to be operated from outside the vacuun tank of the cyclotron. The channel section design is shown in Figure 17.

It was decided that six channel sections should be adequate although an extra section was built to be installed if it seemed profitable. The gap between section 3 and section 4 provides for the use of the internal target probe for internal beam bombardment experiments. The sections are held in place by brass jacks which jack against the upper cyclotron pole tip and hold the sections against a ½ inch thick aluminum plate which is properly spaced away from the lower pole tip. The sections are held against radial thrust by stainless steel dowels into the aluminum plate and the total thrust on the plate is taken by brackets butting against the ½ inch pole cap of the cyclotron. With this method of installation the channel sections can be completly removed or inserted in a very short time. Once the vacuum tank of the cyclotron is opened either operation

FIGURE 16

CHANNEL LAYOUT

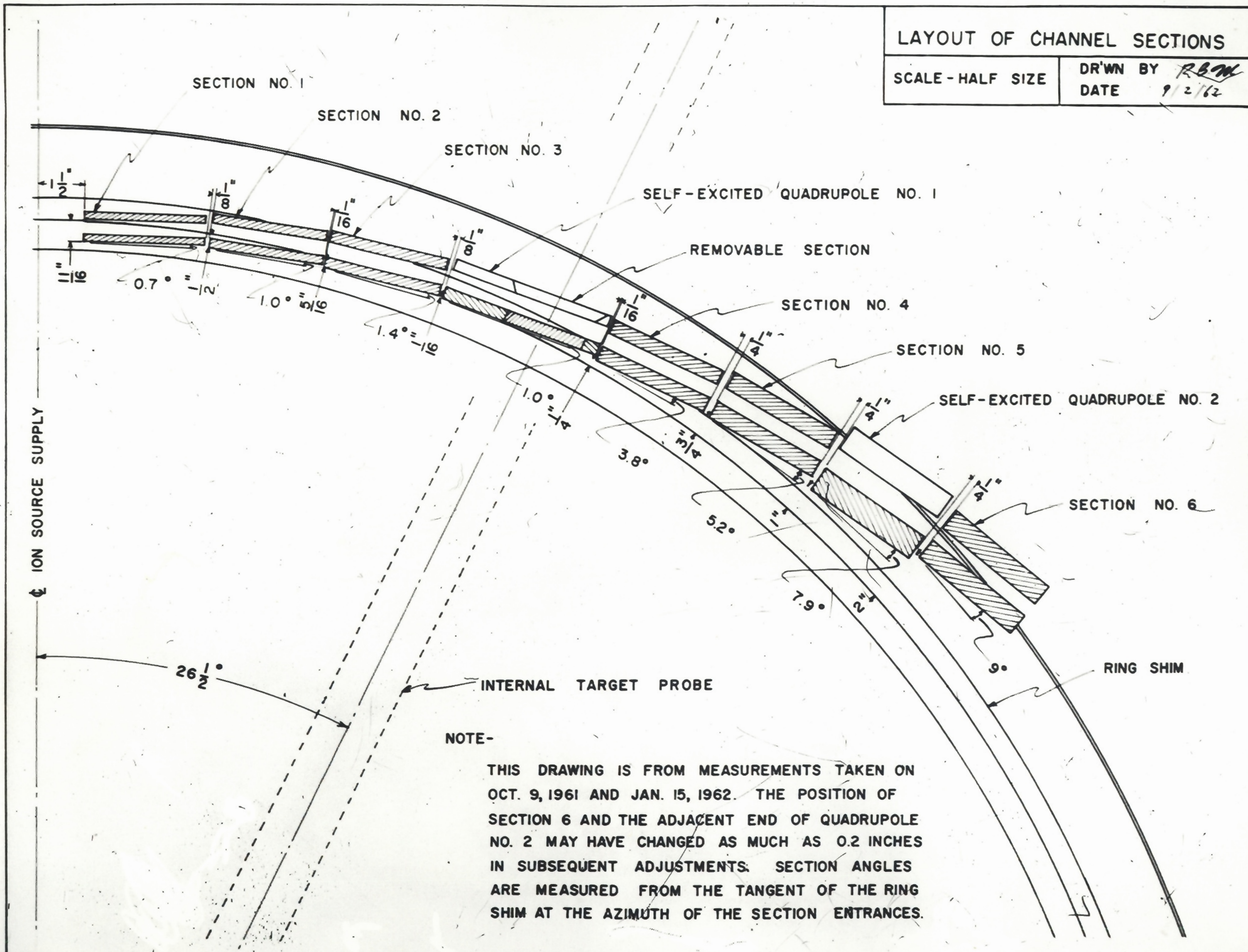

LAYOUT OF CHANNEL SECTIONS

SCALE - HALF SIZE	DR'WN BY RBM DATE 9/2/62

NOTE-

THIS DRAWING IS FROM MEASUREMENTS TAKEN ON OCT. 9, 1961 AND JAN. 15, 1962. THE POSITION OF SECTION 6 AND THE ADJACENT END OF QUADRUPOLE NO. 2 MAY HAVE CHANGED AS MUCH AS 0.2 INCHES IN SUBSEQUENT ADJUSTMENTS. SECTION ANGLES ARE MEASURED FROM THE TANGENT OF THE RING SHIM AT THE AZIMUTH OF THE SECTION ENTRANCES.

FIGURE 17

DETAIL OF CHANNEL SECTIONS

NOTE -

CHANNEL SHOWN IS NO 1. THE DIMENSIONS OF THE MAGNETIC IRON OF ALL CHANNELS ARE LISTED BELOW. ASSOCIATED DIMENSIONS OF BRASS PIECES AND SCREWS ADJACENT TO THE IRON (TOP & BOTTOM) ARE CHANGED ACCORDINGLY BUT ALL OTHER DIMENSIONS REMAIN THE SAME THROUGHOUT. ON CHANNELS 2 & 5 THE WORM & PINION MOUNT IS INVERTED TO GIVE CLEARANCE FOR THE DRIVESHAFTS

CHANNEL NO	WALL THICKNESS	GAP	LENGTH
1	$\frac{1}{4}$"	$\frac{1}{2}$"	4"
2	$\frac{5}{16}$	"	"
3	$\frac{3}{8}$	"	"
4	$\frac{1}{2}$	"	"
5	$\frac{5}{8}$	"	"
6	$\frac{3}{4}$	"	"

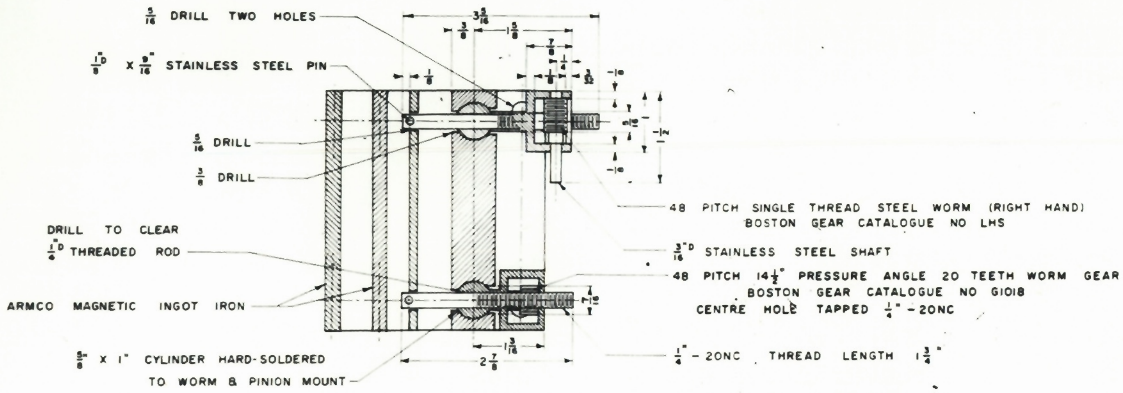

SECTION A-A

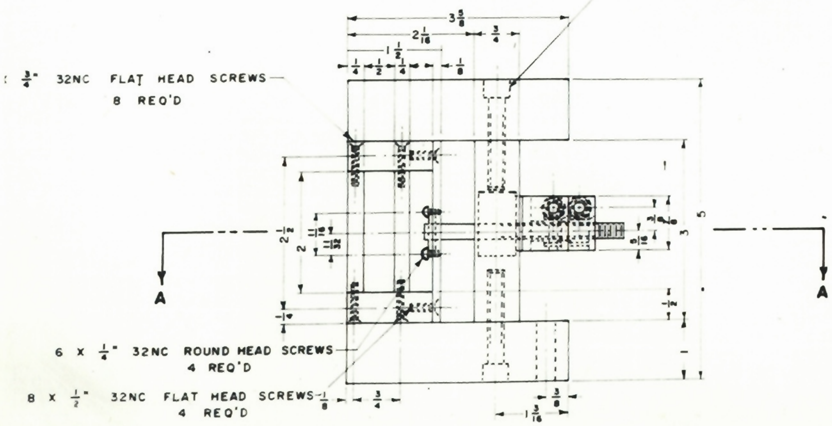

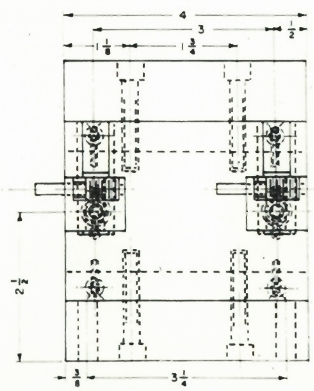

MATERIAL - BRASS UNLESS SPECIFIED OTHERWISE

MCGILL UNIVERSITY RADIATION LABORATORY	
DETAIL OF CHANNEL	
SCALE - FULL SIZE	DATE - AUG. 21, 1961 DR'WN BY

can be carried out in about 5 minutes.

Since the large amount of iron used in the construction of the channel seriously perturbs the magnetic field in a whole quadrant of the cyclotron, it is necessary to correct the field radially inward from the channel so that the internal circulating beam both before and after regenerative deflection will be undisturbed. For the first two or three sections, this correction has to be carried up to within 1/4 or 1/8 inch of the channel wall. Unfortunately the shims needed for this field correction are quite massive and introduce further unavoidable negative field gradient in the channel.

The method of attack was to map the magnetic field in the vicinity of the bare channel sections, calculate the vertical shimming required to correct for the field defect, install this shimming and remap the field. This procedure was repeated until it was felt that an adequate correction had been made. We were helped greatly in this program by having a rapid means of measuring the magnetic field (the apparatus described in Chapter 3) and by having means of calculating the effect of magnetic shims (Appendix B).

In the first attempt only the first three sections were installed. To obtain a relatively undisturbed beam it was found that two conditions had to be met.

1. The shimming had to be carried right up to the channel wall for the first three sections. The shim thickness adjacent to the wall of the first channel section is almost equal to the wall thickness of the channel itself.

2. Except for the shimming very close to the channel wall, a vertical gap of at least $2\frac{1}{2}$ inches had to be maintained. This was no doubt due to the necessity of having a sufficient vertical aperture. A photograph of a typical channel section (section 4) with vertical shims attached, is shown in Plate 6.

After several trials the beam was deflected into the first three channel sections. About 10% of the beam circulating at 36 inches entered the first channel section and about 80% of this appeared at the exit of section 3. Alignment of the sections to obtain this transmission was carried out by observing the beam picked up on an insulated brass block which could be moved along the channel sections from outside the vacuum tank. In this way, after the beam was picked up at the channel entrance, the three channel sections could be aligned in about 4 hours.

When the optimum alignment had been obtained it was found that the channel entrance was 0.3 inches radially inward from the position indicated by the measurements of the beam distribution taken before the channel installation. This indicated that, despite the magnetic shimming, the channel sections had changed the average field in their vicinity and therefore altered the performance of the regenerator deflector. Since a fairly good yield was obtained, no attempt was made to rectify this condition.

The later three sections were installed and aligned in the same manner as the first three. A photograph of the complete channel installation is shown in Plate 7. No serious

PLATE 6

CHANNEL SECTION NO. 4

Note that the vertical magnetic shims move with the channel section as its position is adjusted.

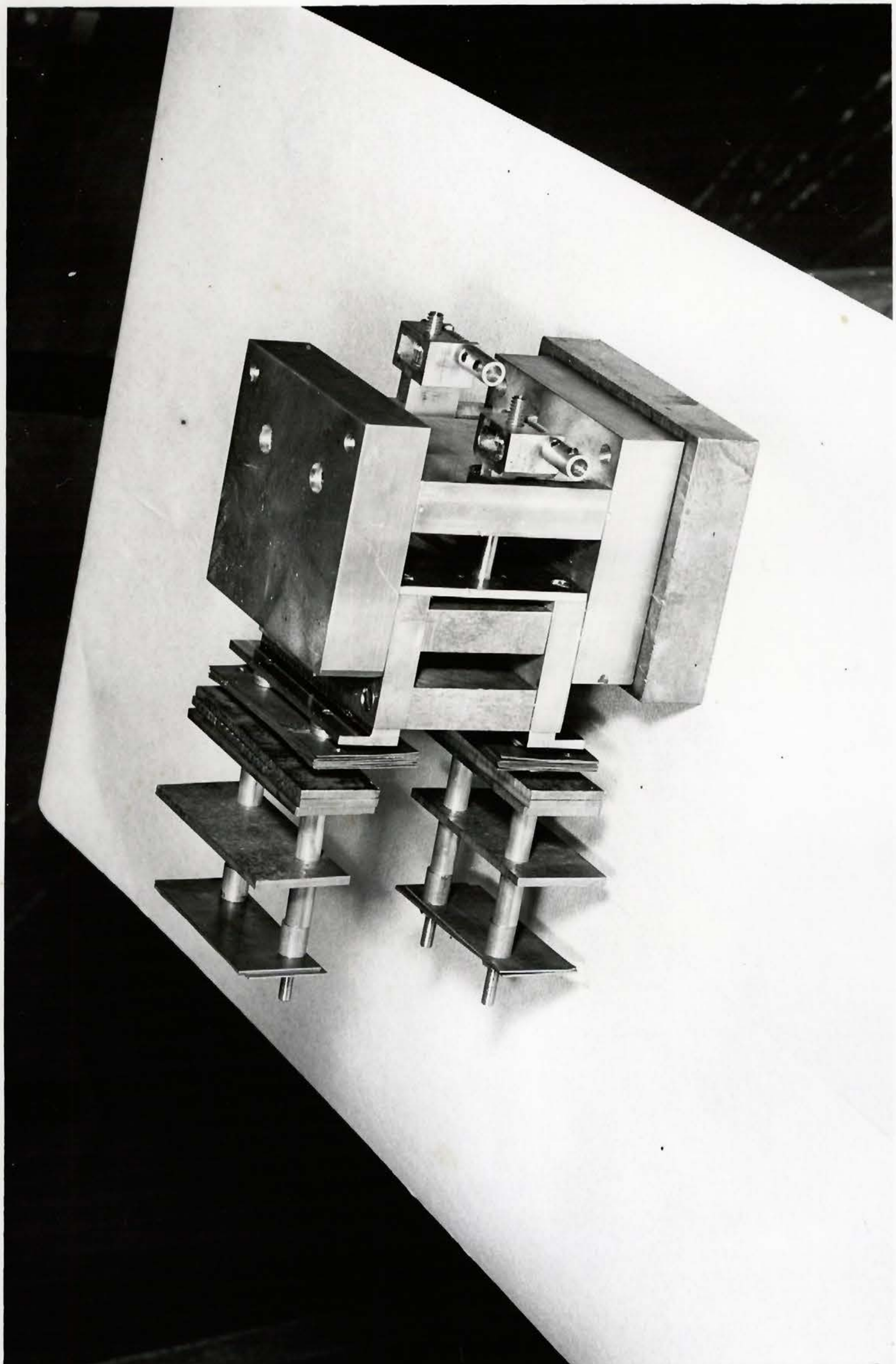

PLATE 7

CHANNEL INSTALLATION

This photograph was taken before the self excited horizontally focusing quadrupoles were installed.

disturbances of the internal beam were found although the fraction of the internal beam that entered the channel has decreased a little (to about 6% of the beam at 36 inches). However, of the beam entering the channel, only 15% remained after all six channel sections had been traversed. Glass plates were set up in the channel sections and the patterns produced by proton bombardment indicated that the loss was due to horizontal divergence of the beam. It was decided that a self excited quadrupole with a positive (horizontally focusing) field gradient should be used to correct this divergence.

A positive field gradient which converges the beam horizontally will cause the beam to diverge vertically. Since this undesirable diverging action depends on the vertical extent of the beam, the horizontally focusing quadrupole should be placed where the vertical extent of the beam is a minimum.

The negative field gradient which caused horizontal divergence of the beam in the first three channel sections converges the beam vertically. The vertical focus occurs at about the entrance of section 4. This gives a region of small vertical extent of the beam in which the self excited quadrupole may be placed in the gap left for the internal target probe between channel sections 3 and 4. The vertical action of a quadrupole in this position would then be small and would only move the vertical focus farther along the length of the channel.

A self excited quadrupole was built with as large a positive field gradient as possible in the limited space available. A simple sketch of the quadrupole geometry is given in Figure 18. A removable section was provided so that the internal

FIGURE 18

GEOMETRY OF MAGNETIC IRON IN SELF EXCITED QUADRUPOLE

No attempt is made to show the non-magnetic parts of this quadrupole. Only the geometry of the magnetic iron is indicated so as to show the induced quadrupole effect.

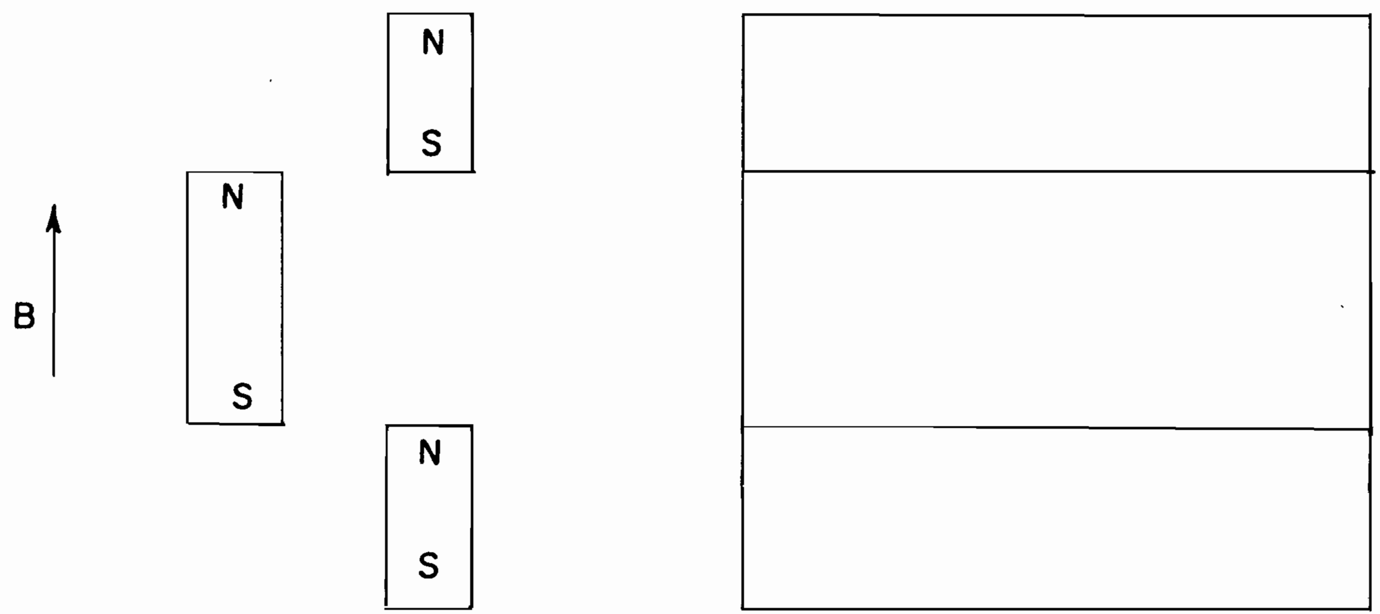

N
S
N
S
N
S
B

target probe could still be used. The field gradient possible was not large enough to completely counteract the horizontal divergence but about 50% of the beam entering the channel now appeared at the channel exit. Subsequent measurements showed that the vertical focal point had moved down the channel to about section 6.

At this time the geometry and the alignment of the channel sections and the self excited quadrupole were fairly well established and it was felt that a review of the total shimming of the extraction system was in order. While we were still obtaining a reasonable fraction of the internal beam at 36 inches, the internal beam loss from radius 22 inches to radius 36 inches was considerable (about 80% or more). By redressing the shimming we were able to increase the fraction of the beam at 36 inches that entered the channel to about 10% but the loss in the region between 22 inches and 36 inches could not be reduced beyond about 60% in the time available for the readjustment. Expressed as a percentage of the internal beam at 16 inches, the extracted beam is a little better than 1% as measured on a Faraday cup. For present normal operation of the machine, the external beam current versus radius is given in Figure 19.

It is the opinion of the writer that at this stage the possibilities of the extraction system have not been fully realized. The percentage of the beam at 36 inches which is deflected into the magnetic channel is good but not as large as the percentage which was deflected with a similar radial gain before the channel was installed. This might be corrected

FIGURE 19

VARIATION OF BEAM CURRENT WITH RADIUS

This curve is intended to show where the internal beam is lost. It is easily seen that there are two regions in which the internal beam decreases in intensity with radius. These occur at about 27 inches and at about 33 inches. These regions correspond to regions of reduced field gradient in the machine. Only about 15% of the beam at 16 inches reaches a radius of 35 inches. The beam which reaches the channel entrance indicated by the dotted line is about 2%.

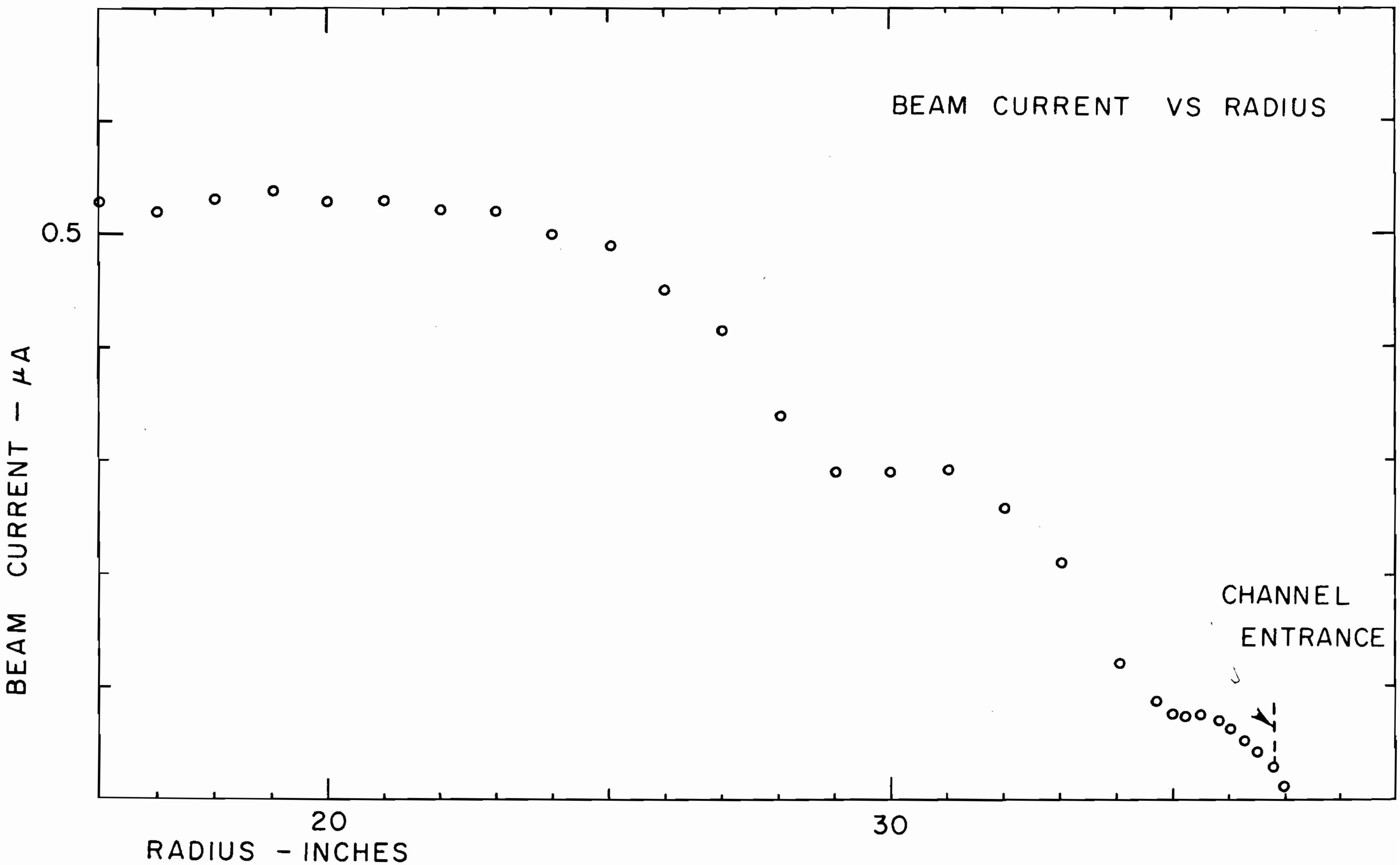
BEAM CURRENT VS RADIUS
CHANNEL
ENTRANCE
0.5
BEAM CURRENT – μA
20
30
RADIUS – INCHES

by readjusting the regenerator strength to match the altered field gradient in the region r = 36 inches to r = 38 inches due to the presence of the channel. However the greatest beam loss in the machine is at inner radii. This beam loss is no doubt due to the variation of dB/dr within the machine. Regions in which dB/dr becomes small not only have smaller vertical focusing forces on the protons but also demand more energy gain per revolution to keep the protons in step with the decreasing frequency on the accelerating dees. If the voltage on the dees cannot provide enough energy to the protons for them to stay in step, the protons fall behind and are lost.

These shallow regions of dB/dr have apparently al ways existed in the machine and have al ways been responsible for beam loss. The installation of the extraction system with the limited vertical aperature of its shimming may have made the effect of these regions a little more marked.

However to correct these faults a thorough survey of the magnetic field of the cyclotron should be carried out. This survey should include planes above and below the median plane to detect vertical asymmetries. For such a mapping the dee system would have to be removed. A calculation of the necessary shimming could then be carried out and the shimming installed and securely fastened inside the machine.

With luck, such a correction could be carried out in one step but the total operation might add about two months to the machine down time. For most counting experiments the current is already too intense. (This is because the proton consists of bursts rather than a steady current. The instantaneous beam current in the burst may reach about 10^{13} protons per second). It was felt therefore that attention should now be given to the problem of focusing the beam into a well behaved roughly parallel beam of good cross section and to building up the necessary experimental equipment to make use of this beam.

CHAPTER 6

FOCUSING THE EXTERNAL BEAM FROM INSIDE THE CYCLOTRON

Focusing of the External Beam from Inside the Cyclotron

Because of the negative horizontal field gradient of the cyclotron magnetic field, the extracted proton beam is fairly well focused vertically but diverges horizontally. The horizontal spread of the external beam before corrective measures were taken is indicated in Figure 20. In an elevation view the beam is roughly parallel.

The beam quality may be expressed as its "area in phase space". For a full discussion of the significance of the area in phase space of a beam of particles the reader is referred to Penner (1961). Only a few pertinent results of this approach are indicated here.

The structure of a beam of protons at any point z along the beam path may be described in a rectangular coordinate system by emittance plots dx/dz versus x and dy/dz versus y. (For horizontal beams, x and y are generally taken to be horizontal and vertical respectively.) For a well behaved beam, the points representing the protons in the beam fall inside a well defined area on each emittance diagram. This area is called the area in phase space.

As one moves along the beam path, the shapes of these areas transform, but for systems in which the magnetic field is a linear function of x and y, the area in each emittance plot is constant. These areas may therefore be used as a measure of the quality of the beam and should be kept as small as possible. The smaller these areas are, the smaller is the divergence of the beam when it is focused to a small spot.

FIGURE 20

HORIZONTAL DIRECTION OF EXTERNAL BEAM IN CYCLOTRON VAULT

The direction of the beam was obtained by exposing X ray plates at the end of various lengths of 4 inch diameter beam pipe. The beam pipe was provided with a 0.050 inch thick aluminum window and was connected to a flexible bellows so that it could be swung horizontally to investigate the horizontal beam spread.

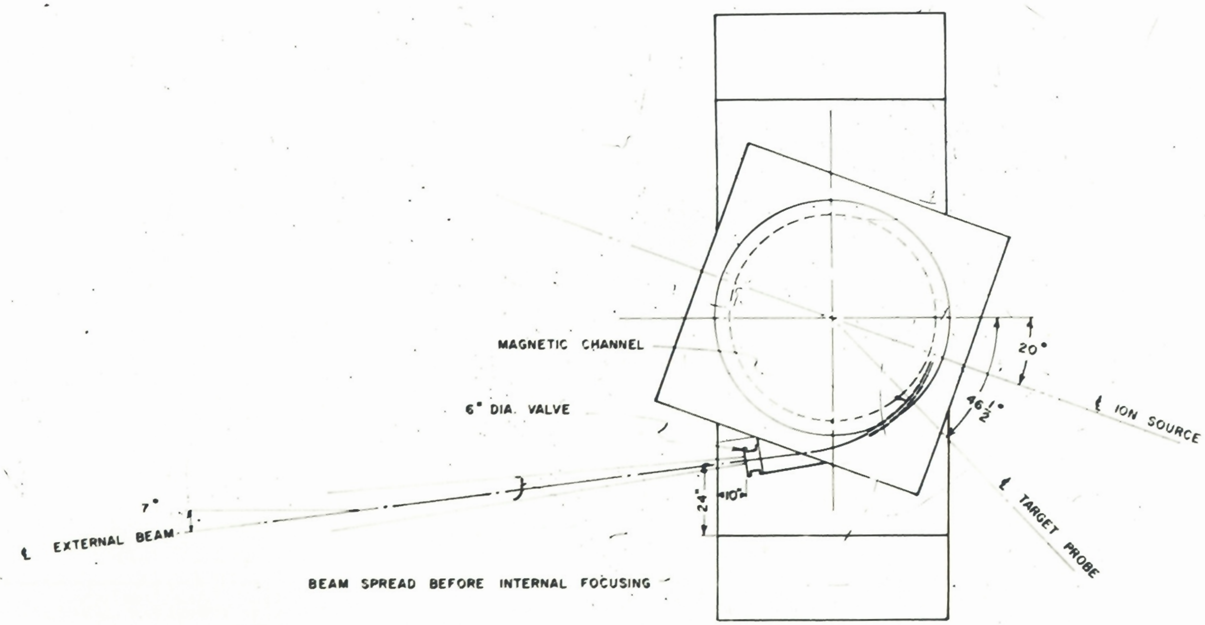

EXTERNAL BEAM DIRECTION	
SCALE - 1 INCH = 2 FEET	DR'N BY [illegible] DATE 11/2/62

It is desirable to be able to focus the beam to a small spot for two reasons. One reason is simply the high specific bombardment obtained. The other is to prevent adding phase space area to the beam structure when it is energy degraded in an absorber. Energy degrading of a synchrocyclotron external beam is necessary in order to obtain energy variation. When a perfectly parallel proton beam is energy degraded it acquires a certain divergence. If such a beam of finite size passes through an absorber, then the area in phase space is increased from zero to an amount equal to the angular divergence multiplied by the size of the beam at the scatterer and so the beam size at the scatterer should be as small as possible. The beam divergence on leaving the absorber may be large but if the cross sectional area is small, then quadrupoles of sufficient aperture to contain the diverging beam can refocus the beam to another small spot on the target.

To obtain a good degraded beam then, two sets of quadrupoles are necessary; a set of large aperture to collect the degraded beam from the absorber and focus it to a small spot on the target and another set to focus the external beam from the cyclotron to a small spot on the absorber.

The large aperture set has already been installed (Pacific Electric Motor Co. Model 6SF-26-10LI: 6 inch aperture, 10 inch long with a maximum field gradient of 4 Kilogauss/inch). The aperture of the other set is dictated by the size of the external beam. A considerable saving in space and quadrupole investment is therefore achieved by making the external beam as small as possible by focusing inside the cyclotron.

The focusing from inside the machine may be accomplished by a second self excited quadrupole. (The first self excited quadrupole, to improve the transmission in the channel, has been described in Chapter 5). To calculate the necessary quadrupole strength it is most convenient to use the method of transfer matrices (Penner 1961). In this method the values of x and dx/dz for a particular proton are represented by a two dimensional vector $\begin{bmatrix} x \\ dx/dz \end{bmatrix}$. The operation of a magnetic system on this proton may be expressed as a 2 x 2 transfer matrix operating on this vector;

$$\begin{bmatrix} x' \\ dx'/dz \end{bmatrix} = M_x \begin{bmatrix} x \\ dx/dz \end{bmatrix} \tag{1}$$

The vector for each proton in the beam locates a point on the emittance plane. As the proton moves through any magnetic system (even as it drifts through a field free region) this point moves in the emittance plane according to (1). The shape of the area encompassing all the proton points (or a sufficiently large percentage of them) changes according to the motion of these points.

Perhaps the most useful structure for an external beam before focusing on a target is one for which the emittance plot in either coordinate is slightly elliptical with its major axis in the 2nd and 4th quadrant. In a field free region protons drift so that they preserve their values of dx/dz and dy/dz and increase their values of x and y by z(dx/dz) and z(dy/dz) respectively. A proton beam with an elliptical emittance with the major axis in the 2nd and 4th quadrant will then drift so that the major axis of the plot rotates into the 1st and 3rd quadrants. In so doing the cross section of the beam diminishes before it expands. This necking down of the beam increases the path length for which the beam size may be held to within a certain limit.

The actual emittance plots of the beam 55 inches beyond the channel exit before the second self excited quadrupole was installed are shown in Figure 21. The points on these plots were obtained by a brass block with a rectangular array of holes placed at z ≅ 55 inches. (Distance along path length is defined as z ≅ 0 at channel exit). The brass block was thick enough to stop the protons and so the holes produced fine pencils of beam. By following the pattern of spots on X ray film placed at various values of z greater than 55 inches, the values of dx/dz and dy/dz for the beam pencils could be determined. The vertical emittance plot obtained is very good while the horizontal plot is indicative of the large horizontal divergence.

The horizontal emittance pattern at z ≅ 55 inches may be thought of as the horizontal emittance pattern at the channel exit operated on by the horizontal transfer matrix of the cyclotron fringing field over the 55 inches of beam path from the channel exit. Let this transfer matrix be M_x. What is required is a quadrupole to be added to this system so that the combined transfer matrix of the quadrupole plus fringing field will give a horizontal emittance pattern outside the

FIGURE 21

EMITTANCE PLOTS AT Z = 55 INCHES (BEFORE FINAL IMPROVEMENTS)

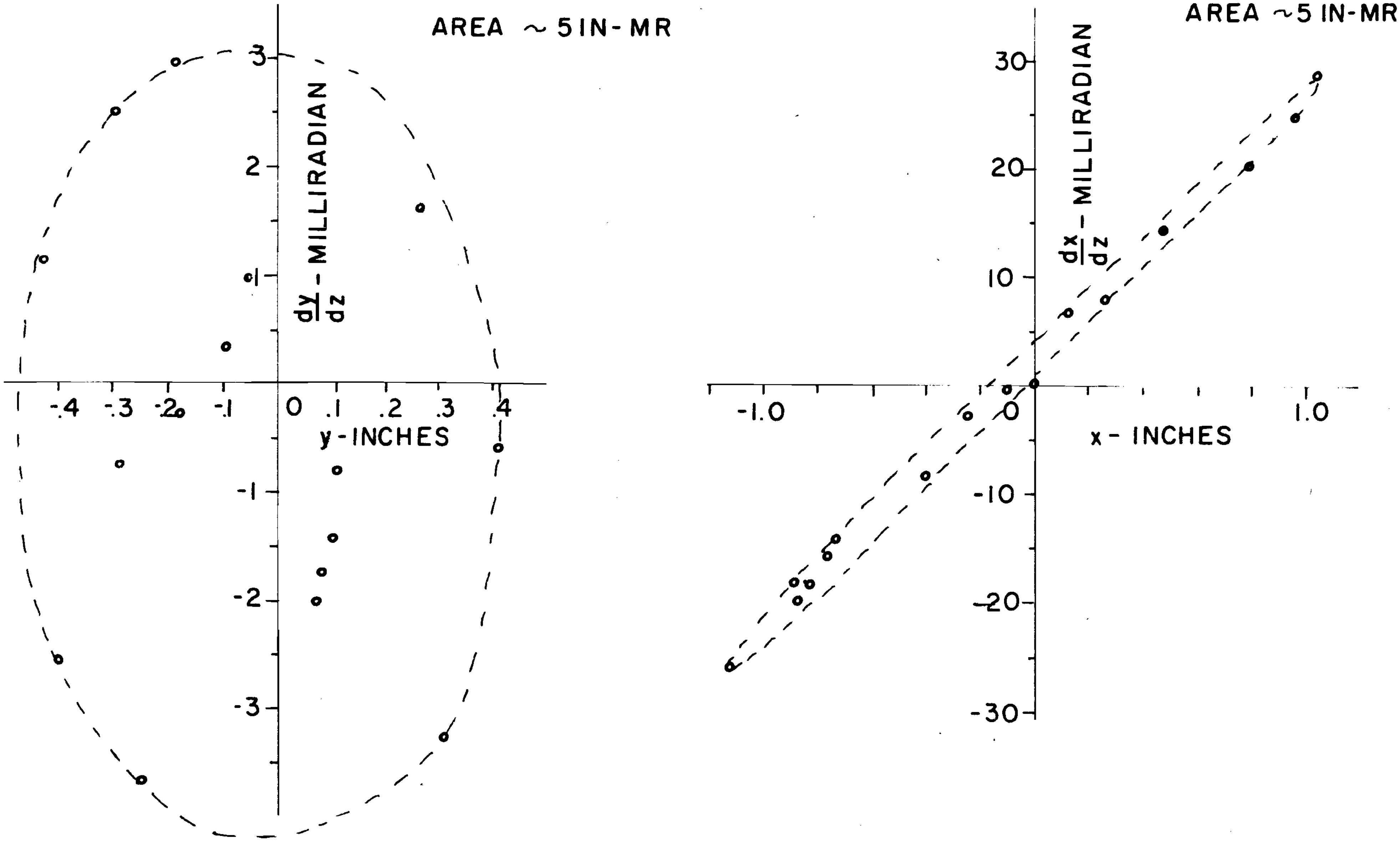

ORIGINAL EMITTANCE PLOTS OF EXTERNAL BEAM

55 INCHES FROM CHANNEL

machine which is slightly elliptical with the major axis preferably in the 2^{nd} and 4^{th} quadrants. At the same time the quadrupole should not disturb the vertical emittance pattern. Therefore, if possible, the quadrupole should be located in a region where the vertical extent of the beam is a minimum.

Fortunately this region occurs in channel section 6. The quadrupole could therefore replace section 6 and section 6 could be placed after the quadrupole. Since the average field reduction in the quadrupole is small, the beam trajectory is altered very little by this change.

The combined transfer matrix of the quadrupole and fringing field may be written as

$$T_x = M_x P_x$$

where P_x is the horizontal transfer matrix for the quadrupole. The procedure in designing the quadrupole was to calculate T_x for trial values of P_x and to apply T_x to the emittance pattern at the channel exit giving a calculated emittance pattern outside the machine. P_x was adjusted until the desired pattern was obtained. In the approximation of this design, the channel exit position and the cyclotron fringing field were assumed unchanged by the quadrupole installation and the quadrupole installation therefore did not change the transfer matrix M_x.

The transfer M_x was calculated by multiplying incremental horizontal transfer matrices of the form

$$\Delta M_x = \begin{bmatrix} 1 & 0 \\ -\frac{1}{Br}\frac{\partial B}{\partial x}\Delta z & 1 \end{bmatrix}$$

where ΔM_x is the transfer matrix for path length Δz and Br is the magnetic rigidity of the proton. The total path length of 55 inches for M_x was taken in 5 inch steps of Δz and the value of $\partial B/\partial x$ for each incremental transfer matrix was taken as the average value over Δz. $\partial B/\partial x$ was calculated as a function of z from a map of the fringing field of the cyclotron.

It may be noted that the above transfer matrices do not include the average field term which expresses the radius of curvature of the particle trajectory. This term disappears because we are referring the particle motion to the curved trajectory of the beam center.

Once the transfer matrix M_x has been evaluated, the emittance pattern at the channel exit can be obtained by applying the inverse of M_x to the measured emittance pattern at z = 55 inches. The resulting emittance patterns are shown in Figure 22. The vertical emittance pattern was obtained in a manner similar to that for the horizontal pattern.

These emittance patterns agreed with a qualitative picture of the beam behaviour inside the channel obtained during the channel installation (Chapter 5). They also agreed with beam patterns produced in X ray films and on a flourescent screen placed in the region of the channel exit. A telephoto lens was used to view the flourescent screen by closed circuit television.

FIGURE 22

EMITTANCE PATTERNS AT CHANNEL EXIT

These emittance patterns were obtained by applying the inverse of the transfer matrix of the cyclotron fringing field gradient to the emittance points in Figure 21. Note that here the vertical emittance pattern shows a greater divergence than the horizontal. This is because the beam has just gone through a vertical focal point. The cyclotron fringing field refocuses the beam vertically before it is out in the cyclotron vault.

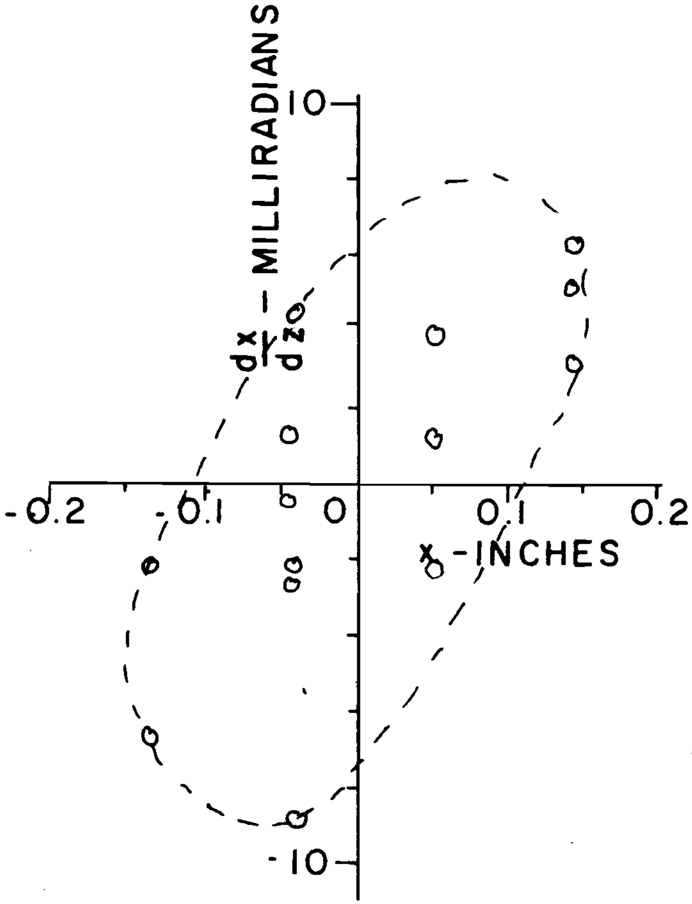

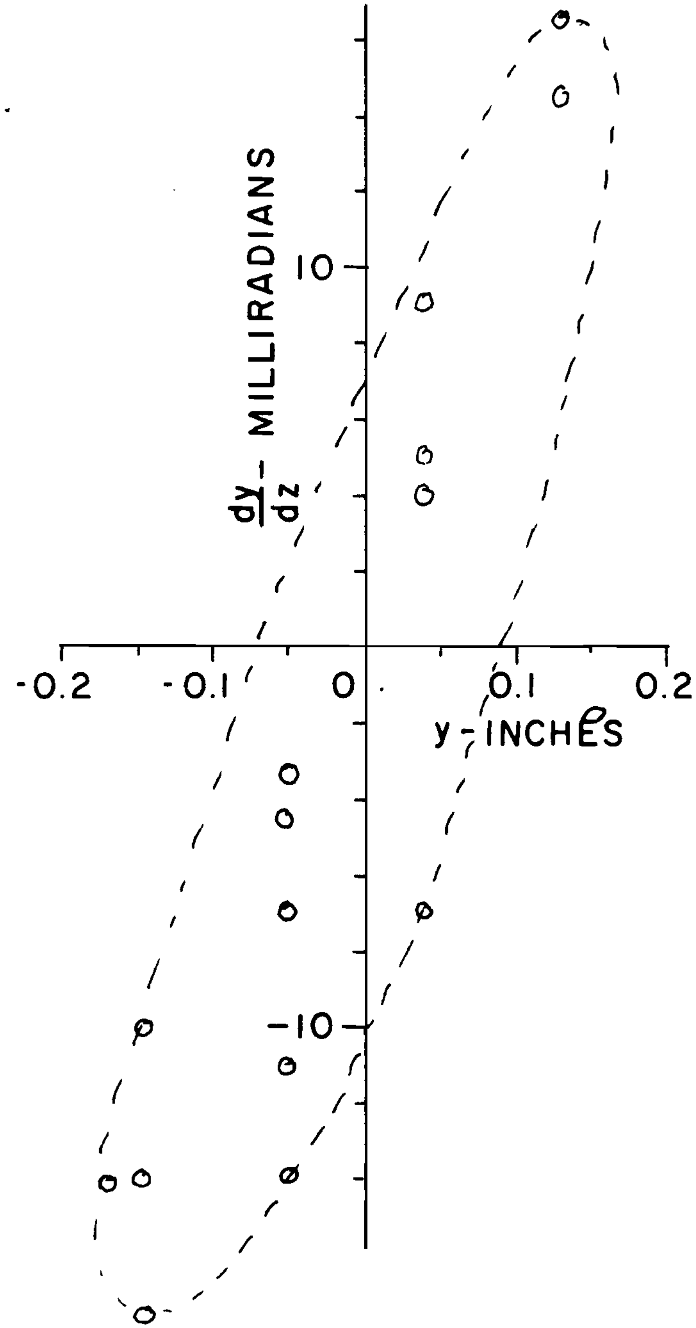

ORIGINAL EMITTANCE PLOTS
AT CHANNEL EXIT

When the horizontal emittance pattern at the channel exit was obtained in this way, the emittance pattern at $z \approx 55$ inches was calculated for trial values of quadrupole strength. The transfer matrix for the quadrupole in the limit of zero length is given by

$$P_x = \begin{bmatrix} 1 & 0 \\ \frac{-1}{B\rho}\,p & 1 \end{bmatrix}$$

where p, the quadrupole strength is defined as $\int dB/dx\, dz$. (For short quadrupoles the above form of the matrix may still be used if p is given by $\int dB/dx\, dz$ and the integration is carried out over values of z for which dB/dx for the quadrupole is significant.) These trial values of P_x were multiplied by M_x and the result applied to the horizontal emittance pattern of Figure 22. It was estimated that a value of p of 35 Kilogauss should be the best quadrupole strength to design for. The methods of Appendix were then used to design a self excited quadrupole (complete with vertical shims to restore the interior field of the cyclotron) which would give this value of integrated field gradient.

The quadrupole was built and installed. The calculations of Appendix B gave sufficiently accurate results for the rather large mass of iron (about 5 lbs) to be installed in the machine, with the correct shimming to prevent the disturbance of the internal beam, without magnetic field measurements being necessary.

It was found that the quadrupole made a decided improvement in the beam pattern but was not strong enough.

This was not unexpected considering the approximations and the roughness of the data involved in the design. After an adjustment of the quadrupole strength (involving an increase of about 15%) the emittance diagrams shown in Figure 23 were obtained. It still appears that the quadrupole could be a little stronger (maybe 5%) but very little is to be gained by such an adjustment.

It is seen in Figure 23 that total emittance pattern in both the horizontal and the vertical plots is not elliptical. However ellipses may be drawn as shown that will encompass about 85% of the beam intensity. The beam outside these ellipses may be removed by a simple horizontal slit central on the median plane which limits the vertical extent of the beam at the channel entrance. This indicates that the small part of the beam removed may be far enough from the median plane of the channel to suffer from the vertical non-uniformity of the field gradient in the channel sections.

The area enclosed by the ellipses is small, indicating a higher quality beam than was apparent before the second self excited quadrupole was installed. An area in phase space of one inch-milliradian is equivalent to an increase of beam size from ½ inch to 1 inch in about 20 feet. At z = 55 inches the beam has a spread of roughly ¾ inch both horizontally and vertically. Using the 6 inch aperture quadrupoles directly, it was estimated that at ½ current the beam size could be reduced to about 0.03 inch x 0.08 inch at 3 feet from the nearest quadrupole iron. With smaller aperture quadrupoles enabling higher field gradients it should be possible to reduce this spot size further.

FIGURE 23

FINAL EMITTANCE PATTERNS AT Z = 55 INCHES

The points on these diagrams were obtained by a remote control slit system at z = 55 inches and a flourescent screen placed about 6 feet away from the slits and viewed by closed circuit television. The 6 feet of drift space was in a vacuum pipe. The dotted contours encompass about 85% of the beam intensity.

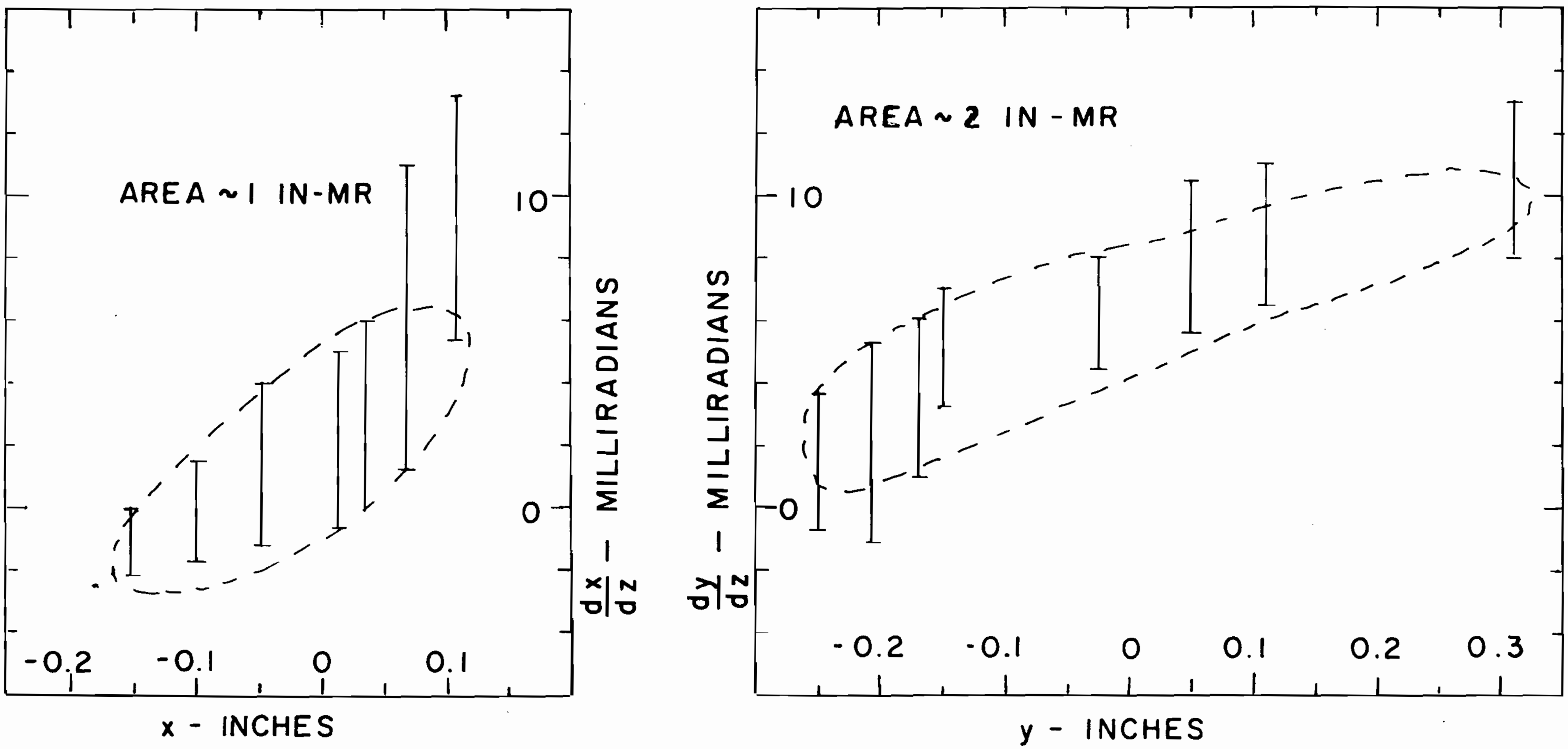

EMITTANCE PLOTS OF FINAL EXTERNAL BEAM

55 INCHES FROM CHANNEL

CHAPTER 7

DESCRIPTION OF THE EXTERNAL BEAM

Description of External Beam

A description of the external beam of protons delivered by the synchrocyclotron at the time of writing follows.

The areas in phase space, indicating the quality of the beam as a measure of the spot size for a given divergence, are 1 inch-milliradian in the horizontal plane and 2 inch milliradians in the vertical plane for about 85% of the beam. The method of obtaining these measurements is outlined in the previous chapter.

The horizontal and vertical spread of the beam at a point 200 inches from the channel exit (about 120 inches from the exit port at the wall of the vacuum tank) is shown in Figure 24. These points were obtained by moving a slit in front of a Faraday sup. It is seen that about 85% of the beam is within a horizontal extent of 0.5 inches and a vertical extent of 0.3 inches.

The set of 6 inch aper_ture quadrupoles manufactured by Pacific Electric Co. are now being used to focus the beam onto a target. With the field gradient in these quadrupoles at half rated current, the beam was focused to a spot having the horizontal and vertical distributions indicated in Figure 25. The points shown as crosses in this figure were obtained by bombarding stacks of teflon strips 1/32 of an inch thick and measuring the relative intensity of the induced radioactivity in each strip. The points shown as circles were obtained by the moving slit system. The difference in the two curves for the vertical pattern is probably due to the error in locating the position of the slit, the millimeter readings being

FIGURE 24

EXTERNAL BEAM SPREAD BEFORE FOCUSING

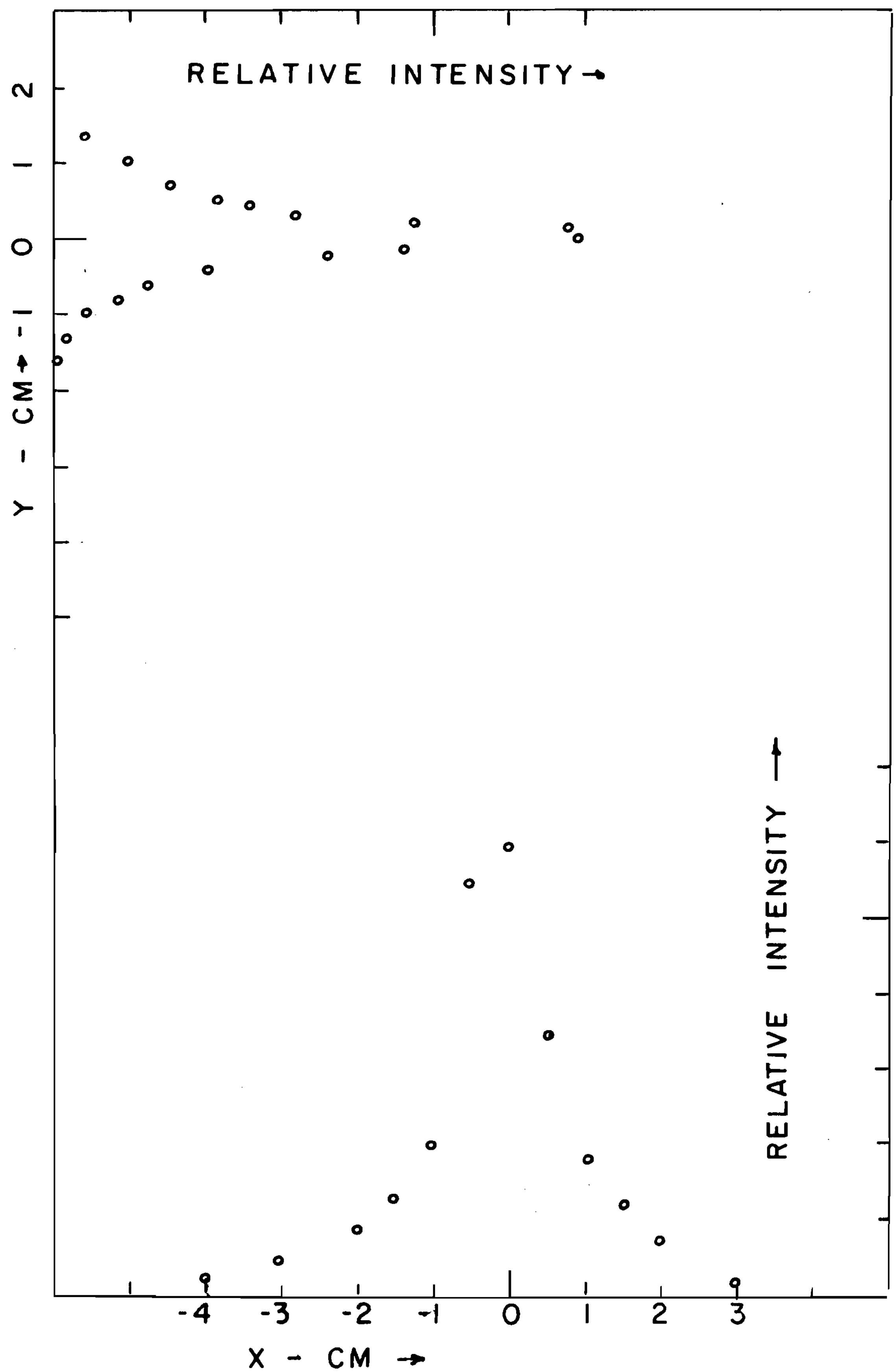
RELATIVE INTENSITY →
Y - CM →
2
1
0
-1
RELATIVE INTENSITY →
-4
-3
-2
-1
0
1
2
3
X - CM →

FIGURE 25

SPREAD OF FOCUSED EXTERNAL BEAM

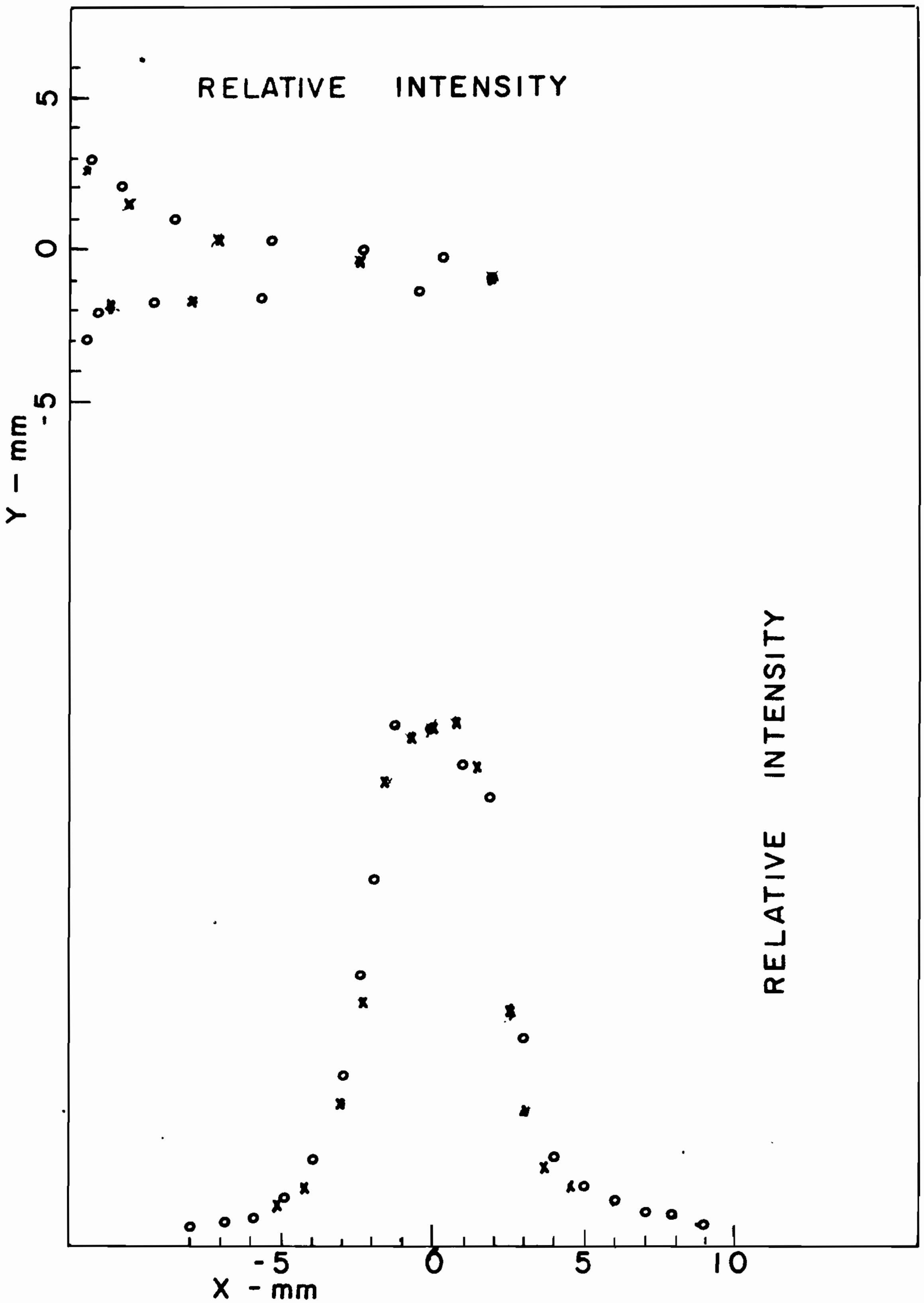
RELATIVE INTENSITY
Y - mm
5
0
-5
RELATIVE INTENSITY
-5
0
5
10
X - mm

estimated by interpolating between half-centimeter divisionsof a scale viewed by closed circuit television.

The Faraday cup output viewed on an oscilloscope indicates that the beam has a pulse length of less than 20×10^{-6} sec. and a repetition rate of 400 per second.

The energy of the protons in the external beam was determined by attenuation in aluminum absorbers. The energy from three separate determinations was measured as 97.1 ± 0.4 Mev with an energy spread determined from the range straggle of less than 1 Mev (width at half maximum intensity). The energy was calculated from the range energy curves of Rich and Madey (1954).

The current of the external beam was obtained with a Faraday cup in a vacuum chamber with a thin entrance window. The current from this cup was measured by a Keithley micromicro-ammeter Model No. 414. The readings on the Faraday cup were checked by C^{11} activation at a beam current of 2.7×10^{-9} ampere. Exact agreement was obtained ($\sim 1\%$) by using the cross section of 61.5×10^{-27} at 97 Mev from Figure 8 of Crandall et. al. (1956).

For an average internal beam current of 0.5×10^{-6} ampere at a radius of 16 inches in the cyclotron the external beam is about 4×10^{-9} ampere. The fraction of the beam which is extracted depends on the internal beam current and increases slightly for higher internal beam current. The interal beam current was measured by a copper block which is moved into the path of the orbiting protons at a radius of 16 inches.

NOTES

NOTES

NOTES

CHAPTER 8

CONCLUSION

Conclusion

In the sense that the engineering of equipment and space to handle the external beam has not yet been completed, the project of magnetic extraction of a proton beam from the McGill synchrocyclotron has not yet been completed. However an external beam of protons has been delivered into the cyclotron vault. A description of this beam has been given in the previous chapter. In conclusion, a few features of the extraction are described.

The complete extraction system is designed for easy removal and installation. Once the wall of the vacuum tank has been removed (taking about 15 minutes) the complete extraction system may be removed or installed in about 10 minutes. This greatly facilitated the adjustment of the magnetic shimming to correct the magnetic field in the vicinity of the extraction system.

Once the necessary readjustment of the magnetic field of the interior of the cyclotron was accomplished by magnetic shimming, the positional adjustment of the regenerator and each channel section was very easily carried out without breaking the cyclotron vacuum. All that was necessary was to remove the cyclotron magnetic field to free the system from the magnetic forces.

These mechanical provisions enabled the extraction project to proceed smoothly and quickly. The total time of the extraction project to date (including design of the system and setting up and calibrating of magnetic field measuring gear) has been about 18 months. The down time of the cyclotron in this period has been about 7 months. The scientific personnel involved in setting up the extraction system was one research associate and one graduate student.

The McGill synchrocyclotron is the smallest proton synchrocyclotron in which a regenerative extraction system has been installed. It has by far the smallest pole gap ($7\frac{1}{2}$ inches compared to 11.7 inches for the Harvard machine). While this narrow pole gap is economical in cyclotron magnet design, it is a handicap in designing a regenerative extraction system. The more rapid decrease of the magnet field in the fringing region of the cyclotron with a narrow pole gap necessitates a stronger regenerator. However because the vertical extent of the beam depends on the magnetic field pattern in the median plane of the machine and this pattern is very much the same in the interior of all synchrocyclotrons, the vertical aperture of this regenerator should be the same as for the machines with the wider gap.

It may be difficult to fit the iron necessary for the stronger regenerator in a narrow pole gap. In fact the aperture of the McGill deflection system had to be reduced somewhat and careful analysis and design was necessary to obtain as large an aperture as possible. However it has been shown by this thesis that with sufficient care in analysis and design, a successful regenerative extraction system can be installed in a smaller synchrocyclotron without experimental adjustment of the regenerator strength and channel size.

APPENDIX A - DESIGN FORMULAE FOR NON-LINEAR REGENERATIVE EXTRACTION

Introduction

In this appendix the design formulae for the non-linear deflection system for the McGill synchrocyclotron are derived from basic principles. Although most of the equations developed here have been published by Le Couteur in the span of three papers (1951, 1953, 1955), there is nowhere an integrated development of the mathematics of non-linear regenerative extraction in sufficiently general terms to be suitable for the McGill synchrocyclotron.

Many details of the mathematical derivations are included so that the casual reader may see more easily the approximations introduced. The approximations in the work of Le Couteur and Lipton (1955) on non-linear regenerative deflection were tailored to suit the Liverpool 156 inch synchrocyclotron and as such do not quite fit the McGill machine because of its different fringing field gradient. Hence, while the development here closely parallels that of Le Couteur it is different in detail because of the slightly different approximations involved.

Development of Equations of Motion in r and z

The basic equation used to determine the motion of protons in a magnetic field is the relativistic Lagrangian

$$L = m_o c^2 (1 - \sqrt{1-\beta^2}) + e\vec{V} \cdot \vec{A} - e\phi \qquad (1)$$

where $m_o c^2$ is the rest energy of the particle, $\vec{V}$ is the velocity of the particle in the coordinate frame in which we calculate $\vec{A}$ the magnetic vector potential and ϕ is the electric scalar potential. The equations of motion are then

$$\frac{d}{dt}\left[\frac{\partial L}{\partial \dot{q}_i}\right] - \frac{\partial L}{\partial q_i} = 0 \qquad (2)$$

where $\frac{\partial L}{\partial \dot{q}_i}$ are generalized momenta p_i . In the present problem ϕ need not be considered since the energy gain per turn of the order of 7 Kev is small compared to the particle kinetic energy of about 100 Mev. The cylindrical coordinate system (r, θ, z) with z along the central axis of the cyclotron will be used. The field B is then given by

$$\vec{B} = \vec{\nabla} \times \vec{A}$$

which implies;

$$B_r = \frac{1}{r}\frac{\partial A_z}{\partial \theta} - \frac{\partial A_\theta}{\partial z}$$

$$B_\theta = \frac{\partial A_r}{\partial z} - \frac{\partial A_z}{\partial r} \qquad (3)$$

$$B_z = \frac{1}{r}\frac{\partial}{\partial r}(r A_\theta) - \frac{1}{r}\frac{\partial A_r}{\partial \theta} .$$

Also

$$\nabla \times \vec{B} = 0$$

or

$$\frac{1}{r}\frac{\partial B_z}{\partial \theta} - \frac{\partial B_\theta}{\partial z} = 0$$

$$\frac{\partial B_z}{\partial r} - \frac{\partial B_r}{\partial z} = 0 \qquad (4)$$

$$\frac{1}{r}\frac{\partial}{\partial r}(r B_\theta) - \frac{1}{r}\frac{\partial B_r}{\partial \theta} = 0 \quad .$$

In a normal synchrocyclotron the magnetic field should be azimuthally uniform to a good approximation. Then $\frac{\partial B_z}{\partial \theta} = \frac{\partial B_r}{\partial \theta} = 0$ and from equation (4) the only possible real solution for B_θ is zero. Then from equation (3)

$$\frac{\partial A_r}{\partial z} = \frac{\partial A_z}{\partial r} = 0$$

and A_r and A_z must be arbitrary constants which one may set to zero. Then

$$B_r = -\frac{\partial A(r,z)}{\partial z}$$

$$B_z = \frac{\partial A(r,z)}{\partial r} + \frac{A(r,z)}{r} \qquad (5)$$

$$L = m_0 c^2 \left(1 - \left(1 - \frac{\dot{r}^2 + r^2\dot{\theta}^2 + \dot{z}^2}{c^2}\right)^{\frac{1}{2}}\right) + e r \dot{\theta} A(r,z) \qquad (6)$$

.

The equation in θ becomes

$$\frac{d}{dt}\left(mr^2\dot{\theta} + erA\right) = 0 \qquad (7)$$

or $$mr^2\dot{\theta} + erA = \text{cost.} \equiv P_\theta$$

and the equations in r and z become

$$\frac{d}{dt}(m\dot{r}) - \frac{\partial L}{\partial r} = 0$$
$$\frac{d}{dt}(m\dot{z}) - \frac{\partial L}{\partial z} = 0 \qquad (8)$$

Now consider the possibility of an orbit stable in r and z which is set up to have $r = r_0$ and $z = 0$. The stability is investigated by expanding $\frac{\partial L}{\partial r}$ and $\frac{\partial L}{\partial z}$ in a Taylor's series about $(r_0, 0)$. Writing $r = r_0 + \rho$,

$$\frac{\partial L}{\partial r} = \left.\frac{\partial L}{\partial r}\right|_0 + \rho\left.\frac{\partial^2 L}{\partial r^2}\right|_0 + z\left.\frac{\partial^2 L}{\partial r \partial z}\right|_0 + \frac{\rho^2}{2}\left.\frac{\partial^3 L}{\partial r^3}\right|_0 + \rho z\left.\frac{\partial^3 L}{\partial z\, \partial r^2}\right|_0$$
$$+ \frac{z^2}{2}\left.\frac{\partial^3 L}{\partial r \partial z^2}\right|_0 + \frac{\rho^3}{6}\left.\frac{\partial^4 L}{\partial r^4}\right|_0 + \frac{\rho^2 z}{2}\left.\frac{\partial^4 L}{\partial r^3 \partial z}\right|_0 + \frac{\rho z^2}{2}\left.\frac{\partial^4 L}{\partial r^2 \partial z^2}\right|_0 + \frac{z^3}{6}\left.\frac{\partial^4 L}{\partial r \partial z^3}\right|_0 + \cdots \qquad (9)$$

$$\frac{\partial L}{\partial z} = \left.\frac{\partial L}{\partial z}\right|_0 + z\left.\frac{\partial^2 L}{\partial z^2}\right|_0 + \rho\left.\frac{\partial^2 L}{\partial r \partial z^2}\right|_0 + \frac{z^2}{2}\left.\frac{\partial^3 L}{\partial z^3}\right|_0 + \rho z\left.\frac{\partial^3 L}{\partial r \partial z^2}\right|_0$$

$$+ \frac{\rho^2}{2}\left.\frac{\partial^3 L}{\partial z \partial r^2}\right|_0 + \frac{z^3}{6}\left.\frac{\partial^4 L}{\partial z^4}\right|_0 + \frac{z^2\rho}{2}\left.\frac{\partial^4 L}{\partial z^3 \partial r}\right|_0 + \frac{z\rho^2}{2}\left.\frac{\partial^4 L}{\partial z^2 \partial r^2}\right|_0 + \frac{\rho^3}{6}\left.\frac{\partial^4 L}{\partial z \partial r^3}\right|_0 + \cdots$$

$$. \qquad (10)$$

For a stable orbit $\left.\frac{\partial L}{\partial r}\right|_0 = \left.\frac{\partial L}{\partial z}\right|_0 = 0$ and $\frac{\partial^2 L}{\partial r^2}$ and $\frac{\partial^2 L}{\partial z^2}$ must be negative. $\frac{\partial^2 L}{\partial r^2}$ and $\frac{\partial^2 L}{\partial z^2}$ may then be considered to be restoring force constants. The other derivatives will determine the coupling between the r and z motion and the degree to which the restoring springs are non-linear. Equating the derivatives $\left.\frac{\partial L}{\partial r}\right|_0$ and $\left.\frac{\partial L}{\partial z}\right|_0$ to zero gives

$$\left.\frac{\partial L}{\partial r}\right|_0 = er\dot{\theta}\frac{\partial A}{\partial r} + e\dot{\theta}A + m\dot{\theta}^2 r\Big|_0 \qquad (11)$$

$$= er\dot{\theta}B_z + m\dot{\theta}^2 r\Big|_0 \doteq 0 \quad ; \qquad \dot{\theta} = -\frac{e}{m}B_{z_0}$$

$$\left.\frac{\partial L}{\partial z}\right|_0 = er\dot{\theta}\left.\frac{\partial A}{\partial z}\right|_0 = -er\dot{\theta}B\Big|_0 = 0 \qquad (12)$$

$$B_{r_0} = 0 \quad .$$

These results are very familiar and no such high-powered methods were needed to obtain them.

Considering higher derivatives;

$$\left.\frac{\partial^2 L}{\partial r \partial z}\right|_0 = -e\dot{\theta}\left(r\frac{\partial B_r}{\partial r} + B_r\right)\Big|_0 = 0$$

and similarly

$$\left.\frac{\partial^3 L}{\partial r^2 \partial z}\right|_0 = 0 \quad .$$

B_r is antisymmetric about the median plane of the cyclotron and therefore all even order derivatives of B_r with respect to z vanish at z = 0. In particular

$$\left.\frac{\partial^3 L}{\partial z^3}\right|_0 = -er\dot{\theta}_0\left.\frac{\partial^2 B_r}{\partial z^2}\right|_0 = 0 \quad .$$

Evaluating the other derivatives in a similar fashion and using equations (4) and (5) and $\frac{\partial^2 B}{\partial z^2} + \frac{\partial^2 B}{\partial r^2} = 0$ the following forms of the equations of motion are obtained;

$$
\begin{aligned}
\frac{1}{\dot{\theta}_0^2}\frac{d^2\rho}{dt^2} = & -\rho\left(1 + \left(\frac{r}{B}\frac{\partial B}{\partial r}\right)_0\right) - \frac{\rho^2}{2}\left(\frac{r}{B}\frac{\partial^2 B}{\partial r^2} + \frac{1}{B}\frac{\partial B}{\partial r} - \frac{1}{r}\right)_0 \\
& + \frac{z^2}{2}\left(\frac{1}{B}\frac{\partial B}{\partial r} + \frac{r}{B}\frac{\partial^2 B}{\partial r^2}\right)_0 + \frac{\rho z^2}{2}\left(\frac{r}{B}\frac{\partial^3 B}{\partial r^3} + \frac{2}{B}\frac{\partial^2 B}{\partial r^2}\right)_0 \\
& - \frac{\rho^3}{6}\left(\frac{r}{B}\frac{\partial^3 B}{\partial r^3} + \frac{2}{B}\frac{\partial^2 B}{\partial r^2} + \frac{1}{rB}\frac{\partial B}{\partial r} + \frac{3}{r^2}\right)_0 \\
& + \frac{\rho z^2}{2}\left(\frac{r}{B}\frac{\partial^3 B}{\partial r^3} + \frac{2}{B}\frac{\partial^2 B}{\partial r^2}\right)_0 + --- \qquad (13)
\end{aligned}
$$

$$
\begin{aligned}
\frac{1}{\dot{\theta}_0^2}\frac{d^2 z}{dt^2} = & \; z\left(\frac{r}{B}\frac{\partial B}{\partial r}\right)_0 + \rho z\left(\frac{1}{B}\frac{\partial B}{\partial r} + \frac{r}{B}\frac{\partial^2 B}{\partial r^2}\right)_0 \\
& - \frac{z^3}{6}\left(\frac{1}{B}\frac{\partial^3 B}{\partial r^3}\right)_0 + \frac{z\rho^2}{2}\left(\frac{r}{B}\frac{\partial^3 B}{\partial r^3} + \frac{2}{B}\frac{\partial^2 B}{\partial r^2}\right)_0 \\
& + --- \qquad (14
\end{aligned}
$$

where B_z is now written as B.

To design the extraction system it is necessary to follow the particles in angle rather than time. For the magnitude of radial deflection expected, the approximation $\frac{d\theta}{dt} = \dot{\theta}_o$ may not be adequate and so it is replaced by $r\frac{d\theta}{dt} = r_o\dot{\theta}_o$ whereupon to first order,

$$\frac{d^2}{dt^2} = \dot{\theta}_0^2\left[1 - \frac{2\rho}{r_o}\frac{d^2}{d\theta^2} - \frac{1}{r_o}\frac{d\rho}{d\theta}\frac{d}{d\theta}\right] \qquad (15)$$

Substituting into equations (13) and (14) the final form of the equations of motion in r and z are obtained;

$$\begin{aligned}\frac{d^2\rho}{d\theta^2} = & -\left[1 + \left(\frac{r}{B}\frac{\partial B}{\partial r}\right)\right]_o\rho - -\left[\frac{r}{B}\frac{\partial^2 B}{\partial r^2} - \frac{3}{B}\frac{\partial B}{\partial r} - \frac{5}{r}\right]_o\rho^2 \\ & + \frac{1}{2}\left[\frac{1}{B}\frac{\partial B}{\partial r} + \frac{r}{B}\frac{\partial^2 B}{\partial r^2}\right]z^2 + \frac{1}{2}\left[\frac{r}{B}\frac{\partial^3 B}{\partial r^3} - \frac{2}{Br}\frac{\partial B}{\partial r}\right]\rho z^2 \\ & - \frac{1}{6}\left[\frac{1}{B}\frac{\partial^3 B}{\partial r^3} - \frac{4}{B}\frac{\partial^2 B}{\partial r^2} - \frac{5}{Br}\frac{\partial B}{\partial r} + \frac{9}{r^2}\right]_o\rho^3 + \frac{1}{r}\left[\frac{d\rho}{d\theta}\right]^2 \\ & + - - -\end{aligned} \qquad (16)$$

$$\begin{aligned}\frac{d^2 z}{d\theta^2} = & \left[\frac{r}{B}\frac{\partial B}{\partial r}\right]_o z + \left[\frac{r}{B}\frac{\partial^2 B}{\partial r^2} - \frac{1}{B}\frac{\partial B}{\partial r}\right]_o\rho z \\ & - \frac{1}{6}\left[\frac{1}{B}\frac{\partial^2 B}{\partial r^2}\right]_o z^3 + \frac{1}{2}\left[\frac{r}{B}\frac{\partial^3 B}{\partial r^3} - \frac{2}{B}\frac{\partial^2 B}{\partial r^2} - \frac{4}{Br}\frac{\partial B}{\partial r}\right]_o z\rho^2 \\ & + \frac{1}{r}\left[\frac{d\rho}{d\theta}\right]\left[\frac{dz}{d\theta}\right] \qquad + - - -\end{aligned} \qquad (17)$$

These equations of motion are equations of displacement in terms of azimuthal angle. Velocities may now be expressed as derivatives with respect to angle rather than time and frequencies describing oscillatory motion are then expressed as multiples of orbital frequency for the equilibrium orbit.

At this point the pattern of the magnetic field in an actual synchrocyclotron is to be considered (see Figure 9, Chapter 3, for the pattern in the McGill machine). The field is fairly well described by saying that $n = - r/B \, \partial B/\partial r$ has a constant value out to a certain radius r_o where it suddenly starts to increase. The region of the cyclotron in which r is less than r_o is considered to be the "interior" of the machine, and the region in which r is greater than r_o is considered to be the "exterior" or "fringing" region.

The equations of motion for protons orbiting in the interior of the machine are

$$\begin{aligned} \frac{d^2\rho}{d\theta^2} &= -\left(\left(\frac{r}{B}\frac{\partial B}{\partial r}\right) + 1\right)\rho = -(1-n)\rho \\ \frac{d^2 z}{d\theta^2} &= \left(\frac{r}{B}\frac{\partial B}{\partial r}\right) z = -n\,z \quad . \end{aligned} \tag{18}$$

These equations of motion show that the protons may oscillate radially about the equilibrium value of r, with a frequency equal to $(1-n)^{\frac{1}{2}}$ and may oscillate vertically about $z = 0$ with a frequency equal to $n^{\frac{1}{2}}$.

For protons orbiting in the fringing area of the cyclotron, the higher derivatives in equations (16) and (17) must be considered. In this region, the field may be expressed as a Taylor's expansion about $r = r_o$;

$$B(\rho) = B + \left(\frac{\partial B}{\partial r}\right)_o \rho + \frac{1}{2}\left(\frac{\partial^2 B}{\partial r^2}\right)_o \rho^2 + \frac{1}{6}\left(\frac{\partial^3 B}{\partial r^3}\right)_o \rho^3 + - - \tag{19}$$

where $\rho = (r-r_o)$ and the expansion holds for $\rho \geqslant 0$.

Le Couteur found that the fringing field of the Liverpool machine could be adequately expressed by keeping only terms of second order. Consequently many of the higher derivatives in the coupled equations of motion (16) and (17) do not appear in his development. However to express the fringing field of the McGill machine it was felt that the term in ρ^3 had to be included. Numerical analysis of the fringing field measurement of Chapter 3 gave the following values as the best fit;

$$r_o = 36 \text{ in.}$$

$$B_o = 16{,}000 \text{ gauss}$$

$$\left[\frac{\partial B}{\partial r}\right]_o = -24 \text{ gauss/in}$$

$$\left[\frac{\partial^2 B}{\partial r^2}\right]_o = -108 \text{ gauss/in}^2$$

$$\left[\frac{\partial^3 B}{\partial r^3}\right]_o = -96 \text{ gauss/in}^3 \quad .$$

In non-linear regenerative deflection of a synchrocyclotron beam useful acceleration of the protons is considered to stop at $r = r_o$. The protons orbiting at this radius then have their orbit centers moved away from the center of the machine so that, eventually, with sufficient motion of the orbit center in one orbit, the protons may be made to enter a magnetic channel. (see Chapter 2 - The Non-Linear Regenerative

Deflection System).

A total deflection of about 2 inches should be adequate to allow the beam to be picked up in a magnetic channel. For $\rho \leq 2$ inches the above coefficients give a calculated magnetic field $B(\rho)$ which agrees with the measured values to within the instrumental accuracy (0.1%). Substituting these values into equations (16) and (17) one obtains

$$\frac{d^2\rho}{d\theta^2} = -0.946\rho(1 - 0.20\rho - 0.03\rho^2 + 0.12z^2) - 0.12z^2$$

$$\frac{d^2z}{d\theta^2} = -(0.054 + 0.24\rho + 0.10\rho^2)z \quad .$$

In these equations the term $0.001\ z^3$ and the velocity^2 terms have been neglected. The equations obtained by Le Couteur and Lipton (1955) for the Liverpool machine were

$$\frac{d^2\rho}{d\theta^2} = -0.955\rho(1 - 0.52\rho) - 0.13\ z^2$$

$$\frac{d^2z}{d\theta^2} = -(0.045 + 0.26\rho)z \quad .$$

The problem in designing the non-linear regenerative deflection system is to obtain sufficient motion of the orbit center while keeping this motion in a straight line towards the channel system and while maintaining vertical stability.

In passing the reader may note that the reason for the familiar vertical "blow-up" for protons oscillating about an equilibrium orbit at n = 0.2, is easily seen. Considering that in this field region, higher derivatives are strong, the coefficient of the term ρz in equation (17) must be significant. The change in $dz/d\theta$ as θ increases from θ_1 to θ_2 may be obtained by integrating equation (17) once with respect to θ. The motion in ρ and z may not be simple harmonic in this region but it is still oscillatory with fundamental frequencies of oscillation. By having the range of integration $(\theta_2 - \theta_1)$ corresponding to a number of complete cycles in z, the term $\left(\frac{r}{B}\frac{\partial B}{\partial r}\right)_0 z$ will give no contribution in the integration. Considering then the contribution of the term ρz, we have

$$\left(\frac{dz}{d\theta}\right)_2 - \left(\frac{dz}{d\theta}\right)_1 \quad \propto \quad \int_{\theta_1}^{\theta_2} \rho z \, d\theta \qquad .$$

If the fundamental frequencies of radial and vertical oscillation are related by integers, the integral on the R. H. S. has a finite value. This value is proportional to the amplitude of the radial oscillation. If the relating integer is large, the value of this integral may not be significant (except for very large radial oscillations) but at n = 0.2, the radial frequency is only twice the vertical frequency.

If the amplitude of the radial oscillation is very small this is still not serious. However for a typical synchrocyclotron a large fraction of the protons may have a radial amplitude of oscillation as large as ½ inch. Since the radial frequency is twice the vertical frequency, the energy of this radial oscillation, if it were transferred completely to the vertical oscillation, would result in a vertical oscillation amplitude of 1 inch. Such a vertical extent of the beam is intolerable.

<u>Character of the Radial Motion</u>

A proton with an equilibrium orbit of radius r_0 but with its orbit center shifted from the center of the machine, moves through two regions of the machine; one in which $\rho < 0$ and the other in which $\rho > o$ (Figure A1).

The character of the radial motion for $\rho < o$ is simple harmonic with frequency, say, Ω . In the region $\rho > o$ it is not simple harmonic but still is oscillatory with a fundamental frequency, say, Ω' where Ω' is a function of the radial oscillation amplitude in this region.

The regenerator is a narrow wedge (in θ) of radial field gradient placed as indicated in Figure A1 in the region $\rho > o$. Its field gradient, integrated over the azimuthal angle for which it is effective, is the quantity which is to be designed to give the required regenerative deflection. In the mathematical treatment of this appendix, the regenerator is considered to subtend practically zero azimuthal angle.

The radial motion is then considered in three parts; the angle g to where the proton crosses r_o after leaving the regenerator, the angle k where the proton remains in the region $\rho < o$ and the angle h to return to the regenerator. In the azimuthal region k the radial oscillation goes through one half cycle. The angle k is therefore given by $\Omega K = \pi$.

In considering the motion of a proton in this system it is most convenient to express the displacement and velocity in one coordinate as a two dimensional vector and to represent the effect on this vector of passing through a region of the machine as a 2 x 2 transfer matrix for this region. If the radial displacement and velocity are expressed in the units used throughout this development, this vector is $\begin{pmatrix} \rho \\ \frac{d\rho}{d\theta} \end{pmatrix}$.
If a particle described by this vector enters the region g,

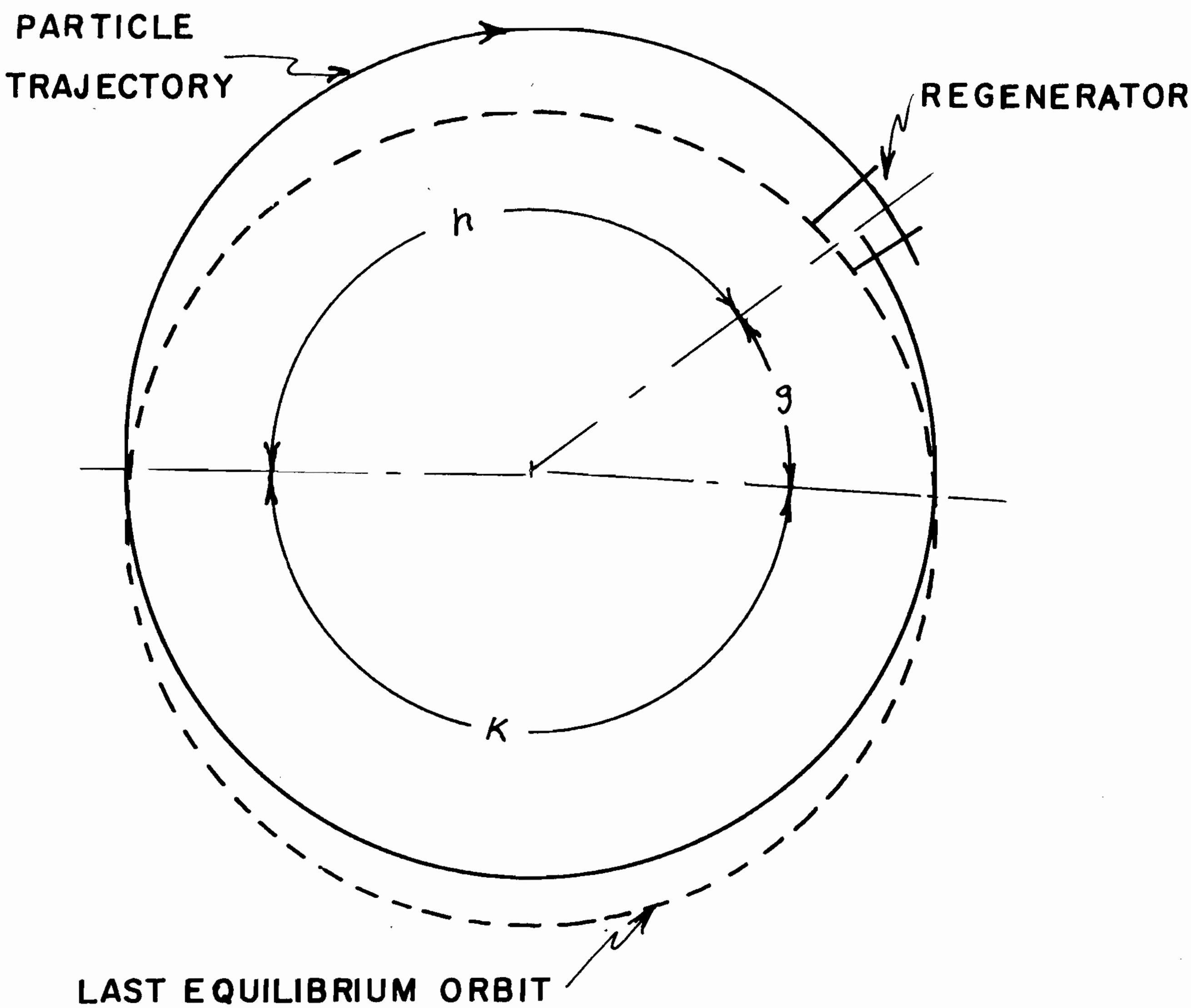

FIGURE A1 - AZIMUTH POSITION OF REGENERATOR then its descriptive vector for the radial motion on leaving g is given by $G_r \begin{pmatrix} \rho \\ \frac{d\rho}{d\theta} \end{pmatrix}$ where G_r is the 2 x 2 transfer matrix representing the change in the radial motion on passing through G.

Measuring θ from the regenerator position, the motion in θ (assuming it to be simple harmonic) is given by

$$\rho = \rho_M \sin(\Omega'\theta + \psi)$$

$$\frac{d\rho}{d\theta} = \Omega'\rho_M \cos(\Omega'\theta + \psi)$$

where ψ represents the phase of the radial motion of the particle as it leaves the regenerator and enters region g. The radial motion at entrance to g is then $\begin{pmatrix} \rho_M \sin\psi \\ \Omega'\rho_M \cos\psi \end{pmatrix}$ and using the usual expansion for the sine and cosine the motion at θ is described by

$$\begin{pmatrix} \rho \\ \frac{d\rho}{d\theta} \end{pmatrix} = \begin{pmatrix} \rho_M \sin\psi \cos\Omega'\theta + \rho_M \cos\psi \sin\Omega'\theta \\ \Omega'\rho_M \cos\psi \cos\Omega'\theta - \Omega'\rho_M \sin\psi \sin\Omega'\theta \end{pmatrix}$$

which may be factored to

$$\begin{pmatrix} \rho \\ \frac{d\rho}{d\theta} \end{pmatrix} = \begin{pmatrix} \cos\Omega'\theta & \frac{1}{\Omega'}\sin\Omega'\theta \\ -\Omega'\sin\Omega'\theta & \cos\Omega'\theta \end{pmatrix} \begin{pmatrix} \rho \sin\psi \\ \Omega'\rho\cos\psi \end{pmatrix}.$$

The transfer matrix for G_r is thus seen to be

$$G_r = \begin{pmatrix} \cos\Omega' g & \frac{1}{\Omega'}\sin\Omega' g \\ -\Omega'\sin\Omega' g & \cos\Omega' g \end{pmatrix}.$$

Similarly for region k and h it may be seen that

$$K_r = \begin{pmatrix} \cos\Omega k & \frac{1}{\Omega}\sin\Omega k \\ -\Omega\sin\Omega k & \cos\Omega k \end{pmatrix}$$

$$H_r = \begin{pmatrix} \cos\Omega' h & \frac{1}{\Omega'}\sin\Omega' h \\ -\Omega\sin\Omega' h & \cos\Omega' h \end{pmatrix} .$$

The transfer matrix for a narrow regenerator may be set as

$$R_r \begin{pmatrix} 1 & 0 \\ -T_r & 1 \end{pmatrix}$$

where

$$T_r \equiv -\frac{1}{\rho}\left[\left(\frac{d\rho}{d\theta}\right)_{out} - \left(\frac{d\rho}{d\theta}\right)_{in}\right]_{REGEN}$$
$$= -\frac{1}{\rho}\,\frac{r_o}{B_o}\left(1 + \frac{\rho}{r_o}\right)^2 \int \Delta B\, d\theta \quad .$$

(ΔB is the field change introduced by the regenerator).

Consider a particle whose motion on entering the regenerator for the m^{th} time is described by $\begin{pmatrix} \rho \\ \frac{d\rho}{d\theta} \end{pmatrix}_m$. As it is about to enter the regenerator for the $m+1^{th}$ time its radial motion may be described by

$$\begin{pmatrix} \rho \\ \frac{d\rho}{d\theta} \end{pmatrix}_{m+1} = A_r \begin{pmatrix} \rho \\ \frac{d\rho}{d\theta} \end{pmatrix}_m$$

where $A_r = H_r K_r G_r R_r$.

Evaluating A_r by multiplying one obtains

$$A_r = \begin{pmatrix} \alpha & \beta \\ \gamma & \delta \end{pmatrix}$$

where

$$\alpha = \cos \Omega' f - \frac{T_r}{\Omega'} \sin \Omega' f$$

$$\beta = \frac{1}{\Omega} \sin \Omega' f$$

$$\gamma = -T_r \cos \Omega' f - \Omega' \sin \Omega' f$$

$$\delta = \cos \Omega' f$$

and

$$f = 2\pi + \left(\frac{\pi}{\Omega'} - \frac{\pi}{\Omega} \right) \quad .$$

If we let $\begin{pmatrix} \rho \\ \frac{d\rho}{d\theta} \end{pmatrix}_0$ represent the particles radial motion on entering the regenerator for the first time we have

$$\begin{pmatrix} \rho \\ \frac{d\rho}{d\theta} \end{pmatrix}_m = A^m \begin{pmatrix} \rho \\ \frac{d\rho}{d\theta} \end{pmatrix}_0 \quad .$$

The matrices G_r, K_r, H_r and R_r have determinant unity and therefore so does A_r. The product of the eigenvalues of A_r must then be unity as well. Let the eigenvalues of A_r be e^{Λ} and $e^{-\lambda}$ and the corresponding eigenvectors be $\begin{pmatrix} u \\ v \end{pmatrix}$ and $\begin{pmatrix} u' \\ v' \end{pmatrix}$. Then

$$A_r \begin{pmatrix} u \\ v \end{pmatrix} = e^{\Lambda} \begin{pmatrix} u \\ v \end{pmatrix}$$

$$A_r \begin{pmatrix} u \\ v \end{pmatrix} = e^{-\Lambda} \begin{pmatrix} u' \\ v' \end{pmatrix} \quad .$$

Since these two eigenvectors are a complete set, the motion of a proton entering the regenerator for the first time is described by

$$\begin{pmatrix} \rho \\ \frac{d\rho}{d\theta} \end{pmatrix}_0 = x \begin{pmatrix} u \\ v \end{pmatrix} + y \begin{pmatrix} u' \\ v' \end{pmatrix}$$

where

$$x = \frac{\left(\frac{d\rho}{d\theta}\right)_0 u' - \rho_0 v'}{u'v - v'u}$$

$$y = \frac{\left(\frac{d\rho}{d\theta}\right)_0 - \rho_0 v}{uv' - vu'} .$$

Then

$$\begin{pmatrix} \rho \\ \frac{d\rho}{d\theta} \end{pmatrix}_m = A_r^m \left(x \begin{pmatrix} u \\ v \end{pmatrix} + y \begin{pmatrix} u' \\ v' \end{pmatrix} \right)$$

$$= x\, e^{m\Lambda} \begin{pmatrix} u \\ v \end{pmatrix} + y\, e^{-m\Lambda} \begin{pmatrix} u' \\ v' \end{pmatrix} .$$

If the regenerator is so built that e^{Λ} is significantly greater than one, after a few revolutions we have

$$\begin{pmatrix} \rho \\ \frac{d\rho}{d\theta} \end{pmatrix}_m = x e^{m\Lambda} \begin{pmatrix} u \\ v \end{pmatrix} .$$

It may be worthwhile to try to clarify this with a graphical sketch (Figure A2). It should be noted that since Ω, Ω' are both less than unity the radial motion, without the regenerator, does not go through a complete cycle in one orbit. The regenerator makes up for this by being a strong radial focusing device which curls the protons back into the machine.

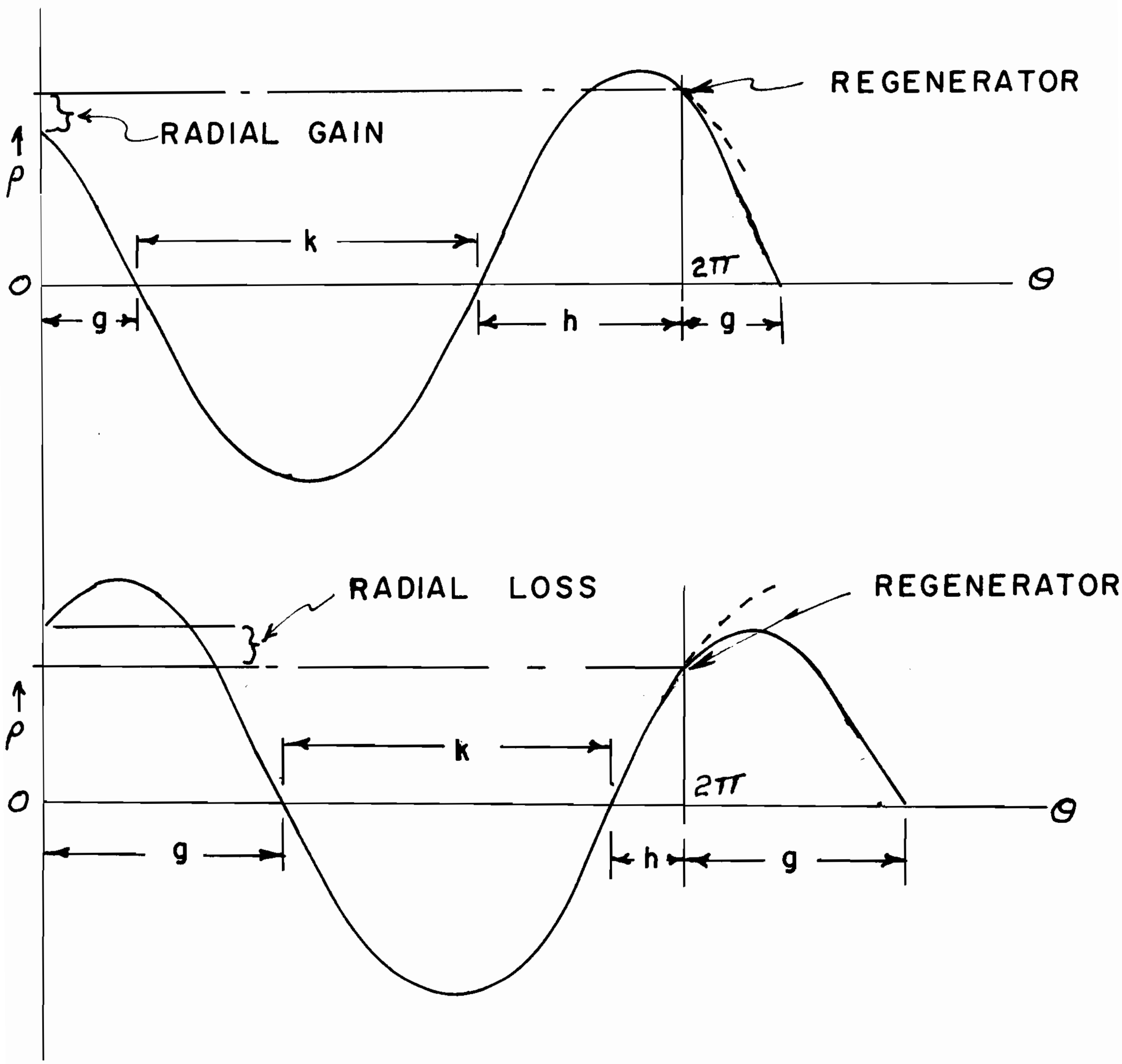

FIGURE A2 REGENERATOR EIGENVECTOR PHASES so that they start the next orbit at the same phase as the previous. The two eigenvector solutions for A_r indicate that there are two starting phases for which the regenerator is able to accomplish this. These are sketched in Figure A2. It is seen that in one case the amplitude of the radial oscillation is increased and in the other it is diminished. These correspond to the eigenvalues e^{Λ} and $e^{-\Lambda}$ respectively.

To evaluate e^{Λ} it is only necessary to note that the sum of the eigenvalues is equal to the spur of the matrix A_r. Then

$$e^{\Lambda} + e^{-\Lambda} = 2\cosh\Lambda = \alpha + \beta$$

$$\cosh\Lambda = \cos\Omega' f - \frac{T_r}{2\Omega'} \sin\Omega' f \quad . \qquad (23)$$

This determines the radial gain factor e^{Λ}. To determine the phase angle of the motion one must determine the eigenvector $\begin{pmatrix} u \\ v \end{pmatrix}$. From

$$A\begin{pmatrix} u \\ v \end{pmatrix} = \begin{pmatrix} \alpha & \beta \\ \gamma & \delta \end{pmatrix}\begin{pmatrix} u \\ v \end{pmatrix} = e^{\Lambda}\begin{pmatrix} u \\ v \end{pmatrix}$$

$$(\alpha - e^{\Lambda})u + \beta v = 0$$

$$\gamma u \qquad (\delta - e^{\Lambda})v = 0$$

which yields the one solution

$$\frac{u}{v} = \frac{\beta}{e^{\Lambda} - \alpha}$$, u or v arbitrary.

For simplicity set $u = \beta$ so that $v = e^{\Lambda} - \alpha$.

Consider again the motion on leaving the regenerator for the m^{th} time. Recall that this may be written as

$$\begin{pmatrix} \rho \\ \frac{d\rho}{d\theta} \end{pmatrix} = \rho_{MAX} \begin{pmatrix} \sin\psi \\ \Omega'\cos\psi \end{pmatrix}$$

where ψ determines the phase of the motion. From

$$\rho_{MAX} \begin{pmatrix} \sin\psi \\ \Omega'\cos\psi \end{pmatrix} = x e^{m\Lambda} \begin{pmatrix} 1 & 0 \\ -T & 1 \end{pmatrix} \begin{pmatrix} u \\ v \end{pmatrix}$$

one obtains

$$\cot\psi = \frac{-T_r u + v}{\Omega' u} = \frac{e^{\Lambda} - \cos\Omega' f}{\sin\Omega' f} \quad . \qquad (24)$$

The radial motion after the regenerator is then given by

$$\rho = \rho_{MAX} \sin(\Omega'\theta + \psi) \quad ; \quad \rho_{MAX} = K e^{m\Lambda} \qquad (25)$$

whereupon ρ vanishes at $\theta = \pi - \frac{\psi}{\Omega'} = g$. The value of g is thus determined.

Character of the Vertical Motion

While achieving the desired radial expansion of the beam it is necessary to avoid vertical instability and for high efficiency of extraction the vertical expansion must be minimized. The choice of radial expansion factor e^{Λ} must take this into account.

As in the discussion of radial motion, the proton is considered to move in three different regions; in region g where the vertical oscillation frequency is effectively ω', in k where it is ω where $\omega < \omega'$ and in h back to the regenerator where it is again ω'. Starting at the radial node between the regions g and k the effect on the vertical motion of one orbit may be written as

$$\begin{pmatrix} z \\ \frac{dz}{d\theta} \end{pmatrix}_{m+1} = A_z \begin{pmatrix} z \\ \frac{dz}{d\theta} \end{pmatrix}_m \qquad A_z = G_z R_z H_z K_z = \begin{pmatrix} a & b \\ c & d \end{pmatrix}$$

where K_z, H_z, G_z, R_z represent the vertical motion transfer matrices in the regions k, h, g, and the regenerator respectively.

Evaluation of these matrices gives

$$K_z = \begin{pmatrix} \cos\omega k & \frac{1}{\omega}\sin\omega k \\ -\omega\sin\omega k & \cos\omega k \end{pmatrix}$$

$$H_z = \begin{pmatrix} \cos\omega' h & \frac{1}{\omega'}\sin\omega' h \\ -\omega'\sin\omega' h & \cos\omega' h \end{pmatrix}$$

$$R_z = \begin{pmatrix} 1 & 0 \\ T_z & 1 \end{pmatrix}$$

$$G_z = \begin{pmatrix} \cos\omega' g & \frac{1}{\omega'}\sin\omega' g \\ \omega'\sin\omega' g & \cos\omega' g \end{pmatrix}$$

$$T \equiv -\left[\left(\frac{dz}{d\theta}\right)_{out}-\left(\frac{dz}{d\theta}\right)_{in}\right]_{REGEN.} = \frac{r_0}{B_0}\left(1+\frac{\rho}{r_0}\right)^2 z\int\frac{\partial(\Delta B)}{\partial r}d\theta$$

$$a = \cos\omega k\cos\omega'(g+h) - \frac{\omega}{\omega'}\sin\omega k\sin\omega'(g+h)$$

$$+\frac{T_z}{\omega'}\sin\omega' g\left(\cos\omega k\cos\omega' h - \frac{\omega}{\omega'}\sin\omega k\sin\omega' h\right)$$

$$b = \frac{1}{\omega}\sin\omega k\cos\omega'(g+h) + \frac{1}{\omega}\cos\omega k\sin\omega'(g+h)$$

$$+\frac{T_z}{\omega'}\sin\omega' g\left(\frac{1}{\omega}\cos\omega' h\sin\omega k + \frac{1}{\omega'}\sin\omega' h\cos\omega k\right)$$

$$c = -\omega\sin\omega k\cos\omega'(g+h) - \omega'\cos\omega k\sin\omega'(g+h)$$

$$-\frac{T_z}{\omega'}\cos\omega' g\left(\omega'\cos\omega k\cos\omega' h - \omega\sin\omega k\sin\omega' h\right)$$

$$d = \cos\omega k\cos\omega'(g+h) - \frac{\omega'}{\omega}\sin\omega k\sin\omega'(g+h)$$

$$+\frac{T_z}{\omega'}\cos\omega' g\left(\cos\omega k\sin\omega' h + \frac{\omega'}{\omega}\sin\omega k\cos\omega' h\right).$$

Constrained vertical motion requires that the eigenvalues of A_Z be of the form $e^{\pm i\lambda}$, i. e. the phase of the vertical oscillation may change in one orbit but not its amplitude. From

$$e^{i\lambda} + e^{-i\lambda} = a + d$$

$$\cos\lambda = \cos(\omega k + \omega'(g+h)) - \frac{(\omega'-\omega)^2}{2\omega\omega'}\sin\omega k\sin\omega'(g+h)$$

$$\frac{T}{2\omega'}\left\{\sin(\omega k+\omega'(g+h)) + \frac{(\omega'-\omega)^2}{2\omega\omega'}\sin\omega k\cos\omega'(g+h) + \frac{\omega'^2-\omega^2}{2\omega\omega'}\sin\omega k\cos\omega'(h-g)\right\} \qquad (26)$$

Let the eigenvectors of A_z be $\begin{pmatrix} u \\ v \end{pmatrix}, \begin{pmatrix} u' \\ v' \end{pmatrix}$. Then for eigenvalue $e^{i\lambda}$

$$A_z \begin{pmatrix} u \\ v \end{pmatrix} = e^{i\lambda} \begin{pmatrix} u \\ v \end{pmatrix}$$

$$(a - e^{i\lambda})u + bv = 0$$

$$cu + (d - e^{i\lambda})v = 0 \quad .$$

These are two linear homogenous equations in u, v for which the determinant of the coefficients of u and v may be shown to be zero. Then u and v are connected by the equation

$$u = \frac{bv}{e^{i\lambda} - a} \quad .$$

In choosing the phase of the particle, one may arbitrarily set u to be real and write v as e^{iy}. Equating imaginary parts one obtains immediately

$$\sin y = \frac{u \sin \lambda}{b} \quad .$$

Equating real parts, after a little manipulation one obtains $u^2 = -\frac{b}{c}$. The eigenvector $\begin{pmatrix} u' \\ v' \end{pmatrix}$ becomes $\begin{pmatrix} u \\ e^{-iy} \end{pmatrix}$. The initial conditions of the vertical motion may be expressed in terms of the eigenvectors as

$$\begin{pmatrix} z \\ \frac{dz}{d\theta} \end{pmatrix}_0 = \text{const} \left(e^{i\varphi} \begin{pmatrix} u \\ e^{iy} \end{pmatrix} + e^{-i\varphi} \begin{pmatrix} u \\ e^{-iy} \end{pmatrix} \right)$$

$$= 2\text{const} \begin{pmatrix} u \cos \\ \cos(\varphi + y) \end{pmatrix} \quad .$$

After N turns the motion becomes

$$\begin{pmatrix} z \\ \frac{dz}{d\theta} \end{pmatrix} = 2 \text{ const} \begin{pmatrix} u\cos(\varphi + n\lambda) \\ \cos(\varphi + \gamma + n\lambda) \end{pmatrix} .$$

The amplitude h_N of the vertical oscillation after N turns is given by

$$h_N^2 = z_N^2 + \left(\frac{\frac{dz}{d\theta}}{\omega}\right)^2$$

$$= \frac{2(\text{const})^2}{\omega}(1 + \omega^2 u^2)(1 + \cos\epsilon \cos 2(\mu + \varphi + n\lambda))$$

where

$$\tan 2\mu = \frac{\sin 2y}{\omega^2 u^2 + \cos 2y}$$

$$\sin\epsilon = \frac{2\omega \sin}{1 + \omega^2 u^2} = \frac{2\sin\lambda}{-\frac{c}{\omega} + b\omega} . \quad (27)$$

Then

$$\frac{h_n}{h_0}^2 = \frac{1 + \cos\epsilon \cos 2(\mu + \varphi + n\lambda)}{1 + \cos\epsilon \cos 2(\mu + \varphi)} .$$

The maximum value of this ratio is

$$\frac{h_{MAX}}{h}^2 = \frac{1 + \cos\epsilon}{1 - \cos\epsilon} \quad (28)$$

Sin ϵ is determined from equation (27) and λ in equation (27) is determined from equation (26). The denominator in expression (27) may be shown to be

$$-\frac{c}{\omega}+b\,\omega = 2\ \sin(\omega\ k+\omega'(g+h)) + \frac{(\omega'-\omega)^2}{\omega\,\omega'}\cos\omega k\sin\omega'(g+h)$$

$$-\frac{T_z}{\omega}\Big\{\cos(\omega k+\ \omega'(g+h))\ +\frac{(\omega'-\omega)^2}{\omega\ \omega'}\cos\omega k\cos\omega'(g+h)$$

$$+\frac{\omega'^2-\omega^2}{2\omega\ \omega'}\cos\omega k\ \cos\ \omega'(h-g)\Big\}\ . \tag{29}$$

Calculation of Radial and Vertical Oscillation Frequencies

To use the above equations it is necessary to know the vertical and radial oscillation frequencies ω' and Ω'. In the case of radial motion, one quarter period may be obtained by calculating the angle in which ρ changes from zero to ρ_{max}. Integrating equation (18) from ρ_{max} to ρ one obtains

$$\left(\frac{d\rho}{d\theta}\right)^2 = 0.946(\rho_M^2-\rho^2) - 0.13(\rho_M^3-\rho^3) - 0.015\ (\rho_M^4-\rho^4)$$
$$-\ 0.24\int_{\rho_M}^{\rho} z^2(1+0.95\rho)\,d\rho\ .$$

z is not a single valued function ~~function~~ of ρ but its maximum value must not be greater than about 0.4 inches. The r.m.s. value should then be of the order of 0.30 inches and one obtains

$$-\int_{\rho_M}^{\rho} z^2(1\ +\ 0.95\,\rho)\,d\rho\ \sim\ 0.08(\rho_M-\rho)+0.04(\rho_M-\rho)$$

$$\left(\frac{d\rho}{d\theta}\right) = -\Big[0.02(\rho_M-\rho)\ +0.95(\rho_M^2-\rho^2)$$
$$-0.13(\rho_M^3-\rho^3)-0.015(\rho_M^4-\rho^4)\Big]^{\frac{1}{2}}\ .$$

One quarter period is given by

$$\frac{\pi}{2\Omega'} = \int_{\rho_{MAX}}^{\rho} \frac{d\rho}{\left(\frac{d\rho}{d\theta}\right)} .$$

This is one form of the general elliptical integral and may be evaluated by the standard methods in terms of the elliptical integral of the first kind. However with a computer a numerical integration is probably easier. The results are plotted in Figure A3.

The effective vertical oscillation frequency may be obtained by averaging the coefficient of z in equation (19) over the approximately π radians for which the proton travels in the region $\rho > 0$. Then on obtains

$$\omega' = \frac{1}{\pi}\int_0^{\pi} (0.054 + 0.24\rho + 0.10\rho)\, d\phi$$

where

$$\rho = \rho_{MAX} \sin\phi .$$

Results of a numerical integration for ω' are also plotted in Figure A3.

Regenerator Field Design.

It is now possible to check the behaviour of regenerator designs. Considering a regenerator field strength

$$\frac{r_o}{B_o}\int_{REGEN} \Delta B \, d\theta = A\rho + B\rho^2$$

where ΔB is the field increment in the regenerator, the problem is to find values of A and B which result in suitable values of e^{Λ} but also keep the vertical expansion within reasonable limits $(h_N/h_o \sim 2$ or $\cos\epsilon \sim 0.6)$. The regenerator radial and vertical actions are given by

$$-T_r \rho = -\frac{r_o}{B_o}\left(1 + \frac{\rho}{r_o}\right)^2 \int \Delta B \, d\theta$$

$$T_z z = \frac{r_o}{B_o}\left(1 + \frac{\rho}{r}\right)^2 \int \frac{\partial(\Delta B)}{\partial r} \, d\theta \quad .$$

To first order

$$T_r \doteq A + \left(B + \frac{2A}{r_o}\right)\rho$$

$$T_z = A + \left(2B + \frac{2A}{r_o}\right)\rho \quad .$$

A plot of the radial gain factor e^{Λ} obtained from equation (20) versus T_r is given in Figure A4. To be able to extract a beam it is necessary to have a radial gain factor of about 1.3 to 1.4 at $\rho = 1\frac{1}{2}$ to 2 inches. It takes a value of $T_r = 0.17$ to initate the regenerator action at $\rho = 0$ and it would seem that a value of $T_r = 0.2$ ($e^{\Lambda} = 1.05$) would be about the smallest practical value. Starting at a trial value of $T_r = 0.20$ at $\rho = 0$ and of $T_r = 0.8$ at $\rho = 1\frac{1}{2}$ inches gives

$$A = 0.2$$

$$B = 0.4 \quad .$$

Computing e^{Λ}, g, and $\cos\epsilon$ from equations (23), (24), (26), (27), (28), (29) and a knowledge of Ω' and ω' gives the values plotted in Figures A4, A5, A6. Calculations were carried out for various values of B.

It should be noted that the appropriate value of T_r at $\rho_{max} = 2$ inches is the value for ρ in the regenerator of about $1\frac{1}{2}$ inches. This is because the regenerator azimuth is not that for maximum radial displacement. The radial displacement at the regenerator is $\rho = \rho_{max} \sin \Omega' g$. The value of g was computed by calculating T_r from

$$T_r = A + \left(B + \frac{2A}{r_o}\right)\rho_{MAX}$$

and then recalculating T_r, after obtaining g, from

$$T_r = A + \left(B + \frac{2A}{r}\right)\rho_{MAX} \sin \Omega' g \quad .$$

A new value of g was obtained from this new T_r and the process cycled until self-consistent values of T_r and g were obtained.

The plot of $\hat{e}$ as a function of ρ_{max} indicates that with an initial displacement of the order of 0.01 inches or less in the regenerator, at least 50 orbits will have to be made to reach $\rho_{max} = 2$ inches. The number of orbits is large because the initial gain factor is so low (1.05) and it may be advisable to increase A if it can be done without causing vertical instability. However it should be noted that 30 of the 50 orbits occur in the first 0.1 inches of displacement.

It would appear from the curves of Figures A4, A5, and A6 that A = 0.2 and B = 0.4 keep the vertical motion restrained and at the same time give the necessary radial displacement. This regenerator strength was the design attempted but the regenerator iron blocks were made up of 1/8 inch plates to facilitate adjustment of the regenerator strength if it should prove necessary.

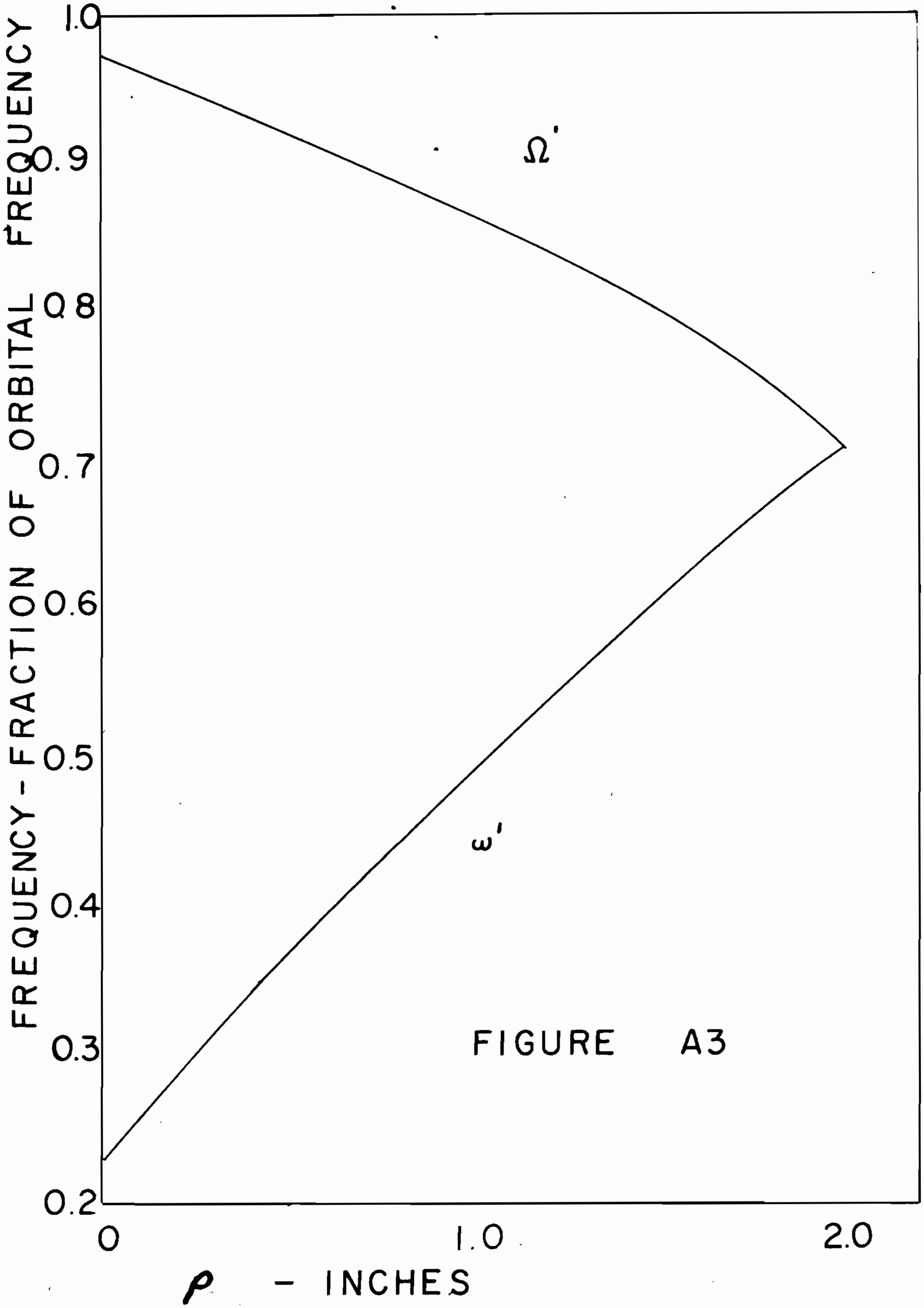
FREQUENCY - FRACTION OF ORBITAL FREQUENCY
1.0
0.9
0.8
0.7
0.6
0.5
0.4
0.3
0.2
Ω'
ω'
0
1.0
2.0
ρ - INCHES

FIGURE A3

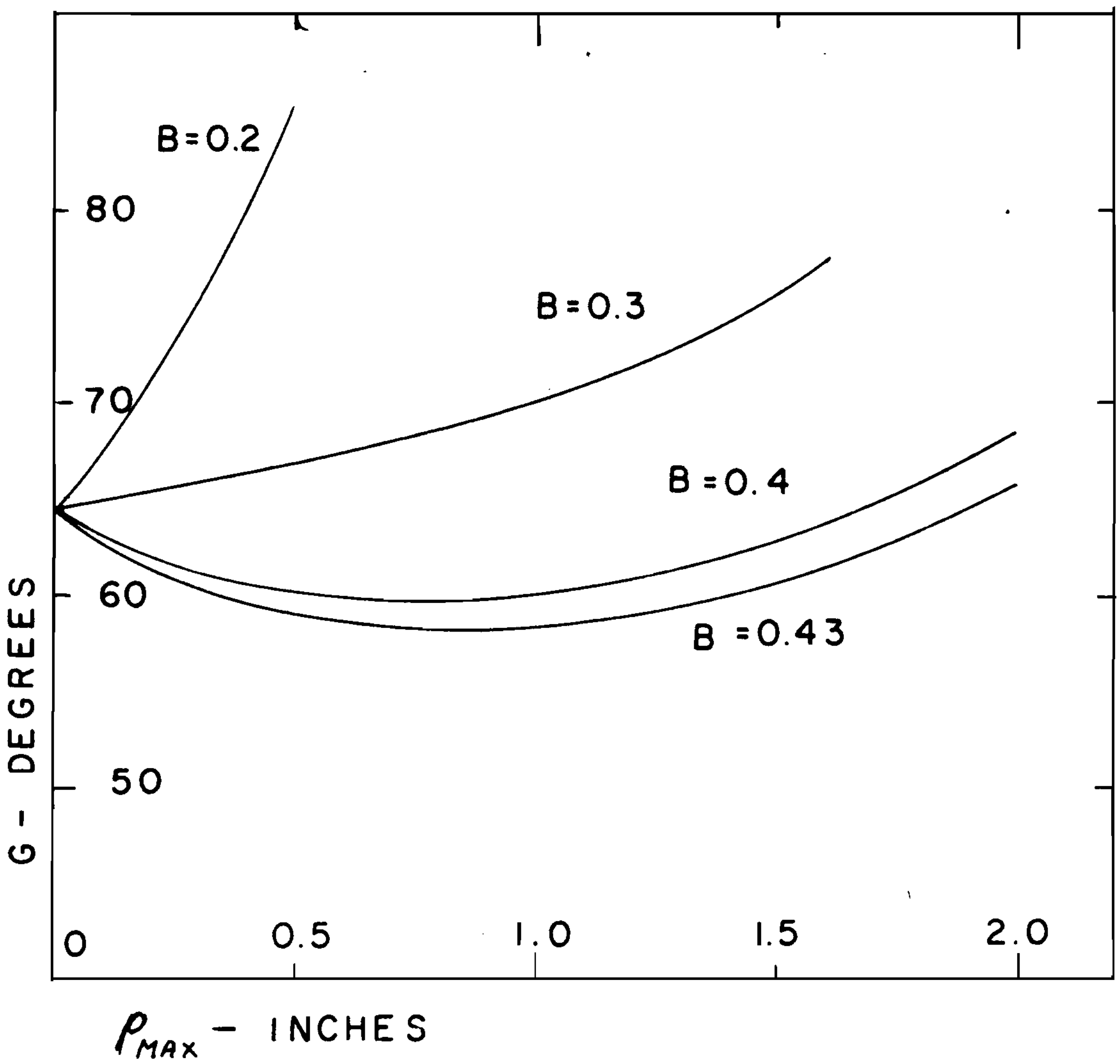

B=0.2
80
B=0.3
70
B=0.4
60
B=0.43
50
G - DEGREES
0
0.5
1.0
1.5
2.0
ρ_{MAX} - INCHES

FIGURE A4

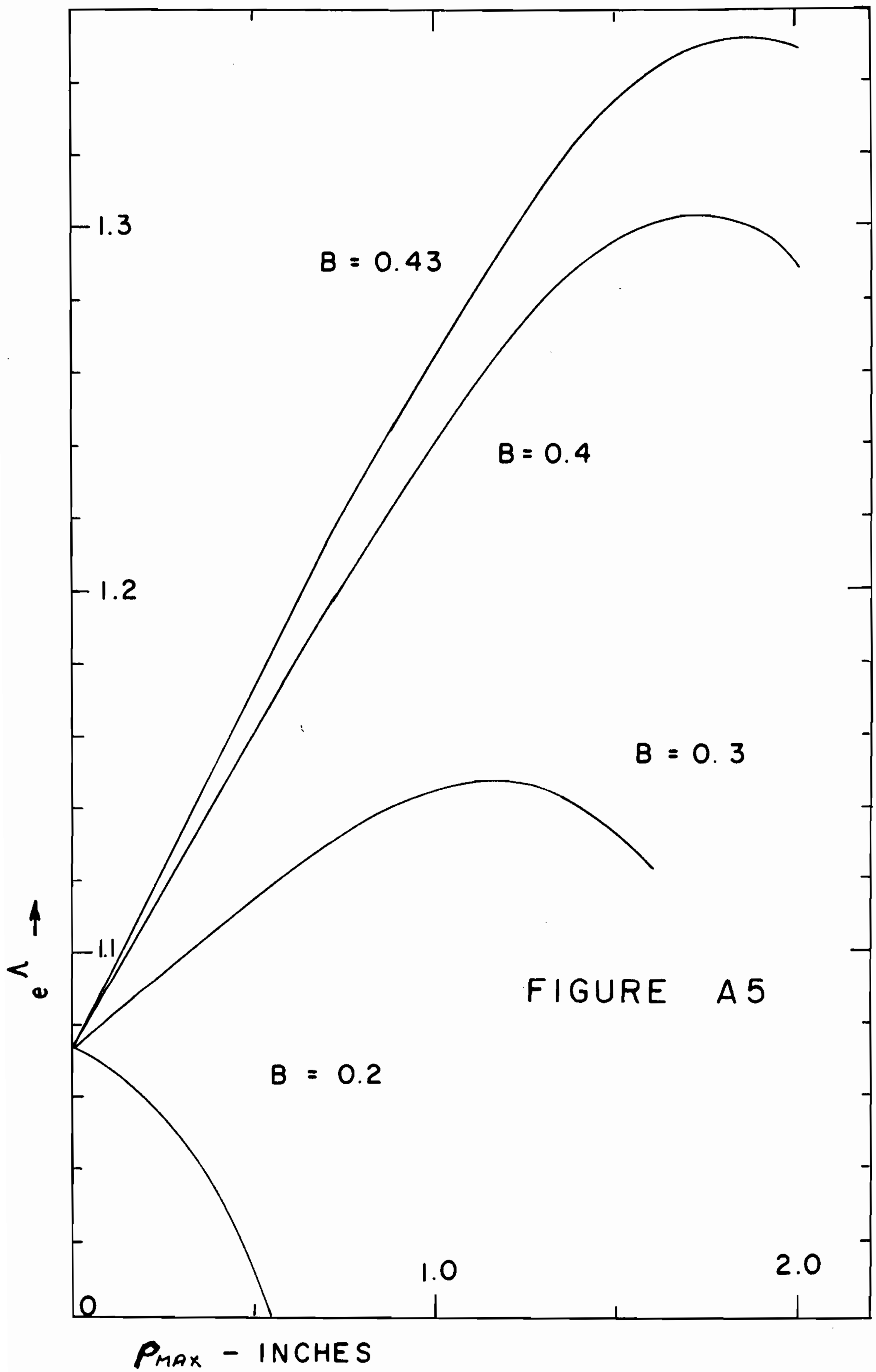

FIGURE A5

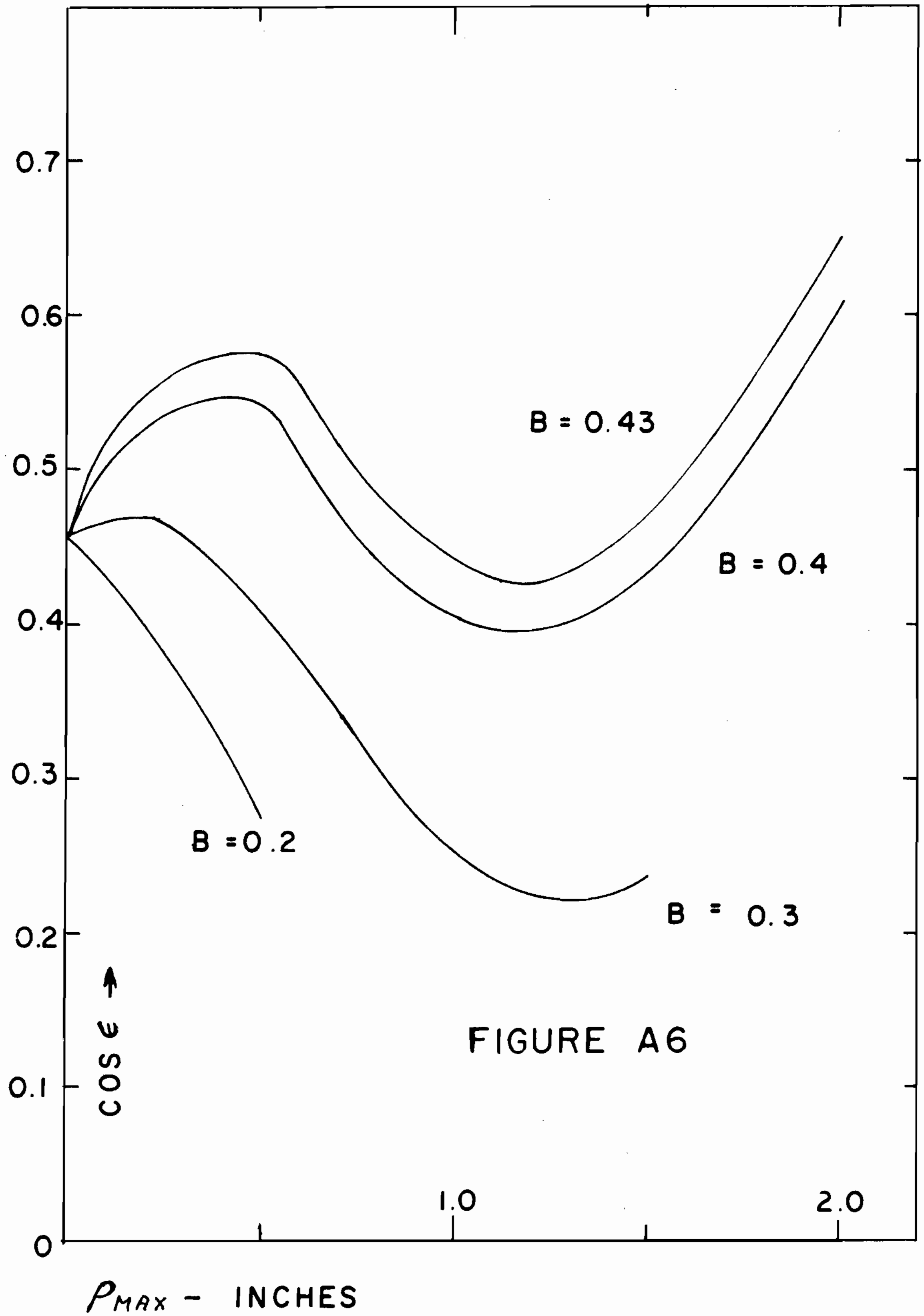

FIGURE A6

APPENDIX B - CALCULATION OF MAGNETIC FIELDS NEAR SATURATED IRON

Introduction

When undertaking a project such as that described in this thesis it is necessary to have some means of computing the magnetic field near pieces of iron placed in the cyclotron pole gap. The method described here gives the field changes in the vicinity of rectangular pieces of iron to within 10% or better.

The starting point of this development is the assumption that any iron placed in the cyclotron pole gap will become saturated, and hence act as a set of sources of magnetic flux with the total flux from each source equal to the saturation flux density of the iron multiplied by the area of the face of the iron which is considered to make up that source. The faces of the iron considered to be the sources of magnetic flux are those perpendicular to the general field direction.

Somewhat the same method of approach was used by A. V. Crewe and J. W. G. Gregory (1955) in the design of the extraction system for the Liverpool synchrocyclotron. However there are probably some refinements in this development which did not appear necessary in theirs; refinements made necessary by the tighter geometry of our smaller machine. The above authors give no details of their computational program.

Differential Form of the Magnetic Field Change

Magnetization curves for Armco Magnetic Ingot Iron show that the "knee" of the saturation curve is at about 20-30 oersteds and beyond this the magnetic flux density in the iron may be expressed as

$$B = B_s + \mu_o H \qquad (1B)$$

where B_s is equal to 21,500 gauss and $\mu_o = 1$ is the permeability of free space. For field strengths greater than several hundred oersteds the flux density the iron is then the saturation flux density B_s added to the flux that would exist if the iron were absent. Since we are dealing with fields of 5000 - 16000 oersteds, this condition is well satisfied. The procedure then is to break up the iron block into elemental columns along the field lines and treat each column as a bar magnet of magnet moment

$$d\,M = \frac{B_s\,dA}{4\pi}\,h \qquad (2B)$$

where dA is the cross sectional area of the column and h is its length (see Figure B1). The total field change in the median plane of the cyclotron is obtained by integrating the effect of these elemental columns. Because pieces of iron placed in the cyclotron gap are placed symmetrically about the median plane it is sufficient to know the field change in the median plane of the added iron. Assuming the direction of the undisturbed field to be positive, this field change outside the iron at a point (x_o, y_o) is

$$d^2B = -\frac{B_s\,dA}{4\pi}\,\frac{h}{\left(\left(\frac{h}{2}\right)^2 + (x - x_o)^2 + (y - y_o)^2\right)^{\frac{3}{2}}} \qquad (3B)$$

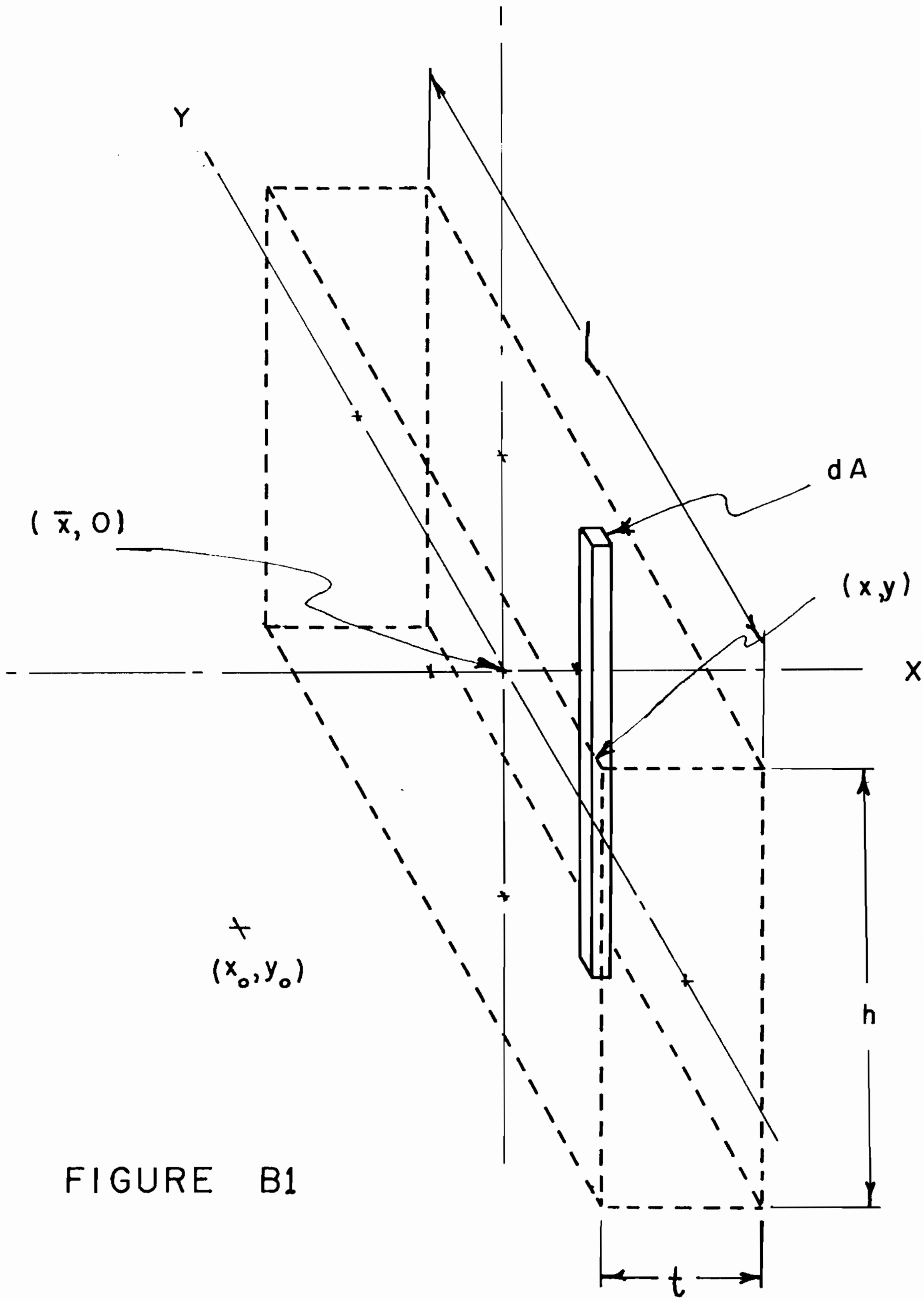

FIGURE B1

Integrating over Length of Bar.

Integrating the differential expression over y one obtains

$$dB = -\frac{B_s\,dx}{4\pi}\,\frac{4h}{h^2 + 4(x-x_o)^2}\left(\begin{array}{c}\dfrac{1}{1+\dfrac{h^2+4(x-x_o)^2}{(L-2y_o)^2}} \\ \dfrac{1}{1+\dfrac{h^2+4(x-x_o)^2}{(L+2y_o)^2}}\end{array}\right). \qquad (4B)$$

If $L-2y_o$ or $L+2y_o$ happen to be negative, the contribution of the corresponding term in this equation becomes negative.

For thin pieces of iron the above integration is entirely adequate, replacing dx by the thickness of the iron.

Integrating over Thickness of Bar

If the iron is thick enough to warrant an integration over x the resulting expression for the field change is

$$\Delta B = -\frac{B_s}{4\pi}\left(\sin^{-1}\frac{1}{(L-2y_o)^2+h^2}\left((L-2y_o)^2 - h^2 - \frac{2h^2(L-2y_o)^2}{h^2+4(x-x_o)^2}\right)\right.$$
$$\left.+\sin^{-1}\frac{1}{(L+2y_o)^2+h^2}\left((L+2y_o)^2 - h^2 - \frac{2h^2(L+2y_o)^2}{h^2+4(x-x_o)^2}\right)\right)\Bigg|_{x_1}^{x_2 = x_1+t}$$

(5B)

where x_2 is greater than x_1 and if x_1 or x_1 and x_2 are negative the corresponding $\sin^{-1}$ terms are subtracted from $-\pi$.

Corrections

For pieces of iron close to the pole tips of the cyclotron, corrections are necessary. Here the situation is analogous to the case of electric charges in the vicinity of a conducting plate. The field may be reproduced by assuming a mirror image of opposite charge on the other side of the plate. If pole tip saturation is not a problem, to a good approximation the pole tip is a magnetic equipotential surface and remains so after the added iron is in place. Mirror images of the mirror images should be of no importance and so the effect of pole tip proximity may be calculated by assuming two new sets of magnetic poles with spacings 2g-h and 2g+h, the set with spacing 2g-h producing a positive field change. (g is the cyclotron gap). A sketch of this assumed source geometry is given in Figure B2.

A computer program based on equation (5B) with the mirror image corrections built in, has been compiled. A similar program based on equation (4B) has also been compiled. In these programs iron pieces such as used in the regenerator may be considered as two sets of primary poles with spacings h_1 causing a positive field change and $h_1 + 2h$ causing a negative field change. As shown in Figure B3, h_1 is the gap between the iron pieces and h is their individual heights.

For thin pieces of iron (of the order of 1/8 inch or less) the computer program based on the differential expression for the field change (equation 4B) may be used. With this program an IBM 650 computer will evaluate the field at one point for one piece of iron in about two seconds. The time for the

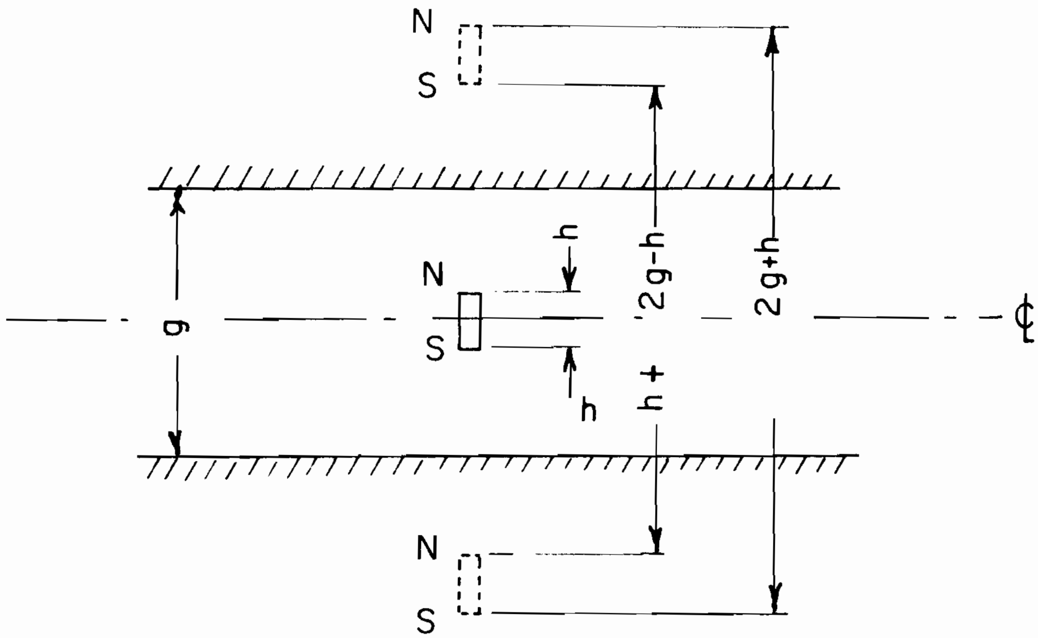

FIGURE B2 - GEOMETRY OF MIRROR IMAGES

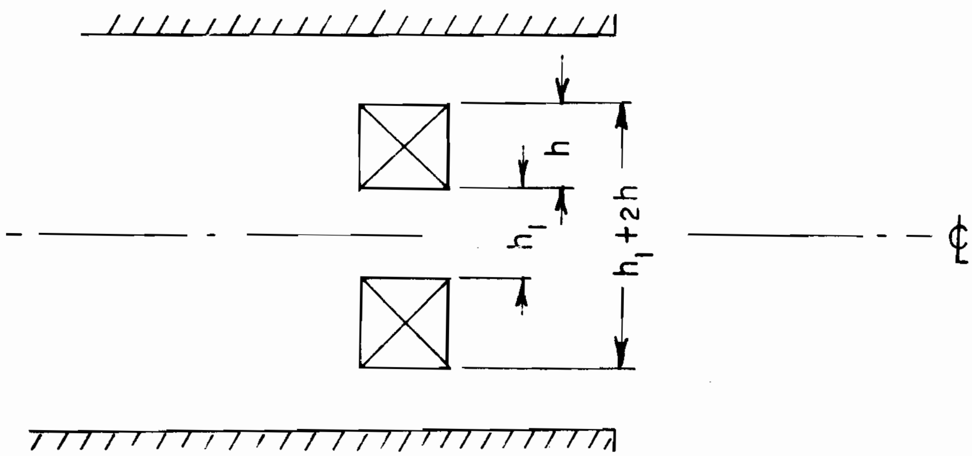

FIGURE B3 - GEOMETRY OF REGENERATOR

program based on the integration of this differential expression (equation 5B), is about 5 seconds for one piece of iron. The computing time for each program is very nearly proportional to the number of pieces of iron. Therefore, for thick pieces of iron that have to be broken up into pieces 1/8 inch thick for the program of equation 4B to give good results, the program based on equation 5B is faster if the pieces are more than ½ inch thick. For extensive field calculations around the thick pieces of iron in the regenerator, the program based on the integration saves considerable computing time.

For heavy blocks of iron near the pole tip some caution must be exercised in the application of this program. For such configurations the iron in the pole tips of the cyclotron may become saturated. This should occur for magnetic flux density in the pole tips approaching 21,000 gauss. The flux density in the pole tips of the McGill synchrocyclotron at a radius of 38½ inches should be normally about 17,000 gauss. Therefore demanding a field change of more than 3,500 gauss at the surface of the pole tip may cause pole tip saturation. This would cause a general depression in the magnetic field in the space between the pole tips at the saturated parts. In the case of the regenerator this effect is noticeable and so the calculated values of the magnetic field cannot be used to design the fine shimming at inner radii. However the measured magnetic field in the principal part of the regenerator turns out to be very close to the calculated values (as a percentage of the field change) and the effect of the depression from pole tip saturation on the regenerator field gradient may be ignored.

In the case of the regenerator an attempt was made to calculate the effect of pole tip saturation. The approach was to calculate the magnetic field change at the pole tip surface due to the regenerator installation. (With a slight modification the existing program was used). The excess of this change over 3,500 gauss was then subtracted at the pole tip and the resultant effect in the median evaluated. This effect was treated as the saturation correction and the results in the fringing area of the regenerator duplicated measured field changes to within instrumental accuracy. However lack of accurate knowledge of both B_s in the pole tip and the flux density normally at the pole tip surface (calculated by conformal mapping of the pole tip geometry) renders the difference highly inaccurate and tends to reduce the value of this approach for design purposes. In most cases it is sufficient to know if pole tip saturation is important. In the cases of channels and self excited quadrupoles no pole tip saturation effects were observed.

BIBLIOGRAPHY

BRUECKNER, K. A., et al. 1961. Phys. Rev. 121, 255.

CALAME, G., et. al. 1957. Nuclear Instr. and Methods 1, 169.

LE COUTEUR, K. J. 1951. Proc. Phys. Soc. (London) B. 64, 1073.

LE COUTEUR, K. J. 1953. Proc. Phys. Soc. (London) B. 66, 25.

LE COUTEUR, K. J. 1955. Proc. Roy. Soc. (London) A. 232, 236.

LE COUTEUR K. J., and LIPTON, S. 1955. Phil. Mag. 46, 1265

COWEN, J. A., and TANTILLA, W. H. 1958. Am. J. Phys. 26, 381

CRANDALL, W. E. et al. 1956. Phys. Rev. 101, 329

CREWE, A. V., and GREGORY, J. W. G. 1955. Proc. Roy. Soc. (lomdon) A, 232, 242

CREWE, A. V., and KRUSE, U. E. 1956. Rev. Sci. Instr. 27, 5

EDEN, R. J. 1959. Nuclear Reactions, edited by P. M. Endt and M. Demeur (North Holland Publishing Co., Amsterdam) p. 1

FREMLIN, J. H., and GOODEN, J. S. 1950. Rept. Progr. in Phys. 50, 295

HONE, D. W. 1951. Ph. D. Thesis, McGill University, Montreal.

KIRKALDY, J. S. 1953. Ph. D. Thesis, McGill University, Montreal.

LIVINGSTON, M. S. 1952. Ann. Rev. Nuclear Sci. 1, 157

MAYO, S., et al. 1958. Nuclear Instr. and Methods 2, 9.

PENNER, S. 1961. Rev. Sci. Instr. 32, 150

PEIERLS, R. E. 1960. Proceedings of the International Conference on Nuclear Structure, Kingston, Ontario, edited by D. A. Bromley and E. W. Vogt (University of Toronto Press) p. 7.

PHILLIPS, R. J. N. 1959. Repts. Progr. in Phys. 22, 562

RICK, M., and MADEY, R. 1954. UCRL-2301

SUWA, S., et al. 1959. Nuclear Instr. and Methods 5, 189

TUCK, J. L., and TENG, L. C. 1951. Phys Rev. 81, 305.

VERSTER, N. F. 1959. Sector Focused Cyclotrons. Proceedings of an Informal Conference, Sea Island, Georgia. p 224